

Coupled models of structured contagion processes in human-environment systems

by

Peter C. Jentsch

A thesis
presented to the University of Waterloo
in fulfillment of the
thesis requirement for the degree of
Doctor of Philosophy
in
Applied Mathematics

Waterloo, Ontario, Canada, 2021

© Peter C. Jentsch

Examining Committee Membership

The following served on the Examining Committee for this thesis. The decision of the Examining Committee is by majority vote.

External Examiner: Tim Reluga
Professor, Mathematics and Biology,
Pennsylvania State University

Supervisors: Chris T. Bauch
Professor, Department of Applied Mathematics, University of Waterloo

Madhur Anand
Professor, School of Environmental Sciences, University of Guelph

Internal Members: Sue Ann Campbell
Professor, Department of Applied Mathematics, University of Waterloo
Zoran Miskovic
Professor, Department of Applied Mathematics, University of Waterloo

Internal-External Member: Paul Fieguth
Professor, Department of Systems Design Engineering,
University of Waterloo

Author's Declaration

This thesis has entirely been authored or co-authored by me. This is a true copy of the thesis, including any required final revisions, as accepted by my examiners.

I understand that my thesis may be made electronically available to the public.

Statement of Contributions

- Chapter 2: MA and CTB conceptualized the study. All authors designed the model. PCJ developed and analysed the model and generated figures. PCJ and CTB wrote the first draft of the manuscript and accessed and verified the data. All authors revised the manuscript critically for important intellectual content, and read and approved the final version of the manuscript. All authors had full access to all the data in the study, and the corresponding author had final responsibility for the decision to submit for publication. The contents of this chapter are based on the corresponding article published in *Lancet Infectious Diseases* [110].
- Chapter 3: Conceptualization by DY, MA, data curation by PCJ, DY, formal analysis by PCJ, funding acquisition by CTB, DY, MA, investigation by PCJ, CTB, DY, MA. Methodology by PCJ, CTB, DY, MA. Project administration by PCJ, CTB, DY, MA. Resources by CTB, DY, MA. Software written by PCJ. Supervision by CTB, DY, MA, validation by PCJ, CTB, DY, MA, visualization by PCJ, CTB. Original draft written by PCJ. Review editing by PCJ, CTB, DY, MA. The contents of this chapter are based on the corresponding article published in *PLoS One* [111].
- Chapter 4: The work in this chapter is based upon a manuscript accepted for publication in *Theoretical Ecology*. All authors conceived ideas for the study. PCJ designed and coded the model, performed analyses, created figures, and drafted the manuscript. All authors revised the manuscript.

Abstract

Models of infectious processes are a common feature in the landscape of applied mathematics. It is rare that these processes are isolated from other significant dynamics in nature, and therefore we can incorporate some of the complexity inherent in real systems by coupling infections to major features of the ecosystems they inhabit. Infectious processes can take many forms, but in this thesis we consider three: the COVID-19 pandemic, the invasion of eastern North American forests by wood-borne pests, and the outbreak cycles of an endemic forest pest. The first chapter covers a model of Sars-CoV-2 in a structured population, coupled with a replicator equation representing sentiment towards the use of non-pharmaceutical interventions. We use this human-environment model of to compare the efficacy of vulnerable-first and transmission-preventing age structured vaccination strategies. The buildup of natural immunity in a population combined with a low vaccination supply, is shown to cause a transmission-preventing vaccination strategy to be more effective. The second chapter considers a spatially structured model of forest pest contagion over an empirically-derived network of forest patches in eastern Canada. Since these pests can frequently be spread long distances by wood transport, we couple this model to the sentiment of local populations towards avoiding firewood transport from outside their area. Three possible countermeasures to the spread of the invasive pest are compared: social incentives, direct interception of infested firewood, and quarantine of patches. The level of effort needed to significantly reduce forest damage with any of these methods is substantial and unlikely to be implemented. The final chapter extends a model of mountain pine beetle (MPB) in western north american pine forests to incorporate tree mortality due to wildfire. We find that wildfire acts as a disturbance that increases the heterogeneity in age structure, and therefore is able to increase the resilience of the forest to outbreaks of MPB. A targeted thinning procedure aimed specifically at increasing heterogeneity in the forest age structure is proposed and shown to be highly effective at reducing the severity of outbreak. The effectiveness of targeted thinning in the manner described further emphasizes the importance of heterogeneity in forest stand structure. Each model tests the importance of indirect protection in preventing the spread of an infectious agent through a specific host population, with respect to key parameters. Models let us use counterfactuals to gain potentially invaluable understanding of these complex human-environment systems.

Acknowledgements

I would like to thank the following people for making this thesis possible.

- My supervisors, Dr. Chris Bauch and Dr. Madhur Anand, for their endless support, understanding, and insight throughout my graduate and undergraduate career.
- Dr. Sue Ann Campbell, Dr. Zoran Miskovic, Dr. Tim Reluga, and Dr. Paul Fieguth for being on my PhD committee.
- Dr. Denys Yemshanov for his patience and mentorship on things forest-related.
- Dr. Mark Penney for the great conversations, collaboration, and opportunity to write an agent-based model in the last six months of my PhD.
- Dr. Christopher Nehaniv for the opportunities to think and present about topics almost completely different from those in this thesis.
- My friends in the Bauch Lab, the applied mathematics department, and outside the university for the time spent not working, and many victorious bar trivia nights.
- Samantha Landry and Emylee Todd for reading and editing the early drafts of this thesis.
- My mom, dad, and siblings, for their support, encouragement, and not asking "so when are you gonna graduate" too often.

Dedication

For Emmy, Max, Sam, and the friends that have helped me get through the past 5 years.

Table of Contents

List of Figures	xi
List of Tables	xxii
1 Introduction	1
1.1 Sars-CoV-2	3
1.2 Imitation dynamics	4
1.3 Forest pests in eastern North America	6
1.4 Mountain pine beetle (MPB) and fire-driven forest ecosystems of the Western Cordillera	7
1.5 Thesis Outline	9
2 Prioritising COVID-19 vaccination in changing social and epidemiological landscapes: a mathematical modelling study	11
2.1 Introduction	12
2.2 Model Overview	14
2.2.1 Structure and parameterisation	14
2.2.2 Model Equations	14
2.2.3 Vaccination process	17
2.2.4 Differences between parameters in the first and second wave	18
2.2.5 Case under-ascertainment	18

2.2.6	Baseline transmission rate	19
2.2.7	Disease progression parameters	20
2.2.8	Initial conditions	20
2.2.9	Particle filtering	21
2.2.10	Vaccination refusal dynamics	22
2.2.11	Model extension for vaccine efficacy against disease only	22
2.2.12	Vaccine scenarios	23
2.3	Results	24
2.4	Discussion	33
3	Go big or go home: a model-based assessment of general strategies to slow the spread of forest pests via infested firewood	37
3.1	Abstract	37
3.2	Introduction	38
3.3	Materials and methods	41
3.3.1	Pest Spread Model	41
3.3.2	Social Dynamics Model	43
3.3.3	Patch-quarantine strategies	44
3.3.4	Parameterization	47
3.3.5	Assessing intervention efficacy	48
3.4	Results	49
3.5	Conclusion	53
3.6	Acknowledgements	57
4	Fire Mitigates Bark Beetle Outbreaks in Serotinous Forests	58
4.1	Introduction	58
4.2	Methods	60
4.2.1	Model Description	60

4.3	Initial conditions	65
4.3.1	Forest thinning protocol (FTP) and controlled burning protocol (CBP)	65
4.3.2	Parameters and simulation design	66
4.4	Results	68
4.4.1	Dynamical regimes	68
4.4.2	Impact of forest thinning protocol (FTP) and controlled burning protocol (CBP)	70
4.5	Discussion	72
5	Conclusion	78
5.1	Summary of findings	78
5.2	Discussion	80
5.3	Limitations and future work	82
5.4	Concluding comments	84
References		85
Appendix		106

List of Figures

1.1	Diagram of population flow in an SIR model	2
1.2	An infection represented by an SIR model, with $\beta = 0.4$, $\gamma = 0.08$, $S(0) = 0.99$, and $I(t) = 0.01$	2
1.3	NPI adoption as a two-player game (between P1 and P2).	5
1.4	An EAB on a penny [176]	7
1.5	MPB-killed lodgepole pines in Manning Park, British Columbia, Canada [212]	7
2.1	A proxy for adherence to NPIs mirrors COVID-19 case reports in both data and model. (a) COVID-19 case incidence by date of report in Ontario, 7-day running average (circles) and ascertained case incidence from best fitting models (lines). (b) Percentage change from baseline in time spent at retail and recreation destinations (orange circles) and at workplaces (green circles) from Google mobility data, and proportion of the population x adhering to NPIs (orange line) and workplace shutdown curve (green line) from fitted model. Parameter values are provided in table 2.1.	26
2.2	Social and epidemiological dynamics interact to determine pandemic waves and vaccine strategy effectiveness. (a) Number of ascertained incident COVID-19 cases, (b) proportion x of the population practicing NPIs, (c) level of school and workplace closure (note that curves for different vaccination strategies overlap), and (d) number of individuals with natural or vaccine-derived immunity versus time. Ontario Population size: 14.6 million. Shutdown occurs at $T = 200\%$ of peak cases in the first wave, vaccination starts in January 2021, vaccination rate is $\psi_0 = 0.5\%$ per week. Other parameter values are provided in table 2.1.	27

2.3	Three model regimes: (a) timely vaccination prevents third wave, (b,c) partial vaccination and indirect protection help during the third wave, and (d) slow and late vaccination fails to prevent third wave. Projections of ascertained incident COVID-19 cases if vaccination begins in (a,b) January or (c,d) September, and if vaccinating (a,c) 1.5% or (b,d) 0.5% of the population per week. Ontario Population size: 14.6 million. $T = 200\%$. Other parameter values are provided in table 2.1.	28
2.4	Percentage reduction in mortality for four strategies depends on vaccination start date and the vaccination rate. Violin plots of the percent reduction in mortality under the four vaccine strategies, relative to no vaccination, as a function of the vaccination rate ϕ_0 , for (a) January and (b) September 2021 availability. Horizontal lines represent median values of posterior model projections. Shutdown threshold $T = 200\%$ and other parameter values are provided in table 2.1. The projected number of deaths in the absence of vaccination was 72000 (95% credible interval 40000–122000) from Jan 1, 2021, to March 14, 2025, and 60000 (31000–108000) from Sept 1, 2021, to March 14, 2025.	29
2.5	More pre-existing natural immunity makes transmission-interrupting strategies more effective. Frequency histogram of the percentage of the population with natural immunity for each strategy, taken from simulations where that strategy reduced mortality most effectively, for (a) oldest first, (b) youngest first, (c) uniform, and (d) contact-based strategies. The most effective strategy is defined as the one that reduced mortality the most across the largest number of model realizations. Vertical dashed lines denote median values of the distribution. Other parameter values are provided in table 2.1.	31
3.1	Camper travel network in Ontario, Quebec and Manitoba. Darker (more orange) lines represent more trips.	48
3.2	Time series of model variables as a function of interventions, direct (raising C_e, panels a - d) and through social pressure (raising U, panels e - h). The former intervention, panels a-d, means an increase of social pressure on people who choose to transport firewood (i.e. increasing the U value), and the latter refers to direct interception of firewood (i.e. increasing the C_e value). Terms $L(t) = \frac{1}{N} \sum_{i=1}^N S_i(t)$, $I(t) = \frac{1}{N} \sum_{i=1}^N I_i(t)$, $B(t) = \frac{1}{N} \sum_{i=1}^N B_i(t)$, $L(t) = \frac{1}{N} \sum_{i=1}^N L_i(t)$ are the averages of the state variables over all patches. $S(t)$ has been omitted for brevity.	51

3.3	Total infestation per node over 5, 10 and 20 years. Neither increasing U nor C_e are effective at long time scales.	52
3.4	Efficacy of social incentives on infestation after time T. Inset graph shows an example of cross-section along the line $f = 0.11$. The influence of infestation on transport strategy, f , can hinder the intervention by public outreach, in the long-term (after approximately 20 years). The inset figure illustrates how one column in the heat map, shown by the dotted line, is constructed from the slopes of linear approximations of $T(t)$ over $U \in [-5, 5]$. The blueness of the lines going left to right is a function of their slope, corresponding to the color of the cells in the heatmap.	53
3.5	Efficacy of social incentives on infestation after time period T with respect to A, the intra-patch infestation parameter. This intervention becomes ineffective over time if A is sufficiently large.	54
3.6	Efficacy of social incentives on infestation after time T intra-patch spreading rate A, affects infestation outcomes. The social incentive to not transport firewood, U , is more effective with lower pest spread rates.	54
3.7	Average total infested trees ($T(t)$) after 5, 10 and 15 years (panels a), b), and c) respectively), assuming the quarantine begins one year after the pest is introduced. Total infestation plotted with respect to the number of nodes quarantined ($ V $) and the length of the quarantine (Δt). The quarantine is effective over 5 years with only 50 patches, provided they are closed for over a year.	55
3.8	Average total infested trees ($T(t)$) after 5, 10 and 15 years (panels a), b), and c) respectively), assuming the quarantine begins two years after the pest is introduced. Total infestation plotted with respect to the number of nodes quarantined ($ V $) and the length of the quarantine (Δt).	55
4.1	Conceptual diagram of compartments (state variables) and transitions between compartments across seasons. See main text and Table 4.1 for definitions of variables and parameters.	63

4.2	Approximate dynamical regimes of the system, where α_1 is the burning rate of juvenile trees, and α_2 is the burning rate of susceptible (mature) trees. a) Average size of largest MPB population (over 500 years at equilibrium) b) Average frequency of MPB outbreaks at equilibrium c) Average size of largest fire season (over 500 years at equilibrium) d) Average frequency of severe fire seasons at equilibrium. The juvenile burning rate (α_1) and susceptible burning rate (α_2) control fire and MPB prevalence. Large α_1, α_2 implies low infestation and also more regularity in the fire regime. All other parameters were set to baseline values (Table 4.1).	69
4.3	Time series of each state variable of a single realization where $\alpha_1 = 0.02$, $\alpha_2 = 0.0025$, showing the regular outbreaks of pests, periodic shifts in fire prevalence, and uneven age distribution generated by MPB outbreaks. a) juvenile distribution at time $t = 2050$ (note different x-axis), b) susceptible population after year t , c) infested tree population after year t , d) number of burned trees after year t . All other parameters were set to baseline values (Table 4.1).	71
4.4	Time series showing realization of model under FTP with $\tau = 0.15$ fraction of $m = 8$ juvenile stands cleared, conducted each year, where $\alpha_1 = 0.02$, $\alpha_2 = 0.0025$. a) juvenile distribution at time $t = 2050$ (note different x-axis), b) susceptible population after year t , c) infested tree population after year t , d) burned forest after year t . Notice the flattening of the age distribution compared to the same parameters with no FTP (Figure 4.3)	73
4.5	Percentage change in average susceptible (mature) forest population compared to no FTP with a) $\tau = 0.15, m = 8$, b) with $\tau = 0.15, m = 8$ applied every 5 years, c) controlled burning with $\tau = 0.15, m = 8$, with respect to burning rates α_1, α_2 . FTP and CBP increase the average population of mature trees in many cases, in addition to reducing outbreak sizes.	74
4.6	Percentage change in maximum MPB infestation size within 500 year period under FTP with a) $\tau = 0.15, m = 8$, b) with $\tau = 0.15, m = 8$ applied every 5 years, c) controlled burning with $\tau = 0.15, m = 8$, with respect to burning rates α_1, α_2 . FTP is always effective at reducing MPB outbreaks, and CBP worsens them if the population of MPB is already low.	74

1	Posterior distributions on inferred non-age structured model parameters for baseline model. Posteriors are composed of 200 candidate parameter sets from the particle filtering, the model was evaluated at these points for all future runs.	107
2	Posterior distributions on inferred age-specific susceptibility modifier parameter ρ_i for baseline model. Three age-specific susceptibility parameters shown here, ρ_1, ρ_2, ρ_3 , were also inferred from particle filtering on the case and mobility data, corresponding to the age brackets 0-20, 20-60, 60+.	107
3	Posterior distributions on inferred age-specific ascertainment rate over time for baseline model. Time dependent ascertainment rates inferred from the data, corresponding to the fraction of actual cases detected by the Ontario testing system.	108
4	Empirical data of cumulative infections due to COVID-19 by age and model posterior predictions. The age-specific total cases at the end of the fitting window, were used to calibrate the model, in an age dependent way. We used only three parameters to capture age specific effects and therefore trade-off some accuracy in the youngest and oldest age groups. . .	109
5	Average of model posterior population seropositivity over time, compared to empirical data. Total seroprevalence in Ontario was assessed during the month of June. We used this value to calibrate the model further.	110
6	Age distribution of vaccination under the contact-based strategy. This strategy vaccines proportionally to the leading eigenvector of the full contact matrix, $C(0)$, to vaccinate people who will, approximately, produce the most secondary infections in a linearized regime.	111
7	Social and epidemic dynamics for early vaccine availability and high vaccination rate. (a) Ascertained incident COVID-19 cases, (b) proportion x of the population practicing NPIs, (c) Intensity of school and workplace closure, (d) percentage of population with natural or vaccine-derived immunity versus time. $T = 200\%$, $\psi_0 = 1.5\%$ per week, vaccine available in January 2021. Other parameters are in Table 2.1.	112

8	Social and epidemic dynamics for late vaccine availability and high vaccination rate. (a) Ascertained incident COVID-19 cases, (b) proportion x of the population practicing NPIs, (c) Intensity of school and workplace closure, (d) percentage of population with natural or vaccine-derived immunity versus time. $T = 200\%$, $\psi_0 = 1.5\%$ per week, vaccine available in September 2021. Other parameters are in Table 2.1.	113
9	Social and epidemic dynamics for late vaccine availability and low vaccination rate. (a) Ascertained incident COVID-19 cases, (b) proportion x of the population practicing NPIs, (c) Intensity of school and workplace closure, (d) percentage of population with natural or vaccine-derived immunity versus time. $T = 200\%$, $\psi_0 = 0.5\%$ per week, vaccine available in September 2021. Other parameters are in Table 2.1.	114
10	Mortality reductions under various values of T and ψ_0, early vaccine availability. Violin plots of the percent reduction in mortality under the four vaccine strategies, relative to no vaccination, as a function of the vaccination rate ψ_0 , for January 2021 availability. Horizontal lines represent median values of posterior model projections. Other parameter values in Table S1. Percentage reductions are relative to no vaccination. Projected number of deaths in the absence of vaccination were 35597.2 (CI: 57465.9,19507.9); 48518.8 (CI: 86853.9,28335.7), 61339.1 (CI: 106623.0,34613.5), 72007.3 (CI: 121754.0,40483.4); 80707.6 (CI: 126732.0,47755.4) after January 1, 2021, for T=50%, 100%, 150%, 200%, and 250%, respectively.	115
11	Mortality reductions under various values of T and ψ_0, late vaccine availability. Violin plots of the percent reduction in mortality under the four vaccine strategies, relative to no vaccination, as a function of the vaccination rate ψ_0 , for September 2021 availability. Horizontal lines represent median values of posterior model projections. Other parameter values in Table S1. Percentage reductions are relative to no vaccination. Projected number of deaths in the absence of vaccination were 25478.8 (CI: 45679.0,13006.7); 39149.6 (CI: 73917.1,20290.9); 50775.1 (CI: 95451.2,25980.9); 60250.7 (CI: 108361.0,30721.9); 68594.0 (CI: 107157.0,36063.6) after September 1, 2021 for T=50%, 100%, 150%, 200%, and 250%, respectively.	116

12	A higher level of natural immunity increases the relative advantage of transmission-interrupting strategies. Median and standard deviation of the percent reduction in mortality under the four vaccine strategies, relative to no vaccination, as a function of the vaccination start date and percent recovered at that time, for (a) $\phi_0 = 1.0\%$ vaccinated per week and (b) $\phi_0 = 2.5\%$ vaccinated per week. Shutdown threshold $T = 200\%$, and other parameter values in Appendix, Table S1.	117
13	Sensitivity analysis exploring a range of vaccine efficacy values, for vaccination rate $\phi_0 = 2.5\%$ per week. Subpanels are parameter planes for January and September availability showing the vaccination strategy that reduces COVID-19 mortality the most as a function of vaccine efficacy in 60+ year-olds versus vaccine efficacy in other age groups. Other parameter values as in Table S1.	118
14	Sensitivity analysis exploring impact of vaccinating behaviour dynamics. $\phi_0 = 2.5\%$ per week, $T = 200\%$. Subpanels are parameter planes for January and September availability showing the vaccination strategy that reduces COVID-19 mortality the most as a function of vaccine social learning rate κ_{vac} and vaccine cost parameter c_{vac} . Other parameter values as in Table S1.	119
15	Epidemic dynamics and social dynamics for both NPI adherence and vaccinating behaviour, when vaccine cost is small, $c_{vac} = 1.1 \times 10^{-4}$. (a) Ascertained incident COVID-19 cases, (b) proportion x of the population practicing NPIs, (c) Intensity of school and workplace closure, (d) percentage of population with natural or vaccine-derived immunity versus time. $T = 200\%$, $\psi_0 = 1.0\%$ per week (maximum rate in absence of vaccine refusal), vaccine available in September 2021, $\kappa_{vac} = 50/\text{day}$. Other parameters are in Table 2.1.	120
16	Epidemic dynamics and social dynamics for both NPI adherence and vaccinating behaviour, when vaccine cost is moderate, $c_{vac} = 2.9 \times 10^{-4}$. (a) Ascertained incident COVID-19 cases, (b) proportion x of the population practicing NPIs, (c) Intensity of school and workplace closure, (d) percentage of population with natural or vaccine-derived immunity versus time. $T = 200\%$, $\psi_0 = 1.0\%$ per week (maximum rate in absence of vaccine refusal), vaccine available in September 2021, $\kappa_{vac} = 50/\text{day}$. Other parameters are in Table 2.1.	121

17	Epidemic dynamics and social dynamics for both NPI adherence and vaccinating behaviour, when vaccine cost is high, $c_{vac} = 3.8 \times 10^{-4}$. (a) Ascertained incident COVID-19 cases, (b) proportion x of the population practicing NPIs, (c) Intensity of school and workplace closure, (d) percentage of population with natural or vaccine-derived immunity versus time. $T = 200\%$, $\psi_0 = 1.0\%$ per week (maximum rate in absence of vaccine refusal), vaccine available in September 2021, $\kappa_{vac} = 50/\text{day}$. Other parameters are in Table 2.1.	122
18	Sensitivity analysis for the scenario where $R_0 = 2.5$ for December 2020 onward. Subpanels are (left) parameter planes for January and September availability showing the vaccination strategy that prevents the most COVID-19 deaths as a function of T and ψ_0 , and (right) percentage reductions in mortality. Other parameter values are as in Table S1.	123
19	Sensitivity analysis for the scenario of 30% heightened ascertainment across all ages from December 2020 onward. Subpanels are parameter planes for January and September availability showing the vaccination strategy that reduces COVID-19 mortality the most as a function of T and ψ_0 (left) and the corresponding posterior parameter distributions for the refitted parameters (right). Other parameter values as in Table S1.	124
20	Sensitivity analysis for the scenario of 30% reduced ascertainment across all ages from December 2020 onward. Subpanels are parameter planes for January and September availability showing the vaccination strategy that reduces COVID-19 mortality the most as a function of T and ψ_0 (left) and the corresponding posterior parameter distributions for the refitted parameters (right). Other parameter values as in Table S1.	125
21	Sensitivity analysis for the scenario of four times the baseline social learning rate from December 2020 onward. Subpanels are parameter planes for January and September availability showing the vaccination strategy that reduces COVID-19 mortality the most as a function of T and ψ_0 (left) and the corresponding posterior parameter distributions for the refitted parameters (right). Other parameter values as in Table S1.	126
22	Sensitivity analysis for the scenario of one-fourth the baseline social learning rate from December 2020 onward. Subpanels are parameter planes for January and September availability showing the vaccination strategy that reduces COVID-19 mortality the most as a function of T and ψ_0 . Other parameter values as in Table S1.	127

23	Sensitivity analysis for the scenario where efficacy against disease v^D is not the same as efficacy against transmission v^T. Subpanels show percentage reduction in mortality for the four strategies versus v^D when $v^T = 0.75$ but v^D ranges from 0.75 to 0.95, for January and September availability. Other parameter values as in Table S1. Note that mortality in this plot is computed from March 15, 2020 to March 14, 2025.	128
24	Posterior parameter distributions and model outputs for more stringent particle filtering criteria under Bayesian particle filtering algorithm. Top left panel shows (a) COVID-19 case incidence by date of report in Ontario, 7-day running average (circles) and ascertained case incidence from best fitting models (lines). (b) Percentage change from baseline in time spent at retail and recreation destinations (orange circles) and at workplaces (green circles) from Google mobility data, and proportion of the population x adhering to NPIs (orange line) and workplace shutdown curve (green line) from fitted model. Top right panel shows posterior parameter distribution for age-specific susceptibility modifier, ρ_i . Bottom panel shows other posterior parameter distributions. Other parameter values as in Appendix, pp. 1-11.	129
25	Sensitivity analysis for more stringent particle filtering criteria under Bayesian particle filtering algorithm. Subpanels are parameter planes for January and September availability showing the vaccination strategy that reduces COVID-19 mortality the most as a function of T and ψ_0 (left) and violin plots showing percentage reduction in mortality (right). Horizontal lines represent median values of posterior model projections. Shutdown threshold $T=200\%$ and other parameter values in Appendix, pp. 1-11. Percentage reductions are relative to no vaccination. Projected number of deaths in the absence of vaccination was 72,000 (95% credible interval: 40,000 to 122,000) from January 1, 2021 to March 14, 2025 for (a) and 60,000 (95% credible interval: 31,000 to 108,000) from September 1, 2021 to March 14, 2025 for (b). Ontario Population size: 14.6 million.	130

- 26 **Model fit to data and baseline projections of mortality reductions under the four vaccine strategies, when behaviour is held constant over time.** Top left: a) COVID-19 case incidence by date of report in Ontario, 7-day running average (circles) and ascertained case incidence from best fitting models (lines). (b) Percentage change from baseline in time spent at retail and recreation destinations (orange circles) and at workplaces (green circles) from Google mobility data, and proportion of the population x adhering to NPIs (orange line) and workplace shutdown curve (green line) from fitted model. Bottom left: Violin plots of the percent reduction in mortality under the four vaccine strategies, relative to no vaccination, as a function of the vaccination rate θ , for (a) January and (b) September 2021 availability. Horizontal lines represent median values of posterior model projections. Shutdown threshold $T=200\%$. Percentage reductions are relative to no vaccination. Projected number of deaths in the absence of vaccination was 72,000 (95% credible interval: 40,000 to 122,000) from January 1, 2021 to March 14, 2025 for (a) and 60,000 (95% credible interval: 31,000 to 108,000) from September 1, 2021 to March 14, 2025 for (b). Ontario Population size: 14.6 million. Right: Each parameter combination on the plane is colour coded according to which of the four strategies prevented the most deaths, on average across all model realizations, for (a) January and (b) September 2021 availability. Other parameter values in Appendix, pp. 1-11. 131
- 27 **Epidemic dynamics and social dynamics for both NPI adherence and vaccinating behaviour, when behaviour is held constant over time.** (a) Ascertained incident COVID-19 cases, (b) proportion x of the population practicing NPIs, (c) Intensity of school and workplace closure, (d) percentage of population with natural or vaccine-derived immunity versus time. $T = 200\%$, $\psi_0 = 0.5\%$ per week, vaccine available in January 2021. Other parameters are in Table 2.1. 132
- 28 Maximum MPB infestation size within 500 year period, under FTP with respect to τ fraction of m juvenile stands cleared. a) ($\alpha_1 = 0.02$, $\alpha_2 = 0.0025$), b) ($\alpha_1 = 0.01$, $\alpha_2 = 0.006$), c) ($\alpha_1 = 0.03$, $\alpha_2 = 0.0012$) 133
- 29 Maximum MPB infestation size within 500 year period, under FTP with respect to τ fraction of m juvenile stands cleared, conducted every five years. a) ($\alpha_1 = 0.02$, $\alpha_2 = 0.0025$), b) ($\alpha_1 = 0.01$, $\alpha_2 = 0.006$), c) ($\alpha_1 = 0.03$, $\alpha_2 = 0.0012$) 133

30	Maximum MPB infestation size within 500 year period, under CBP with respect to τ fraction of m juvenile stands cleared, conducted each year. a) ($\alpha_1 = 0.02$, $\alpha_2 = 0.0025$), b) ($\alpha_1 = 0.01$, $\alpha_2 = 0.006$), c) ($\alpha_1 = 0.03$, $\alpha_2 = 0.0012$.)	134
----	--	-----

List of Tables

2.1	Parameter definitions, values, particle filtering ranges, and sources.	25
3.1	Parameters and default values	45
4.1	Parameters and baseline values of compound fire and pest model. Except for α_i and the noise magnitude, all parameters were obtained from Duncan et al. [67]	67

Chapter 1

Introduction

I am writing this introduction sitting in my living room in Kitchener, Ontario, staring at the dead ash tree which overlooks the empty lots bordering my home. Ash (*Fraxinus sp.*) were a common group of trees planted along city streets in the eastern United States and Canada until the introduction of the emerald ash borer (*Agrilus planipennis*, EAB) to North America in the 1990s [51]. In the past two decades, the emerald ash borer (*Agrilus planipennis*, EAB) has spread throughout the region, killing about 99% of the ash trees in the regions they invade [50, 93]. Once a prominent feature of deciduous woodlands in this area, *Fraxinus* is now limited to rare pockets that have escaped the insect, and seedlings too small to be infested. This narrative is a familiar one. The American chestnut (*Castanea dentata*) was once a major part of the carolinian forests, an important source of lumber and food. It was almost completely wiped out as the chestnut blight (*Cryphonectria parasitica*) spread throughout eastern North America in the 19th and 20th centuries. Infectious agents in this way shape the landscapes we inhabit and the ecosystems we exist within. Of course, infectious agents are not limited to arboreal hosts: I have been in my living room staring at this dead ash tree for the past year, sheltering from the global COVID-19 pandemic.

The various waves of the Black Death, the 1918 influenza pandemic, the HIV/AIDS pandemic, and the current COVID-19 pandemic, have irreversibly shaped our culture. Endemic infectious disease was a massive driving force in the formation of human societies everywhere until very recently. Only in the past century have some parts of the world been able to escape the spectre of endemic diseases such as malaria, polio, influenza, and measles, primarily through the invention of vaccination and understanding of disease spread dynamics. John Snow is considered to be one of the first epidemiologists, for his study of the spatial distribution of London Cholera outbreaks [190, 41], but the tools used in the field have evolved considerably since that time. Compartmental models have been one of

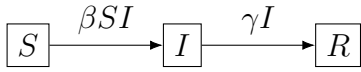


Figure 1.1: Diagram of population flow in an SIR model

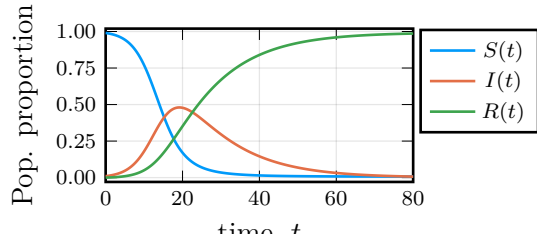


Figure 1.2: An infection represented by an SIR model, with $\beta = 0.4$, $\gamma = 0.08$, $S(0) = 0.99$, and $I(t) = 0.01$.

the main tools used to forecast outcomes and mitigation strategies during recent outbreaks of infectious agents [40]. Due to the ongoing pandemic, the general public is probably more aware than ever before of these models.

Compartmental models for the spread of infectious diseases are usually considered to have been introduced to the field by public health researchers, such as Hamer, Kermack, and McKendrick [89, 113, 41, 71]. This class of models divides the population into homogeneous compartments, and describe the rate of movement between these compartments. The quintessential compartmental model is the SIR model (equations 1.4), so-called for its division of a population into susceptible (the $S(t)$ variable), infected (the $I(t)$ variable), and recovered (the $R(t)$ variable) compartments.

$$\frac{dS}{dt} = -\beta SI \quad (1.1)$$

$$\frac{dI}{dt} = \beta SI - \gamma I \quad (1.2)$$

$$\frac{dR}{dt} = \gamma I \quad (1.3)$$

$$(1.4)$$

The SIR model (Figures 1.1, 1.2) describes a population undergoing an infection that confers complete immunity after one has been infected, under a great number of simplifying assumptions: each compartment is totally homogenous, the probability that an individual recovers is constant per unit time, and the law of mass action. The law of mass action assumes that each individual in the I compartment has a uniform probability β of infecting

any given individual in the S compartment per unit time. It follows that for each I individual, βS people are expected to be infected per unit time, and therefore the total number of infections is expected to be βSI , which is the term removed from the S compartment and added to the I compartment. However, except during office icebreaker games, people do not mix homogeneously, so the assumption of homogeneity is a major drawback. Therefore, a common extension to this model is to add more structure, usually through further subdivision of the compartments [95]. For example, heterogeneity primarily dependent on population age can be represented by a chain of compartments [94]. This idea can be also taken to its continuum limit yielding a system of hyperbolic partial differential equations [15] which describe the evolution of a continuous age distribution. Spatial heterogeneity in host populations can be treated with reaction diffusion equations [172], but it can also be represented by systems of ordinary differential equations connected in a network, sometimes called a metapopulation model [101, 123, 59, 149]. In contrast to a continuum of hosts distributed through space, this network formulation represents homogenously mixed groups that exchange hosts or infections with other homogenous groups. The popularity of this approach is probably due to their ability to easily represent different spatial topologies, and its resemblance to modern population patterns as tight communities of individuals connected by transport [24]. From the initial work on these models, the invention of computers and numerical integration methods have enabled researchers to get useful results from even the most complex elaborations on this theme.

1.1 Sars-CoV-2

It is difficult to overstate the damage and loss of life that the ongoing COVID-19 pandemic has caused or exacerbated in the past year [140, 1]. The first human case of Sars-CoV-2 occurred in late 2019 in central China, almost certainly transmitted from an animal host, very likely a bat [13, 171, 219]. The virus soon spread throughout the world, and was declared a pandemic by the World Health Organization (WHO), on March 11th, 2020 [2]. Prior to the development, manufacture, and distribution of an effective vaccine, non-pharmaceutical interventions (NPIs) were the only option for control of the virus. We can distinguish two types of NPIs, scalable NPIs which require population participation (e.g. face masks, social distancing, hand washing) and those that do not (e.g. surface cleaning, increased ventilation). Compartmental models have been invaluable in modeling the spread of Sars-CoV-2 [196] and assessing the planning and efficacy of NPIs. Anderson et al. [16] use a compartmental model to assess efficacy of provincial lockdown restrictions on infection rates in British Columbia, Canada. They define two SEIR (Susceptible-Infected-

Recovered-Exposed) models, one which corresponds to individuals using NPIs (primarily contact reduction), and another where NPIs are absent. Data from British Columbia, at least when the study was conceived, only contained the number of reported cases for each day, so the authors also include a stochastic model for estimating the delay from the actual case occurrence date to case report date. Fitting these models to the data they show that indeed, physical distancing policy was able to reduce the contact rate of people in British Columbia, more than was necessary to push R below 1. In the months prior to widespread immunization, people around the world endured various levels of NPI policy. Government policy on NPIs has ranged from comprehensive quarantine procedures (in e.g. New Zealand, South Korea, Singapore, Vietnam) to almost nothing at all (e.g. some of the United States, Sweden, Brazil). In the outcomes of the aforementioned countries, empirical research, and modelling studies, NPIs have been shown to be an effective method for the control of COVID-19 [75, 74, 65].

1.2 Imitation dynamics

The demonstrated effectiveness of NPIs implies that the immense morbidity and mortality over the past year is not simply a natural disaster but a humanitarian one. Since our survival depends on our ability to construct a world in which people are incentivized to centre the well-being of others, any attempt to model human outcomes of the pandemic should also attempt to model the incentive structures we operate within. Game theory provides a simple, but effective framework for many of the aforementioned systems [17, 109]. In a game theoretical sense, scalable NPI usage can be viewed as a prisoners dilemma in that everyone either cooperates or defects with the practice of using certain NPIs, and the decision to defect or to cooperate is based on a combination of the perceived payoff to do so, and the influence of the rest of the population [174]. Table 1.3 shows the payoff matrix of this 2-player game. Of course in real life, we are all playing this game, all the time, with everyone.

The simplest way to approximate the time evolution of a such a game is with the one-dimensional replicator equation, which approximates these dynamics in terms of the population average [98]. Specifically, we introduce a variable $x(t)$ which represents the proportion of people adopting a strategy, then the replicator equation 1.5 gives the time-evolution of $x(t)$ in terms of the payoff for cooperating over defecting, $p(x, t)$. We see immediately that this equation, disregarding $p(x, t) = 0$, has two steady states: $x = 1$ and $x = 0$. Given $p(x, t)$ constant, the population will approach whichever point it is initially closer to.

P1 \ P2	use NPI	don't use NPI
use NPI	low risk, NPIs unpleasant	med risk
don't use NPI	med risk, NPIs unpleasant	high risk
med risk	high risk	

Figure 1.3: NPI adoption as a two-player game (between P1 and P2).

$$\frac{dx}{dt} = \sigma x(1-x)p(x, t) \quad (1.5)$$

This formulation has been also used to model vaccination sentiment in a variety of scenarios [152, 29, 27, 28]. In this context, “cooperation” refers to the strategy of getting a widely-available vaccine, and the cooperation payoff function is usually of the form in equation 1.6. The population is assumed to have a constant payoff to avoid vaccination (in many cases, just due to inconvenience) and a payoff to vaccinate proportional to I , the prevalence of infection in the model.

$$p(x, t) = -c + \rho I \quad (1.6)$$

A prisoner’s dilemma formulation and model based upon equation 1.5 coupled to an application-specific model (in the above case, disease dynamics), can also be applied to human-environment models in ecology. In particular, it has been used to model conservation responses coupled to ecosystem dynamics in contexts such as forest-grassland mosaics [102, 92], global climate [47], coral reefs [195], agricultural land use [83]. I will focus on the application of imitation dynamics to forest pest transport, and the use of NPIs in the context of the COVID-19 pandemic.

1.3 Forest pests in eastern North America

The term “forest pests” covers a broad range of infectious agents that are responsible for forest tree damage and mortality. Major invading forest pests in eastern North America include: the Asian longhorned beetle (*Anoplophora glabripennis*), the butternut canker (*Ophiognomonia clavigignenti-juglandacearum*), *Lymantria dispar dispar*, dutch elm disease *Ophiostoma ulmi*, and the aforementioned EAB (Figure 1.4). Together, these non-native pests kill 5.53 teragrams of carbon worth of trees each year, on an order of magnitude comparable to forest fires in North America [73]. Non-native insect invaders are usually introduced by accident. The majority of recently introduced species are a result of careless global trade, with new individuals arriving in lumber, live plants, or similar goods [42]. Models for the spread of these insects are often inspired by models for infectious diseases in humans. Research in mathematical ecology generally uses the related Lotka-Volterra model for host-parasitoid dynamics [71], but SIR models can be a natural choice because they focus on the time-evolution of the host populations, which is often the more useful quantity [71].

Barlow et al. [25] couple a compartmental model of an invading forest pest to human travel patterns. Humans have been shown to be a common vector for forest pests [45, 115, 213], so our effect on the long-distance spread of forest pests is important to understand. They assume that forests occur as homogenously mixed patches, each with its own compartmental dynamics. Transport between each patch is assumed to be proportional to local sentiment towards firewood transport. Their model for human travel behavior uses imitation dynamics, where the payoff for travel is a function of the price of firewood and the perceived level of pest infestation in a patch. Barlow et al. show that, at least with a small number of patches, lowering the cost of firewood is generally effective at reducing equilibrium infestation. Education on the risk of firewood transport, corresponding to an increase the level of concern for infestation levels in a local patch, can also be effective in their model. They find that a drawback of education as a tactic is that resilience to pest reintroduction is low, because transport behavior returns to normal after pests populations have dropped. In chapter 3 we extend their model to a realistic transport network, and include pest mitigation strategies that explicitly use the spatial heterogeneity in the model.



Figure 1.4: An EAB on a penny [176]



Figure 1.5: MPB-killed lodgepole pines in Manning Park, British Columbia, Canada [212]

1.4 Mountain pine beetle (MPB) and fire-driven forest ecosystems of the Western Cordillera

The coniferous forests of the western cordillera of North America are the subject of the model presented in chapter 4. The Canadian section of these forests are primarily composed of a mixture of *Pinus* sp., namely lodgepole pine (*Pinus Contorta*), but also ponderosa pine (*Pinus ponderosa*) [43]. The fire regimes in these forests are generally characterized by frequent, low to mixed severity fires depending on elevation and climactic conditions [3, 19]. In these regions, there are also a few other dominant forest types: those dominated by Douglas Fir (*Pseudotsuga menziesii*), and those dominated by subalpine spruce (*Abies lasiocarpa*). These other forest types become dominant in areas which experience wetter or cooler climates, as they are less drought tolerant, and also less fire resistant [107]. Therefore, the lodgepole pine forests are dependent on a frequent fire regime to maintain climax lodgepole forests. They are very rapidly growing when young, possess (usually) serotinous cones, and maintain massive seed banks in the soil to rapidly colonize the area after disturbances [130, 131].

Besides wildfire, MPB (*Dendroctonus ponderosae*) is the most significant disturbance in these forest types. Endemic to this ecosystem, MPB most commonly attacks lodgepole pine in Canada [179] (Figure 1.5), but it can attack and reproduce within all of the pine

species in North America, and during outbreaks has been recorded to attack spruce and fir trees within its range [79]. MPB, and bark beetles more generally, exhibit highly cyclic lifestyles. For most of the year, they exist in the phloem of the tree first as eggs, then as larvae, until they are mature enough to emerge and fly to new hosts. The emergence of MPB occurs in late summer, although it is heavily dependent on the climate that year [32]. While their flight capability is limited, MPB can use air currents to colonize trees over 20km away from their place of birth [186]. When individuals find a suitable host, they release pheromones that attract other flying beetles and triggering a mass attack behaviour. This behaviour functions to overwhelm the defenses of the host tree. A successful attack results in the MPB laying their eggs in the phloem of the new host tree, and the cycle repeats. Older trees with thicker phloem are most susceptible to MPB attack, and they are generally the first to be colonized, with MPB attacking progressively less suitable hosts as population densities rise [179]. Endemic periods of low MPB density give rise to outbreaks based on a variety of factors, such as density of good hosts, climate, and possibly wildfire damage [179]. Although MPB has always exhibited outbreak cycles, in the past two decades, outbreak sizes have exceeded historically recorded levels probably due to increases in winter temperatures and higher densities of mature trees [33, 179]. Recently, jack pine *Pinus banksiana* stands in northern Alberta, and the Northwest Territories, have been attacked by MPB as they expand their range north and eastward [64, 51]. Understanding the holistic dynamics of these ecosystems, and the role that MPB takes within them, will be key to understanding the causes and effects of these unprecedented population levels.

An early model of bark beetle (a larger group to which MPB belongs) dynamics is that of Berryman et al. [34]. Their model is not a compartmental one, rather they explicitly represent tree (host) and MPB (pathogen) populations. It is assumed that trees $T(t)$ exhibit logistic growth up to a constant carrying capacity, and die according to a function $g(T(t), B(t))$ where $B(t)$ is the population of bark beetles at time t . Bark beetles also exhibit logistic growth, but their carrying capacity is proportional to $g(T, B)$. The crux of this model is the shape of the function g . This function exhibits a threshold in T that decreases as the beetle population B increases, describing the ability for outbreak bark beetle populations to more easily overcome defenses of vigorous trees. They conclude from this model that thinning forest stands is useful to maintain resilience to bark beetle outbreaks. Their approach is reflected in a more recent model by Lewis et al [124], which extends the idea to an integral project model that explicitly represents the vigor distribution of the stand, and its effect on beetle reproduction.

Mechanistic population models are widespread in bark beetle dynamics, but most wildfire modelling has a distinctly different flavour. In the past few decades, the field has largely converged to physics based models which explicitly represent combustion chemistry, forest

geography, and atmospheric fluid dynamics [127, 139, 23]. This comes from a need to produce detailed forecasts on the precise extent, severity, and velocity of wildfires, often in real time. There are some examples of compartmental-style models explicitly modeling wildfires [53], but when they are coupled to forest pests often fire is modeling implicitly [57].

1.5 Thesis Outline

In the first chapter, an age-structured impulsive differential equation model of COVID-19 is coupled to the aforementioned imitation dynamics for physical distancing. It is parameterized with case data from Ontario, Canada and population location data from Google. Two primary categories of vaccination strategy were considered in this model: vaccination of the most vulnerable populations (older age groups), or vaccination of the most transmitting populations (according to contact distribution estimates). We analyze how the timing, supply rate, and shutdown policies will affect the best vaccination policy through numerical simulation of the model.

The second chapter extends the forest pest and firewood transport model of Barlow et al. [25] to a large empirically derived network of human movement patterns between susceptible forest patches. Numerical analysis of this model is done to compare the effectiveness of three major policy categories in reducing the spread of invasive pests throughout forested areas in Eastern Canada. We consider direct interception of human-mediated transport of forest pests, changing behavioural incentives to transport firewood, and quarantine of the most central areas, and combinations thereof. These strategies are assessed with respect to total tree infections over periods of 5, 10, and 20 years.

The third chapter extends an age-structured, discrete time model of mountain pine beetle population [67] to include a simplified model of yearly burn sizes. The effect of changing fire disturbance regimes on the forest stand structure is explored through numerical simulations of the parameter space. Since MPB outbreak patterns seem to strongly depend on the density of mature trees, they are therefore sensitive to stand structure, in particular the creation of large-even aged stands created by severe forest fires. We discuss the dynamical regimes of this system, and argue that outbreak dynamics can be significantly influenced by heterogeneity in stand structure. The final chapter will summarize and contextualize these results, discuss their limitations, and outline opportunities for future work.

Each chapter studies a compartmental model of a contagious process in a human-environment system, where the host population is given structure in either age or space.

We compare various mitigation strategies such vaccine prioritization for Sars-CoV-2, and forest stand thinning in our MPB-wildfire model. Counterfactuals are used to determine the most effective mitigation strategies for each system. The three chapters are followed by a synthesis and summary of the results from each chapter, discussion of their limitations, and opportunities for future work.

Chapter 2

Prioritising COVID-19 vaccination in changing social and epidemiological landscapes: a mathematical modelling study

During the COVID-19 pandemic, authorities must decide which groups to prioritise for vaccination in a shifting social–epidemiological landscape in which the success of large-scale non-pharmaceutical interventions requires broad social acceptance. We aimed to compare projected COVID-19 mortality under four different strategies for the prioritisation of SARS-CoV-2 vaccines. We developed a coupled social–epidemiological model of SARS-CoV-2 transmission in which social and epidemiological dynamics interact with one another. We modelled how population adherence to non-pharmaceutical interventions responds to case incidence. In the model, schools and workplaces are also closed and reopened on the basis of reported cases. The model was parameterised with data on COVID-19 cases and mortality, SARS-CoV-2 seroprevalence, population mobility, and demography from Ontario, Canada (population 14.5 million). Disease progression parameters came from the SARS-CoV-2 epidemiological literature. We assumed a vaccine with 75% efficacy against disease and transmissibility. We compared vaccinating those aged 60 years and older first (oldest-first strategy), vaccinating those younger than 20 years first (youngest-first strategy), vaccinating uniformly by age (uniform strategy), and a novel

This chapter is based on the paper: Jentsch, Peter C., Madhur Anand, and Chris T. Bauch. "Prioritising COVID-19 vaccination in changing social and epidemiological landscapes: a mathematical modelling study." *The Lancet Infectious Diseases* (2021).

contact-based strategy. The latter three strategies interrupt transmission, whereas the first targets a vulnerable group to reduce disease. Vaccination rates ranged from 0.5% to 5% of the population per week, beginning on either Jan 1 or Sept 1, 2021. Case notifications, non-pharmaceutical intervention adherence, and lockdown undergo successive waves that interact with the timing of the vaccine programme to determine the relative effectiveness of the four strategies. Transmission-interrupting strategies become relatively more effective with time as herd immunity builds. The model predicts that, in the absence of vaccination, 72000 deaths (95% credible interval 40000–122000) would occur in Ontario from Jan 1, 2021, to March 14, 2025, and at a vaccination rate of 1.5% of the population per week, the oldest-first strategy would reduce COVID-19 mortality by 90.8% on average (followed by 89.5% in the uniform, 88.9% in the contact-based, and 88.2% in the youngest-first strategies). 60000 deaths (31000–108000) would occur from Sept 1, 2021, to March 14, 2025, in the absence of vaccination, and the contact-based strategy would reduce COVID-19 mortality by 92.6% on average (followed by 92.1% in the uniform, 91.0% in the oldest-first, and 88.3% in the youngest-first strategies) at a vaccination rate of 1.5% of the population per week. Interpretation The most effective vaccination strategy for reducing mortality due to COVID-19 depends on the time course of the pandemic in the population. For later vaccination start dates, use of SARS-CoV-2 vaccines to interrupt transmission might prevent more deaths than prioritising vulnerable age groups.

2.1 Introduction

The COVID-19 pandemic has imposed a massive global health burden as waves of infection to move through populations around the world [140]. Both empirical analyses and mathematical models conclude that non-pharmaceutical interventions (NPIs) are effective in reducing COVID-19 case incidence [16, 156, 201]. However, pharmaceutical interventions are highly desirable given the socio-economic costs of lockdown and physical distancing. Hence, dozens of vaccines are in development [133], and model-based analyses are exploring the question of which groups should get the COVID-19 vaccine first [44, 46].

When vaccines become available, we will face a very different epidemiological landscape from the early pandemic. Many populations will already have experienced one or more waves of COVID-19. As a result of natural immunity, the effective reproduction number R_{eff} (the average number of secondary infections produced per infected person) will be reduced from its original value of approximately $R_0 = 2.2$ in the absence of pre-existing immunity [96]. Epidemiological theory tells us that as R (or R_0) decline toward 1, the indirect benefits of transmission-blocking vaccines become stronger. For instance, if $R_{eff} \approx$

1.5, such as for seasonal influenza, only an estimated 33% percent of the population needs immunity for transmission to die out in a homogeneously mixing population [14, 68]. This effect was evidenced by the strong suppression of influenza incidence in Australia in Spring 2020 due to NPIs targeted against COVID-19 [20].

This effect has stimulated a literature comparing the vaccination of groups that are responsible for most transmission to vaccination of groups that are vulnerable to serious complications from the infection. Natural immunity to SARS-CoV-2 will likely continue to rise in many populations on account of further infection waves. Given these likely changes to the epidemiological landscape before the vaccine becomes available, we suggest this question is worthy of investigation in the context of COVID-19.

The social landscape will also look very different when vaccines become available and this aspect is crucial to understanding the pandemic. Scalable non-pharmaceutical interventions (NPIs) like physical distancing, hand-washing and masks are often one of the few available interventions when a novel pathogen emerges. Flattening the COVID-19 epidemic curve was possible due to a sufficient response by populations willing to adhere to public health recommendations. Therefore, pandemic waves are not simply imposed on populations – they are a creation of the population response to the pathogen. They exemplify coupled socio-epidemiological systems exhibiting two-way feedback between disease dynamics and behavioural dynamics interact with one another [157].

Approaches to modelling coupled social-epidemiological dynamics vary[174, 181, 77, 206, 78]. Some models have used evolutionary game theory to model this two-way feedback in a variety of coupled human-environment systems [157, 27, 102, 47, 10, 218, 6]. Evolutionary game theory captures how individuals learn social behaviours from others while weighing risks and benefits of different choices. In this framework, individuals who do not adopt NPIs can “free-ride” on the benefits of reduced transmission generated by individuals who do adopt NPIs [174].

Here, our objective is to compare projected COVID-19 mortality under four strategies for the prioritisation of COVID-19 vaccines: older individuals first, children first, uniform allocation, and a novel strategy based on the contact structure of the population. We use an age-structured model of SARS-CoV-2 transmission, including evolutionary game theory to model population adherence to NPIs and changes to mobility patterns. We use scenario and sensitivity analysis to identify how strategy effectiveness responds to possible changes in the social-epidemiological landscape that may occur before and after vaccines become available.

2.2 Model Overview

2.2.1 Structure and parameterisation

We developed an age-structured SEPAIR model (Susceptible, Exposed, Presymptomatic, Asymptomatic, Symptomatic, Removed) with ages in 5-year increments. Upon infection, individuals enter a latent period where they are infected but not yet infectious (“Exposed”). After the latent period, individuals become presymptomatically infectious, and then either symptomatically or asymptomatically infectious, before finally entering the Removed compartment when their infectiousness ends. We did not model testing or contact tracing explicitly, although we assume infected individuals are ascertained at some rate. Transmission occurs through an age-specific contact matrix, susceptibility to infection is age-specific, and we include seasonality due to changes in the contact patterns throughout the year. To infer model parameters, we fitted the model to Ontario COVID-19 case notifications stratified by age and time, Ontario seroprevalence data, and Ontario mobility data. Use of seroprevalence data ensured that our estimates of transmission were not biased by case under-reporting. Remaining model parameter values were fixed using Ontario demographic and mortality data, and literature on COVID-19 serial interval and incubation periods. The system of differential equations comprising our model is solved numerically with `DifferentialEquations.jl` in the Julia language [169].

Both schools and workplaces are closed when the number of ascertained active cases surpasses 50%, 100%, 150%, 200%, or 250% of the peak ascertained active cases that occurred during the first wave (the “shutdown threshold”, T), and are re-opened again when cases fall below that threshold. Individuals interact with other individuals at a specified rate and switch between adherence and non-adherence to NPIs, including mobility restrictions, by comparing the cost of practicing NPIs against the cost of not practicing NPIs and thereby being subject to an increased risk of infection according to the prevalence of ascertained cases. Both school and workplace closure and population level of adherence to NPIs reduce transmission according to a specified efficacy.

2.2.2 Model Equations

Transmission dynamics are given by an SEPAIR model, modified to take population adherence to NPIs and school/workplace closure into account, and divided into age classes $i \in [1, 16]$, where each age class contains a 5 year cohort, except for the oldest age group which comprises the ages 75 and over. The model equations are:

$$\frac{dS_i^1}{dt} = S_i^1 \left(-r\rho_i \xi(t) \sum_{j=1}^{16} C_{ij}(t) \left(\frac{I_{s_j} + I_{a_j} + P_j}{N_j} \right) - \tau \right) \quad (2.1)$$

$$\frac{dS_i^2}{dt} = S_i^2 \left(-r\rho_i \xi(t) \sum_{j=1}^{16} C_{ij}(t) \left(\frac{I_{s_j} + I_{a_j} + P_j}{N_j} \right) - \tau \right) \quad (2.2)$$

$$\frac{dE_i}{dt} = (S_i^1 + S_i^2) \left(r_i \xi(t) \sum_{j=1}^{16} C_{ij}(t) \left(\frac{I_{s_j} + I_{a_j} + P_j}{N_j} \right) - \sigma_0 E_i + \tau \right) \quad (2.3)$$

$$\frac{dP_i}{dt} = \sigma_0 E_i - \sigma_1 P_i \quad (2.4)$$

$$\frac{dI_{a_i}}{dt} = \eta \sigma_1 E_i - \gamma_a I_{a_i} \quad (2.5)$$

$$\frac{dI_{s_i}}{dt} = (1 - \eta) \sigma_1 E_i - \gamma_s I_{s_i} \quad (2.6)$$

$$\frac{dR_i}{dt} = \gamma_a I_{a_i} + \gamma_s I_{s_i} \quad (2.7)$$

$$\frac{dD_i}{dt} = \Omega(D(t)) \quad (2.8)$$

where $\xi(t) = [1 + s \sin(\frac{2\pi}{365}(t - \phi) - \frac{\pi}{2})]$ determines the seasonally varying transmission rate with phase ϕ and amplitude s .

Parameter values are defined in Table 2.1. The vaccination dynamics are an impulsive process applied each day, described below. S_i^1 is the number of unvaccinated susceptible individuals in age group i , and S_i^2 is the number of susceptible individuals in age group i who have received a standard two dose course of vaccination but were not immunized. $E_i(t)$ is the number of exposed but not yet infectious individuals in age group i (i.e., individuals in the latent period). $I_{a_i}(t)$ is the number of asymptomatic infectious individuals in age group i and $I_{s_i}(t)$ is the number of symptomatic infectious individuals in age group i . $R_i(t)$ is the number of Removed (recovered, vaccinated, and deceased) individuals in compartment i .

The variable $D(t) \in [0, 1]$ in the model equation $dD(t)/dt = \Omega(D(t))$ represents the public health authority's reaction to the prevalence of ascertained cases and it evolves according to:

$$\Omega(D(t)) = \begin{cases} k_1(1 - D(t)) & \sum_{i=1}^{16} \alpha_i(I_{a_i} + I_{s_i}) > T \\ -k_2 D(t) & \sum_{i=1}^{16} \alpha_i(I_{a_i} + I_{s_i}) \leq T \end{cases} \quad (2.9)$$

This represents closure being triggered when ascertained cases exceed a threshold T , and being lifted when cases drop below that threshold again.

The proportion x of individuals who practice NPIs such as mask wearing, handwashing, and physical distancing, starts off at $x(0) = 0.01$ and evolves as:

$$\frac{dx}{dt} = \kappa x(1-x) \left(\frac{\sum_{i=1}^{16} \alpha_i(I_{a_i} + I_{s_i})}{\sum_{i=1}^{16} N_i} - cx \right) + p_{ul}(1-2x) \quad (2.10)$$

where κ is the social learning rate, c is the incentive to not practice NPIs, and α_i is the fraction of total cases ($I_a + I_s$) that are reported, also known as the ascertainment rate. The p_{ul} term is a phenomenological term that represents the effects of social heterogeneity and influence from external populations that prevents the system from remaining arbitrarily close to $x = 0$ or $x = 1$ for unrealistic periods of time. These equations describe a population where individual sample other individuals at some time rate and switch between adherence and non-adherence to NPIs with a probability proportional to the expected gain in utility $\sum_{i=1}^{16} \alpha_i(I_{a_i} + I_{s_i}) - cx$. We refer the reader to existing literature for details on the derivation of this equation [27, 102, 195, 28, 152].

$C_{ij}(t, x)$ is the average number of contacts per day and consists of contacts at workplaces, schools, households, and other locations, which vary depending on government shutdown policies as well as individual adherence to NPIs like physical distancing and mask use:

$$C_{ij}(t, x) = C_{ij}^W(t) + C_{ij}^S(t) + (1 - \epsilon_P x)(\bar{C}_{ij}^O + \bar{C}_{ij}^H) \quad (2.11)$$

The contacts in each of the aforementioned places can vary as follows. At workplaces, which can be closed by public health authorities:

$$C_{ij}^W(t) = \begin{cases} (1 - \epsilon_W)\bar{C}_{ij}^W & t - t_{delay} > t_{close}, t - t_{delay} < t_{open}^w \\ \bar{C}_{ij}^W & t - t_{delay} < t_{close}^w \\ (1 - D(t)(1 - \epsilon_W))\bar{C}_{ij}^W & t - t_{delay} > t_{open}^w \end{cases} \quad (2.12)$$

where \bar{C}_{ij}^W is the normal (non-pandemic) number of contact-hours per day between individuals of age i and j at the workplace [217]; $\bar{C}_{ij}^W(1 - D(t)\epsilon_P)$ is the reduced rate under workplace closure efficacy $0 < \epsilon_W < 1$ and closure level $D(t)$; and t_{delay} represents the delay between the decision to adopt NPIs and their impact on transmission [125]. Lower than perfect efficacy may stem either from occasional use of workplace for critical needs

or non-authorized access, workplaces that remain open because they provide essential services, etc. t_{close}^W and t_{open}^W are the times of closing and re-opening workplaces, respectively. Similarly, for schools we have:

$$C_{ij}^S(t) = \begin{cases} 0 & t - t_{delay} > t_{close}^s, t - t_{delay} < t_{open}^s \\ \bar{C}_{ij}^S & t - t_{delay} < t_{close}^s \\ (1 - D(t))\bar{C}_{ij}^S & t - t_{delay} > t_{open}^s \end{cases} \quad (2.13)$$

All other places of exposure are governed by social processes with imperfect ability of public health authorities to enforce mandates, and hence are governed by voluntary population adherence to NPIs such as mask use and physical distancing as per the $\epsilon_P x(t)$ term in the equation, where ϵ_P is efficacy of individual adoption of NPIs. In principle, contact hours spent at home should increase as workplaces and schools are closed, but we assume that infection probabilities will saturate rapidly with contact hours in the home. Each of the conditional functions in equations (2.12,2.13), are represented in the model as a smoothed step function with a steep slope, and we restrict them between 0 and 1 if the smoothing process would cause the closure level $D(t)$ to exceed 1.0. Finally, our interventions (school and workplace shutdown) do not distinguish between preventing contacts in “home” versus “other” locations. We assume the same efficacy of NPIs in home as in “other” locations. On one hand, individuals are less likely to use NPIs at home. On the other hand, contacts at home are repeated and thus there is a saturating effect that can somewhat reduce the infection risk, compared to the diversity of contacts experienced in the general community. Additionally, our case notifications are not broken down by the location of infection and thus we have limited ability to parameterize two difference NPI efficacy in home and “other” locations. As a result, we assume the same efficacy in both settings.

2.2.3 Vaccination process

Each day, the total number of individuals vaccinated is equal to $\sum_{i=1}^{16} \phi \frac{S_i(t)}{N_i}$, and the number of individuals immunized against transmission of the virus is $\sum_{i=1}^{16} v_{T_i} \frac{S_i(t)}{N_i - V_i}$ on account of imperfect vaccination. The factor $\frac{S_i(t)}{N_i - V_i}$ represents vaccination of each person with equal probability, so the probability of vaccinating a susceptible person decreases with the fraction of susceptible individuals out of the non-vaccinated people. If there are less than ϕ_i individuals in group S_i^1 , then the remainder of the vaccine is spread evenly among the remaining non-vaccinated groups. Individuals who are vaccinated but not immunized due to imperfect efficacy are moved to the corresponding S_i^2 . We assume that a course of vaccination will not be administered to a person more than twice.

The fraction of people who are vaccinated against disease but not against transmissibility is $v_{D_i} - v_{T_i}$. We assume this fraction of people is still able to transmit the disease normally, and therefore we account for them by reducing the mortality rate (see Supp. Mortality computation).

2.2.4 Differences between parameters in the first and second wave

To account for the differences in social response, to the first and second waves of the infection, we assume that the social dynamics variables κ (the social learning rate), and c (the incentive not to distance). We assume that these variables are functions of time, which transition between two values at a time $t_{switch} = 160$ days after the beginning of the pandemic.

$$\kappa = \kappa(t) = \kappa_2 \left(\frac{\tanh(k_s(t - t_{switch})) + 1}{2} \right) + \kappa_1 \left(1 - \frac{\tanh(k_s(t - t_{switch})) + 1}{2} \right) \quad (2.14)$$

$$c = c(t) = c_2 \left(\frac{\tanh(k_s(t - t_{switch})) + 1}{2} \right) + c_1 \left(1 - \frac{\tanh(k_s(t - t_{switch})) + 1}{2} \right) \quad (2.15)$$

We chose the rate of switch, $k_s = 0.05$ to take 2 - 4 weeks.

2.2.5 Case under-ascertainment

Case under-ascertainment of the i th age group is represented by the following function:

$$\alpha_i(t) = \begin{cases} \alpha_{i,2} & t > t_{switch} \\ \alpha_{i,1} \left(\frac{t_{switch}-t}{t_{switch}} \right) & t \leq t_{switch} \end{cases} \quad (2.16)$$

where where $\alpha_{1,1}, \alpha_{2,1}, \alpha_{3,1}$ corresponds to the ascertainment in the age groups $(0, 20), (20, 60), > 60$ at $t = 0$, respectively. We assume that the ascertainment rises to a value of $\alpha_{1,2}, \alpha_{2,2}, \alpha_{3,2}$ in the age groups $(0, 20), (20, 60), > 60$ respectively, at $t = t_{switch}$, denoting the increase in ascertainment throughout the first wave and into the second wave. We multiply the infections in each age group i at time t by the corresponding $\alpha_i(t)$ after the simulation is finished.

2.2.6 Baseline transmission rate

We can compute r as a function of the next-generation matrix, $M = -\Theta\Sigma^{-1}$ [66], where Θ and Σ are defined as in equations 2.17, 2.18, and so M is a function of $R_0, \sigma_0, \sigma_1, \gamma_a, \gamma_s, \eta, C(t)$, and N . These matrices come from the rate at which infected individuals enter and leave the infection compartments when the system is linearized about the $I_a = 0, I_s = 0, P = 0$ equilibrium. The basic reproduction ratio, R_0 , of the infection is the spectral radius of M , written $\rho(M)$. We can pull r out of this expression and write r in terms of the other parameters: $r = \frac{R_0}{\rho(M)}$.

$$\Theta = \begin{bmatrix} 0 & \dots & 0 & \frac{rC_{1,1}(0)N_1}{N_1} & \dots & \frac{rC_{1,n}(0)N_1}{N_n} & \frac{rC_{1,1}(0)N_1}{N_1} & \dots & \frac{rC_{1,n}(0)N_1}{N_n} & \frac{rC_{1,1}(0)N_1}{N_1} \\ \dots & \frac{rC_{1,n}(0)N_1}{N_n} & & & & & & & & & \\ \vdots & \ddots & \vdots & \vdots & \vdots & \ddots & \vdots & \ddots & \vdots & \vdots & \vdots \\ \ddots & \vdots & & & & & & & & & \\ 0 & \dots & 0 & \frac{rC_{1,n}(0)N_n}{N_1} & \dots & \frac{rC_{n,n}(0)N_n}{N_n} & \frac{rC_{1,n}(0)N_n}{N_1} & \dots & \frac{rC_{n,n}(0)N_n}{N_n} & \frac{rC_{1,n}(0)N_n}{N_1} \\ \dots & \frac{rC_{n,n}(0)N_n}{N_n} & & & & & & & & & \\ 0 & \dots & 0 & 0 & 0 & \dots & 0 & 0 & \dots & 0 & 0 \\ \dots & 0 & & & & & & & & & \\ \vdots & \ddots & \vdots & \vdots & \ddots & \vdots & \vdots & \ddots & \vdots & \vdots & \vdots \\ \ddots & \vdots & & & & & & & & & \\ 0 & \dots & 0 & 0 & 0 & \dots & 0 & 0 & \dots & 0 & 0 \\ \dots & 0 & & & & & & & & & \\ 0 & \dots & 0 & 0 & 0 & \dots & 0 & 0 & \dots & 0 & 0 \\ \dots & 0 & & & & & & & & & \\ \vdots & \ddots & \vdots & \vdots & \ddots & \vdots & \vdots & \ddots & \vdots & \vdots & \vdots \\ \ddots & \vdots & & & & & & & & & \\ 0 & \dots & 0 & 0 & 0 & \dots & 0 & 0 & \dots & 0 & 0 \\ \dots & 0 & & & & & & & & & \end{bmatrix} \quad (2.17)$$

$$\Sigma = \begin{bmatrix} -\sigma_0 & \dots & 0 & 0 & \dots & 0 & 0 & \dots & 0 & 0 \\ \dots & 0 & & & & & & & & \\ \vdots & -\sigma_0 & \vdots & \vdots & \ddots & \vdots & \vdots & 0 & \vdots & \vdots \\ 0 & \vdots & & & & & & & & \\ 0 & \dots & -\sigma_0 & 0 & \dots & 0.0 & 0 & \dots & 0 & 0 \\ \dots & 0 & & & & & & & & \\ 0 & \dots & 0 & -\sigma_1 & \dots & 0 & 0 & \dots & 0 & 0 \\ \dots & 0 & & & & & & & & \\ \vdots & \ddots & \vdots & \vdots & -\sigma_1 & \vdots & \vdots & \ddots & \vdots & \vdots \\ \ddots & \vdots & & & & & & & & \\ 0 & \dots & 0 & 0 & \dots & -\sigma_1 & 0 & \dots & 0 & 0 \\ \dots & 0 & & & & & & & & \\ 0 & \dots & 0 & \eta\sigma_1 & \dots & 0 & -\gamma_a & \dots & 0 & 0 \\ \dots & 0 & & & & & & & & \\ \vdots & \ddots & \vdots & \vdots & \eta\sigma_1 & \vdots & \vdots & -\gamma_a & \vdots & \vdots \\ \ddots & \vdots & & & & & & & & \\ 0 & \dots & 0 & 0 & \dots & \eta\sigma_1 & 0 & \dots & -\gamma_a & 0 \\ \dots & 0 & & & & & & & & \\ 0 & \dots & 0 & (1-\eta)\sigma_1 & \dots & 0 & 0 & \dots & 0 & -\gamma_s \\ \dots & 0 & & & & & & & & \\ \vdots & \ddots & \vdots & \vdots & (1-\eta)\sigma_1 & \vdots & \vdots & \ddots & \vdots & \vdots \\ -\gamma_s & \vdots & & & & & & & & \\ 0 & \dots & 0 & 0 & \dots & (1-\eta)\sigma_1 & 0 & \dots & 0 & 0 \\ \dots & -\gamma_s & & & & & & & & \end{bmatrix} \quad (2.18)$$

2.2.7 Disease progression parameters

Transition rates for the duration of the asymptomatic infectious period and the proportion of symptomatic cases were obtained from COVID-19 epidemiological literature [147, 120, 197]. We computed the mortality due to COVID-19 by applying the case fatality rate obtained from [150], interpolated to 16 age groups.

2.2.8 Initial conditions

The point $t = 0$ was chosen to be the day at which the province of Ontario recorded more than 50 cases, March 10th 2020, to reduce the effects of stochasticity in the early case

counts. Let the number of observed cases of COVID-19 in age group i on March 10th 2020 be ω_i . We use the age distribution of ω_i to determine the age distribution for $I_a(t) + I_s(t)$. The true number of cases that day is ω_i/α_i , where α_i is the ascertainment rate of cases in group i . Since we do not know the actual number of active cases, $I_{a_i}(t) + I_{s_i}(t)$ at $t = 0$, we assume the number of active cases is equal to the true number of incident cases multiplied by a constant I_0 , which is also treated as a model variable to be fitted. Therefore, $I_{s_i}(0) = \eta I_0 \frac{\omega_i}{\alpha_i}$ and $I_{a_i}(0) = (1 - \eta) I_0 \frac{\omega_i}{\alpha_i}$. Similarly, we assumed that the numbers of presymptomatic and exposed cases at $t = 0$ are proportional to the number of ascertained incident cases in each age group, ω_i . We fit the variables P_0 and E_0 so that $P(0) = P_0 \frac{\omega_i}{\alpha_i}$ and $E(0) = E_0 \frac{\omega_i}{\alpha_i}$. We assumed that $S_i^1(0) = N_i - (I_a(0) + I_s(0) + E(0) + P(0))$, so the total number of susceptible, unvaccinated individuals $\sum_{i=1}^{16} S_i^1(0)$ is the population of the region (minus the number who begin in the infected compartments), and $S_i^2(0) = 0$, $E_i(0) = 0$, $R_i(0) = 0$ for all i . Lastly, we assumed that at $t = 0$, only 1% of individuals are physical distancing, so $x(0) = 0.01$, and that $D(0) = 0$.

2.2.9 Particle filtering

We calibrated the model with data from Ontario, Canada. Since the workplace closure opening and closing rates, k_1 and k_2 , are not coupled with the model, we fit a step function of the form

$$f(t) = \epsilon_W (\tanh k_1(t - t_{close}^W) - \tanh k_2(t - t_{close}^W))$$

to the "workplaces_percent_change_from_baseline" field of the Google mobility data [84] for the province. We applied a particle filtering approach using intervals around selected parameters. Intervals used for sampling appear in Table 2.1. We fit the 7-day moving average of incident cases on each day across all age groups to the number of cases registered by Public Health Ontario on that day [200], and also the total number of cases at the end of the fitting window for each age group. The decrease in contact-hours due to social distancing, $x(t)$, was fit to the decrease in the "Retail and Recreation" hours recorded by Google mobility [84]. The 1.1% (0.8%, 1.3%) of Ontario residents seropositive for COVID-19 in June 2021 was also used as a fitting criterion [168]. The posterior distribution of the parameters was estimated with the approximate Bayesian computation scheme described in [203], with uniform priors and 200 particles, using the KissABC [9] library for the Julia language. The acceptance threshold was chosen to given acceptable variation and evaluation time.

2.2.10 Vaccination refusal dynamics

In an extension to the model explored the dynamics of the model with the added complication of vaccine refusal. We introduce a variable $y(t)$ to represent that fraction of the population willing to be vaccinated for the virus, governed by imitation dynamics similar to the social distancing equation 2.10. We add the following equation 2.19 to the rest of the model equations [27, 28].

$$\frac{dy}{dt} = \kappa_{vac}y(1 - y) \left(\frac{\sum_{i=1}^{16} \alpha_i(I_{a_i} + I_{s_i})}{\sum_{i=1}^{16} N_i} - c_{vac} \right) \quad (2.19)$$

In the above equation, the vaccination decisions of the population are governed by a payoff function, where c_{vac} is the payoff not to vaccinate, and the payoff to vaccinate is proportional to current the number of ascertained active infections. The initial condition for this variable, y_0 is assumed to be 0.67 from [135].

The population in age group i that refuses to be vaccinated is $N_i(1 - y(t))$. We implement this mechanic in the model by assuming that the number of people vaccinated each day in age group i , ψ_i is unchanged, except that the compartment $S_{v_i}^1$ is considered to be empty when $N_i(1 - y(t))$ people remain.

2.2.11 Model extension for vaccine efficacy against disease only

We conducted the sensitivity analysis scenario distinguishing vaccine efficacy against disease only versus vaccine efficacy against both infectivity and disease by adjusting the case fatality rates according to vaccine coverage in the population and assumed efficacies. The adjustment factor is determined by the relative sizes of $S_1(t)$ and $S_2(t)$. Let $\xi_1(S_1(t)) = \xi S_1(t)$ be the rate at which individuals in $S_1(t)$ are infected, and similarly $\xi_2 = \xi S_2(t)$ the rate at which individuals in $S_2(t)$ are infected. Let $S_3(t)$ be the number of people at t who are immunized but still able to transmit the virus, and $\xi_3 = \xi S_3(t)$. We also assume that

$$\frac{\xi_1(t)}{\xi_3(t)} = \frac{1 - v_{D_i}}{v_{D_i} - v_{T_i}} \quad (2.20)$$

which applies given that the timescale of infection in individuals is fast compared to the whole duration of the pandemic. The proportion of unvaccinated people who are infected at t is $\frac{\xi_1(t)}{\xi_1(t) + \xi_2(t) + \xi_3(t)}$, and the fraction of vaccinated but not immunized people infected at t is $\frac{\xi_2(t)}{\xi_1(t) + \xi_2(t) + \xi_3(t)}$. From equation 2.20, and the model equations, we can adjust the

probability that a given person who is infected also dies at time t as

$$\text{Adjusted mortality at } t \text{ for age group } i = \frac{S_{1i}(t) + S_{2i}(t)}{S_{1i}(t) + S_{2i}(t) \frac{1-v_{Ti}}{1-v_{Di}}} \times \text{Cases at } t \times \text{measured CFR} \quad (2.21)$$

2.2.12 Vaccine scenarios

We considered two dates for the onset of vaccination: 1 March 2021 and 1 September 2021. These correspond to the end dates of a two-dose course of vaccination lasting two weeks. We assumed it was possible to vaccinate 0.5%, 1.0%, 1.5%, 2.5%, or 5.0% of the population per week (the “vaccination rate”, 0). Our baseline scenario assumed a vaccine with 75% efficacy in all ages, against both infection and transmission.

The “oldest first” strategy administers the vaccine to individuals 60 years of age or older, first. After all individuals in this group are vaccinated, the vaccine is administered uniformly to other ages. The “youngest first” strategy is similar, except it administers the vaccine to individuals younger than 20 years of age first. The “uniform” strategy administers vaccines to all age groups uniformly, from the very start. The “contact-based” strategy allocates vaccines according to the relative role played by different age groups in transmission. This tends to prioritise ages 15-19 primarily, 20-59 secondarily, and the least in older or younger ages. The “oldest first” strategy targets a vulnerable age group while the other three strategies are designed to interrupt transmission.

2.3 Results

The Google mobility data that we use as a proxy for adherence to NPIs closely mirrors the COVID-19 case notification data over the time period used for fitting (2.1, open orange circles). Since a heightened perception of COVID-19 infection risk simulates the adoption of NPIs²⁶, which in turn reduces SARS-CoV-2 transmission [16, 156], this exemplifies a coupled social-epidemiological dynamic. The mirroring may furthermore represent convergence between social and epidemiological dynamics, which has been predicted for strongly coupled systems [187]. Moreover, the fit of the social submodel to the mobility data is as good as the fit of the epidemic submodel to case notification data (Figure 2.1), despite the fact that our social model consists of significantly fewer equations and a similar number of parameters as our epidemiological model. This shows how modelling population behaviour during a pandemic can be accomplished with relatively simple models.

The model predicts additional pandemic waves from Fall 2020 onward, not only with respect to COVID-19 cases but also population adherence to NPIs and periods of school and workplace closure (Figure 2.2). The impact of the four strategies on COVID-19 cases and deaths depends on when the vaccine becomes available and how quickly the population can get vaccinated. Across a large parameter regime, vaccinating 60+ year-olds first prevents the most deaths out of all four strategies if vaccination begins in January 2021, whereas the uniform or contact-based strategies prevent the most deaths if vaccination begins in September 2021, unless the vaccination rate is very small or very large. More specifically, we identify three regimes for model dynamics. We explore them through plots of infection incidence over time (Figure 2.3); plots of the percentage reduction in mortality under all four strategies, as they depend on the vaccination rate (Figure 2.4) and shutdown threshold (Appendix, Figure 10, 11); and plots showing which of the four strategies prevents the most deaths as a function of the shutdown threshold and the vaccination rate (Figure 2.3).

In the first regime, vaccination starts soon and the vaccination rate is relatively high (January availability, vaccinating 1.0% or more of the population per week). A third wave in Fall 2021/Winter 2022 is thereby prevented (Figure 2.3a and Appendix, Figure 7). In this regime, enough people are vaccinated sufficiently far in advance to prevent a third wave, but the “oldest first” strategy prevents more deaths than the other strategies (Figure 2.4a, 2.3a).

In the second regime, either vaccination starts early but the vaccination rate is too low (January availability, 0.5% or less vaccinated per week, Figure 2.2, 2.3b, 2.4a), or vaccination starts late but the vaccination rate is high (September availability, vaccinating 1.5% or more per week, Figure 2.3c, 2.4b and appendix, Appendix, Figure 8). In this

Table 2.1: Parameter definitions, values, particle filtering ranges, and sources.

Parameter	Meaning	Value [Range]	Source
N_i	Population in age group i	0 – 4: 790169; 5 – 9: 789190 10 – 14: 790803; 15 – 19: 887072 20 – 24: 1003052; 25 – 29: 1015105 30 – 34: 1009090; 35 – 39: 969949 40 – 44: 926440; 45 – 49: 938990 50 – 54: 1027557; 55 – 59: 10416495 60 – 64: 892016; 65 – 69: 741824 70 – 74: 557203; 75+: 204431	[192], interpolated
μ_i	COVID-19 case fatality rate in age group i	0 – 4: 0.002; 5 – 9: 0.001 10 – 14: 0.0005; 15 – 19: 0.0005 20 – 24: 0.0010; 25 – 29: 0.002 30 – 34: 0.0031; 35 – 39: 0.0048 40 – 44: 0.0078; 45 – 49: 0.0135 50 – 54: 0.0253; 55 – 59: 0.0455 60 – 64: 0.0784; 65 – 69: 0.1378 70 – 74: 0.2623; 75+: 0.5815	[150], interpolated
C_{ij}	contact rate between class i and j	see Methods	[166]
R_0	basic reproduction rate of infection	calibrated, [1.5, 2.5]	[96, 84, 200]
r	probability of transmission per contact	derived from next generation matrix	[66]
σ_0	inverse of latent period for exposed individuals	calibrated, [0.3, 2.0]	[84, 200, 147, 120, 197]
σ_1	inverse of latent period for presymptomatic individuals	calibrated, [0.3, 2.0]	[84, 200, 147, 120, 197]
γ_a	inverse of infectious period for asymptomatic individuals	0.25/day	[147, 120, 197]
γ_s	inverse of infectious period for symptomatic individuals	calibrated, [0.0, 0.05]	[84, 200, 147, 120, 197]
$\alpha_{1,1}$	Ascertainment rate of class i in the first wave (before t_{switch})	calibrated, [0.01, 1.0]	see Methods
$\alpha_{1,2}$	Ascertainment rate of class i in the first wave (before t_{switch})	calibrated, [0.01, 1.0]	see Methods
$\alpha_{1,3}$	Ascertainment rate of class i in the first wave (before t_{switch})	calibrated, [0.2, 1.0]	see Methods
$\alpha_{2,1}$	Ascertainment rate of class i in the second wave (after t_{switch})	calibrated, [0.01, 1.0]	see Methods
$\alpha_{2,2}$	Ascertainment rate of class i in the second wave (after t_{switch})	calibrated, [0.01, 1.0]	see Methods
$\alpha_{2,3}$	Ascertainment rate of class i in the second wave (after t_{switch})	calibrated, [0.2, 1.0]	see Methods
ρ_1	Age-specific susceptibility modifier, ages 0-20	calibrated, [0.25, 3.0]	see Methods
ρ_2	Age-specific susceptibility modifier, ages 20-60	calibrated, [0.25, 3.0]	see Methods
ρ_3	Age-specific susceptibility modifier, ages 60+	calibrated, [0.25, 3.0]	see Methods
η	fraction of symptomatic infections	0.15	[141]
ϵ_P	efficacy of physical distancing	calibrated, [0.3, 0.9]	[84, 200]
κ	social learning rate	calibrated, [1000, 16000]	[84, 200]
s	seasonality	calibrated, [−0.3, 0.3]	[84, 200]
ϕ	seasonality phase	−30 days	see Methods
v_{T_i}	Vaccine efficacy against transmissibility and disease for individuals in group i	75%	[153]
v_{D_i}	Vaccine efficacy against disease only for individuals in group i	75%	[153]
I_0	Initial ratio of active cases to incident cases	calibrated, [1, 10]	[84, 200]
P_0	Initial ratio of presymptomatic cases to incident cases	calibrated, [1, 10]	
E_0	Initial ratio of exposed cases to incident cases	calibrated, [1, 10]	
ψ_i	Number of vaccines allocated for individuals in group i each day	varied by scenario	
T	Threshold in active reported cases for school/workplace closure	varied by scenario	
k_1	Workplace shutdown rate	0.31432	fitted, see Methods
k_2	Workplace opening rate	0.0056	fitted, see Methods
c	Incentive not to distance	calibrated, [0.0, 0.5]	[84, 200]
p_{ul}	social heterogeneity parameter	calibrated, [0.00, 0.05]	[84, 200]
t_s^{close}	School shutdown date	March 14th, 2020	[82]
t_s^{open}	School opening date	September 8th, 2020	[81]
t_w^{close}	Work shutdown date	March 17th, 2020	[167]
t_w^{open}	Work opening date	June 12th, 2020	[167]
ϵ_w	Work shutdown effectiveness	0.86	fitted, see Methods
t_{switch}	Beginning of second wave	160 days	see Methods
t_{delay}	Delay in impact of interventions on transmission	28 days	[125]
k_s	Rate of change from first to second wave	0.05	see Methods
κ_{vac}	Social learning rate of vaccination	[3e5, 20e5]	fitted, see Methods
c_{vac}	Incentive not to vaccinate	[1.0e − 9, 15e − 9]	fitted, see Methods

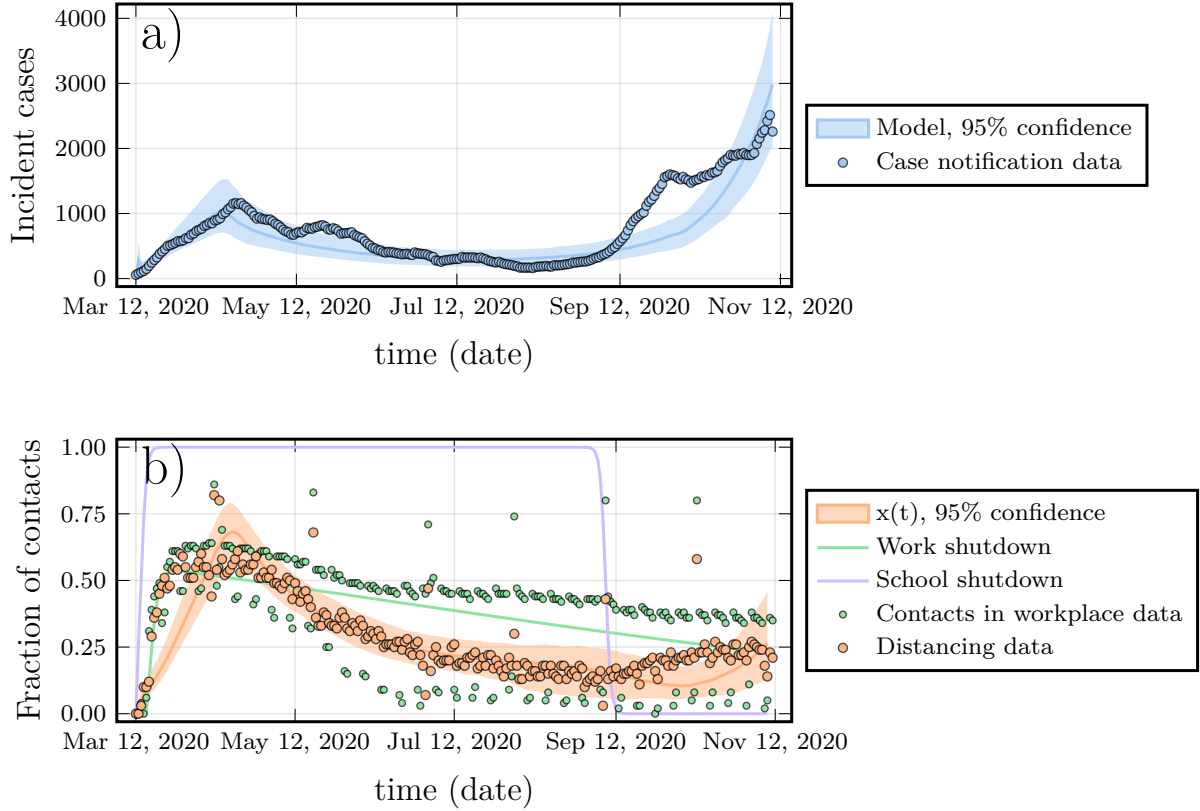


Figure 2.1: A proxy for adherence to NPIs mirrors COVID-19 case reports in both data and model. (a) COVID-19 case incidence by date of report in Ontario, 7-day running average (circles) and ascertained case incidence from best fitting models (lines). (b) Percentage change from baseline in time spent at retail and recreation destinations (orange circles) and at workplaces (green circles) from Google mobility data, and proportion of the population x adhering to NPIs (orange line) and workplace shutdown curve (green line) from fitted model. Parameter values are provided in table 2.1.

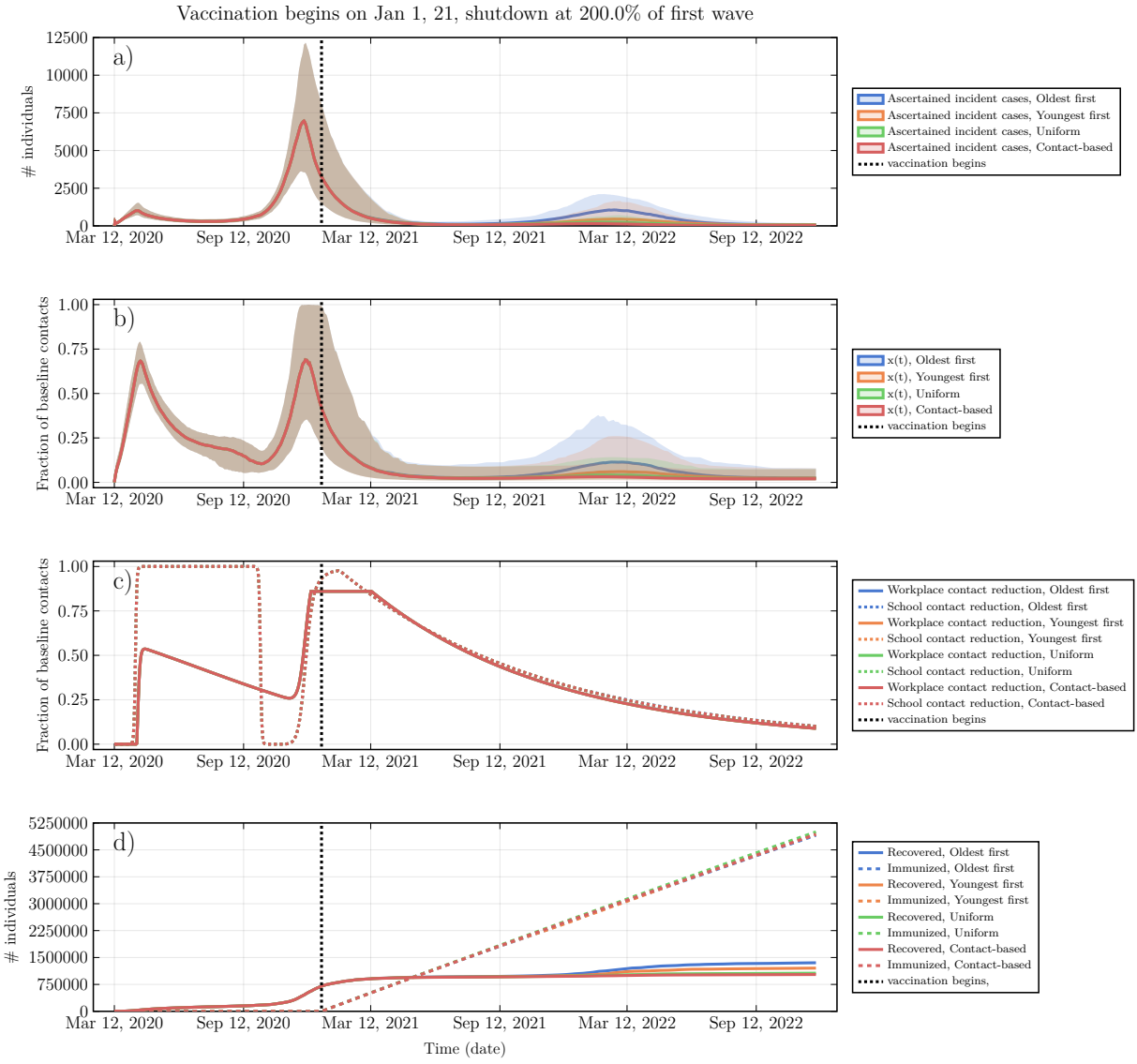


Figure 2.2: Social and epidemiological dynamics interact to determine pandemic waves and vaccine strategy effectiveness. (a) Number of ascended incident COVID-19 cases, (b) proportion x of the population practicing NPIs, (c) level of school and workplace closure (note that curves for different vaccination strategies overlap), and (d) number of individuals with natural or vaccine-derived immunity versus time. Ontario Population size: 14.6 million. Shutdown occurs at $T = 200\%$ of peak cases in the first wave, vaccination starts in January 2021, vaccination rate is $\psi_0 = 0.5\%$ per week. Other parameter values are provided in table 2.1.

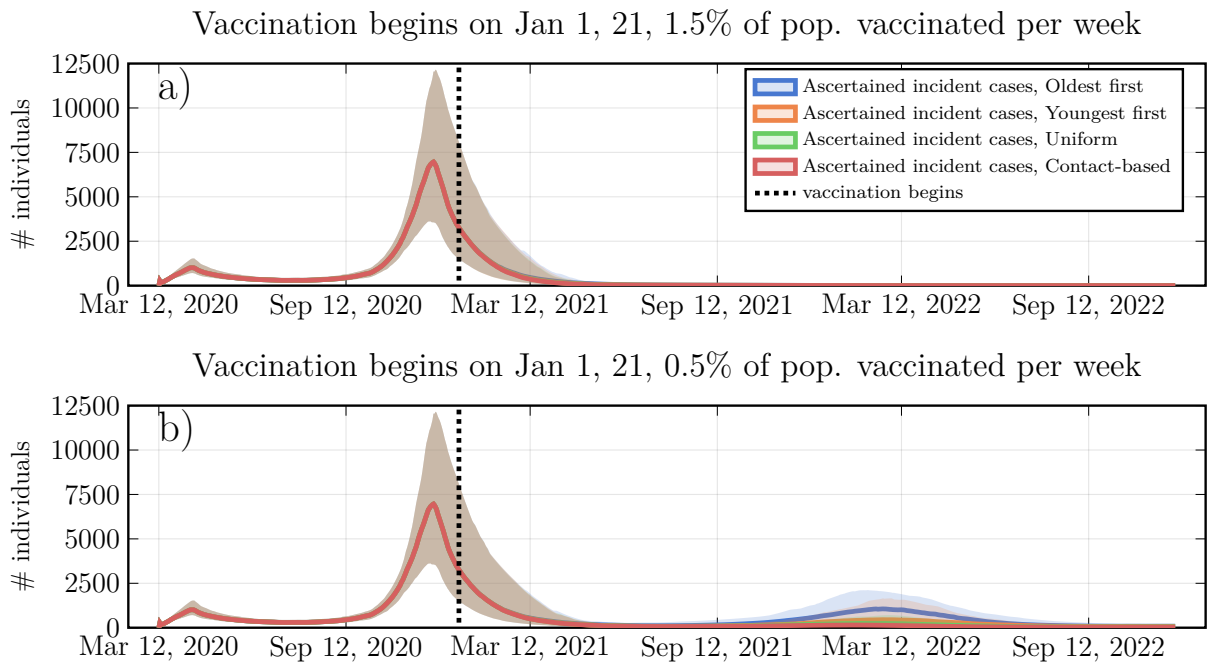


Figure 2.3: Three model regimes: (a) timely vaccination prevents third wave, (b,c) partial vaccination and indirect protection help during the third wave, and (d) slow and late vaccination fails to prevent third wave. Projections of ascertained incident COVID-19 cases if vaccination begins in (a,b) January or (c,d) September, and if vaccinating (a,c) 1.5% or (b,d) 0.5% of the population per week. Ontario Population size: 14.6 million. $T = 200\%$. Other parameter values are provided in table 2.1.

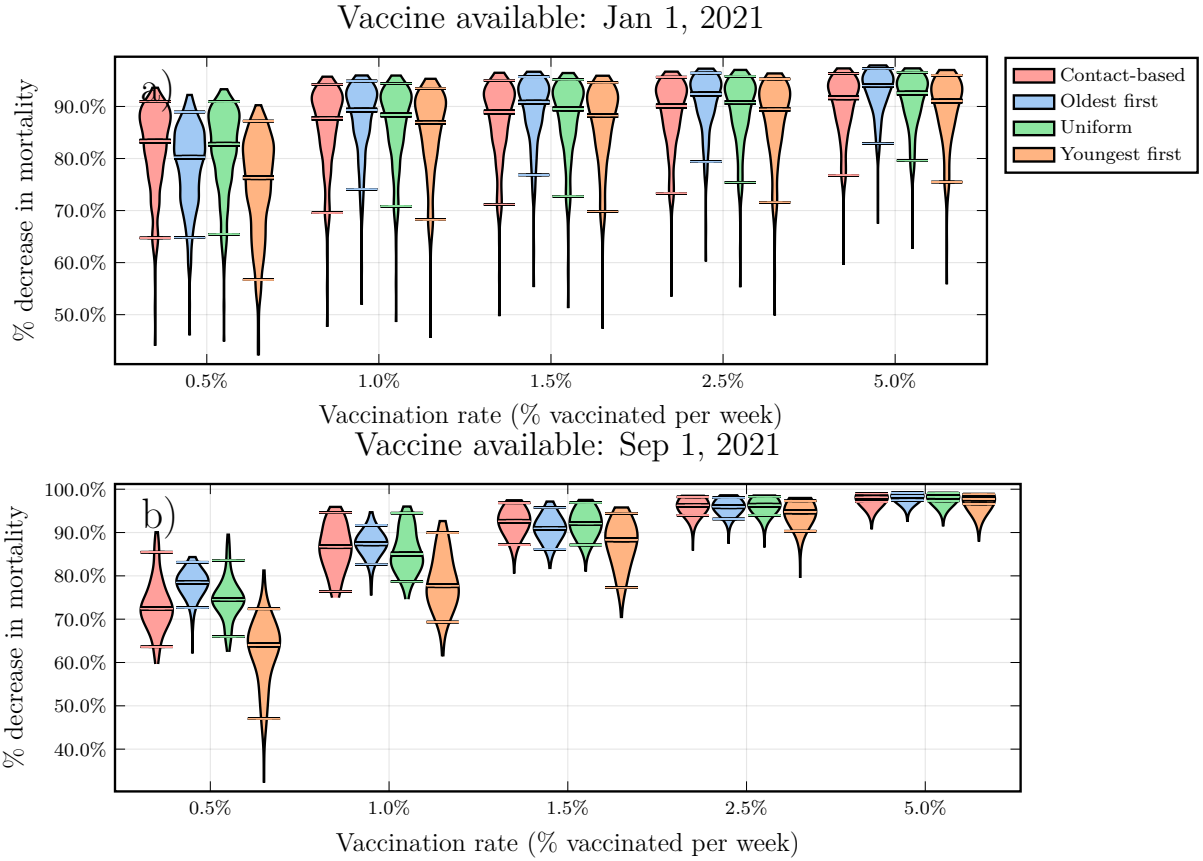
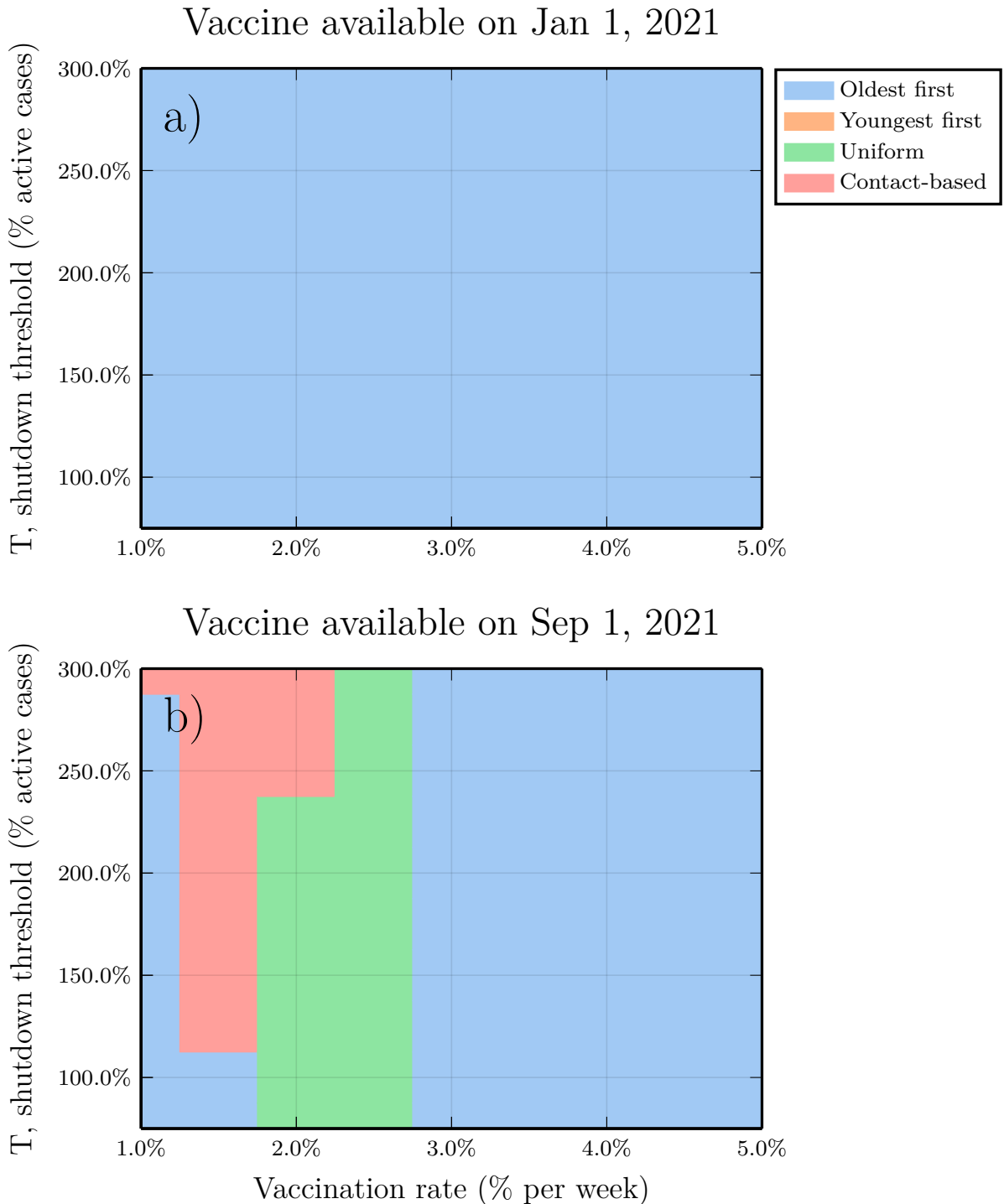


Figure 2.4: Percentage reduction in mortality for four strategies depends on vaccination start date and the vaccination rate. Violin plots of the percent reduction in mortality under the four vaccine strategies, relative to no vaccination, as a function of the vaccination rate ϕ_0 , for (a) January and (b) September 2021 availability. Horizontal lines represent median values of posterior model projections. Shutdown threshold $T = 200\%$ and other parameter values are provided in table 2.1. The projected number of deaths in the absence of vaccination was 72000 (95% credible interval 40000–122000) from Jan 1, 2021, to March 14, 2025, and 60000 (31000–108000) from Sept 1, 2021, to March 14, 2025.



Best of four strategies depends on shutdown threshold T and vaccination rate ϕ_0 . A later start to vaccination favours transmission-interrupting strategies for moderate vaccination rates. Each parameter combination on the plane is colour coded according to which of the four strategies prevented the most deaths, on average across all model realizations, for (a) January and (b) September 2021 availability. Other parameter values are provided in table 2.1.

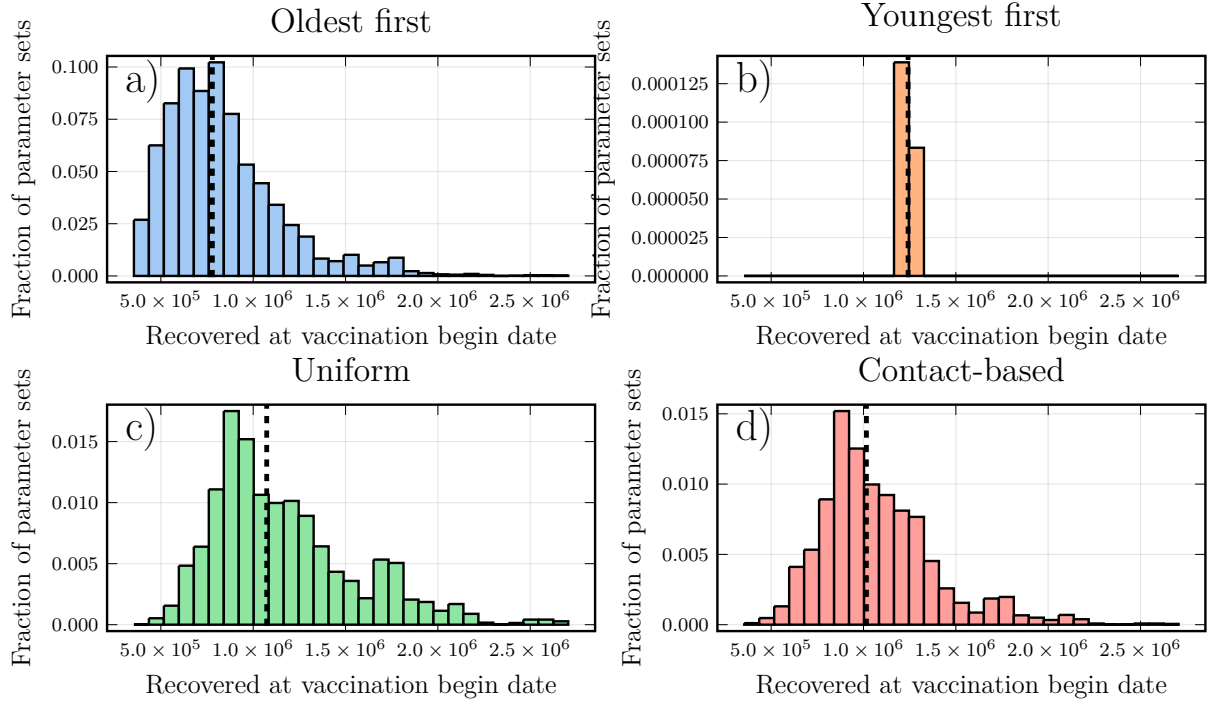


Figure 2.5: More pre-existing natural immunity makes transmission-interrupting strategies more effective. Frequency histogram of the percentage of the population with natural immunity for each strategy, taken from simulations where that strategy reduced mortality most effectively, for (a) oldest first, (b) youngest first, (c) uniform, and (d) contact-based strategies. The most effective strategy is defined as the one that reduced mortality the most across the largest number of model realizations. Vertical dashed lines denote median values of the distribution. Other parameter values are provided in table 2.1.

intermediate scenario, a sufficient proportion of the population is vaccinated for indirect protection from the vaccine to become important during the third wave, but not enough individuals are vaccinated to completely prevent it. As a result, the uniform and contact-based strategies are more effective than the 60+ first strategy, but the “youngest first” strategy does worst of all (Figure 2.2b, 2.3c, 2.4, 2.3). The under-performance of the youngest first strategy occurs because in populations with strong age-assortative mixing²⁶, the indirect benefits of vaccination are “wasted” if vaccination is first concentrated in specific age groups before being extended to the rest of the population. The 60+ first strategy is less affected by this because the COVID-19 case fatality rate is high in this age group. However, as the vaccination rate becomes very high, the effectiveness of all four strategies converges, since the entire population is vaccinated quickly (Figure 2.4b).

In the third regime, vaccination starts late and the vaccination rate is low (September availability, 1.0% or less vaccinated per week; Figure 2.3d and Appendix, Figure 9). This scenario does not allow enough time for indirect protection from vaccination to become strong. As a result, the oldest first strategy prevents more deaths than the other three strategies (Figure 2.4b, 2.3b). Overall mortality is higher for all strategies, on account of the delayed rollout of the vaccine. The relative performance of the strategies in these three regimes is generally unchanged across the full range of values for the shutdown threshold (Appendix, Figure 10, 11).

Frequency histograms across all stochastic model realizations showing what percentage of the population has natural immunity at the start of a vaccine program, when a particular strategy was shown to work best, illustrate the role of indirect protection (Figure 2.5). In simulations where the “oldest first” strategy did best, the percentage of the population with natural immunity tends to be relatively low. This is expected, since indirect protection from vaccines is weaker when few people have natural immunity upon which vaccine indirect protection can build. But when the uniform or contact-based strategy does best, more simulations exhibit a high level of natural immunity at the start of vaccination. We note that the variance in these histograms is high, which underscores the role of other factors in the model such as timing and interaction between social and epidemiological dynamics. In a similar vein, if we plot the percentage reduction in mortality for hypothetical vaccination start dates ranging from September 2020 to September 2021, we observe that the transmission-interrupting strategies become relatively more effective than the “oldest first” strategy for later vaccination start dates, because herd immunity has time to increase before the start of the vaccine program (Appendix, Figure 12).

We also studied how the best strategy changes depending on vaccine efficacy ranging from 40-90% in 60+ year-olds and in ≥ 60 year-olds (Appendix, Figure 13). For January vaccine availability, the “oldest first” strategy is best, even when vaccine efficacy is lower in

60+ year-olds than in those under 60 years of age. For September vaccine availability, the uniform or contact-based strategies do best, except when vaccine efficacy in 60+ year-olds is higher than 70% and also exceeds the vaccine efficacy in <60 year-olds.

We modelled dynamics of vaccinating behaviour after vaccines become available (Appendix, Figures 14, 15, 16). Due to lack of empirical data, we explored a wide range for the social learning rate and the perceived relative cost of vaccination versus infection. The results suggest that a sufficiently high perceived cost of vaccination allows the uniform or contact-based strategies to outperform the “oldest first” strategy, especially for January vaccine availability, except when the vaccine social learning rate is also high (Appendix, Figure 14). Vaccine refusal increases as the vaccine cost rises (Appendix, Figuresgs 14, 15, 16). Since vaccine refusal in the targeted age group forces vaccination of other age groups instead, it makes all strategies behave more like the uniform strategy, although age-specific behaviours could change these predictions.

We ran simulations with $R_0=2.5$ for December 2020 onward and found that “oldest first” was more effective across a broader region of parameter space for September availability, particularly at higher vaccination rates (Appendix, Figure 18). This is expected, since indirect protection is less effective when R_0 is higher. We also ran simulations with 30% higher and lower ascertainment for December 2020 onward to capture potential changes to COVID-19 testing and found that it had little impact on which strategy was most effective (Appendix, Figures 19, 20). Similarly, higher or lower social learning rates for NPIs had little impact on the predictions (Appendix, Figures 21, 22).

We also analyzed a scenario where the vaccine efficacy against disease can be greater than the vaccine efficacy against infectivity. We found that increasing the efficacy against disease up to 95%, while holding the efficacy against infectivity constant at 75%, caused a slight improvement in the effectiveness of all four strategies, especially for the “oldest first” and uniform strategies (Appendix, Figure 23). Finally, we generated results for our baseline scenario, but using a more stringent acceptance threshold for our Bayesian particle filtering algorithm. We found that our results were qualitatively unchanged (Appendix, Figure 25).

2.4 Discussion

Our social-epidemiological model suggests that if a COVID-19 vaccine becomes available sufficiently late in the pandemic, using SARS-CoV-2 vaccines to interrupt transmission might prevent more COVID-19 deaths than using the vaccines to target those 60+ years

of age, depending on when the vaccine becomes available and how quickly the population can be vaccinated. These results are driven by the fact that the vaccine may only become available after populations have had one or more waves of immunizing infections. As a result, the effective reproduction number R_{eff} could be significantly closer to 1 than the basic reproduction number $R_0 \approx 2.2$ that applies to susceptible populations. In this regime, vaccines that reduce transmission have disproportionately large indirect protective effects [14].

The Google mobility data that we use as a proxy for adherence to NPIs closely mirrors the COVID-19 case notification data over the time period used for fitting (Figure 1, open orange circles). Since a heightened perception of COVID-19 infection risk simulates the adoption of NPIs [214], which in turn reduces SARS-CoV-2 transmission [16, 156], this exemplifies a coupled social-epidemiological dynamic. This mirroring may represent convergence between social and epidemiological dynamics, which has been predicted for strongly coupled systems [187]. Moreover, the fit of the social submodel to the mobility data is as good as the fit of the epidemic submodel to case notification data, despite the fact that our social model consists of significantly fewer equations and a similar number of parameters as our epidemiological model. This shows how modelling population behaviour during a pandemic can be accomplished with relatively simple models.

Several studies have used compartmental models to study prioritisation of age groups for COVID-19 vaccination [44, 46, 137]. These models vary widely in terms of study populations, representation of population heterogeneity, interventions, and assumptions about when vaccination starts. Similar to our results, Matrajt et al [137] find that the level of pre-existing immunity strongly dictates outcomes: when pre-existing immunity is high, strategies that distribute the vaccine more evenly across age groups rather than prioritising older age groups. Buckner et al [46] find that targeting 60+ year-olds is best for reducing mortality. They assumed that vaccination begins in December 2020, and they base initial conditions on case notifications in the United States in that month. Similarly, Bubar et al [44] find that vaccinating 60+ year-olds works best for reducing mortality for vaccine programs starting in July 2020 in Belgium, or August 2020 in New York City. Our results agree with Refs. [44, 46] for the scenario of January 2021 vaccine availability. However, we find more deaths can be prevented by first vaccinating other age groups for a September 2021 start. Such a late vaccine start date was not analyzed in [44, 46] although their findings might change if the models were re-initialized to accommodate vaccination starting in September 2021.

Our analysis was limited by its focus on prioritisation of age groups. We did not model other sources of heterogeneity such as geography, socio-economic status, sex, or race—all of which are important determinants of disease burden in this highly unequal

pandemic. We did not model outbreaks in long-term care facilities, where the dynamics of transmission and indirect protection differ from the general population. Similarly, we did not distinguish healthcare or other essential workers. However, many of these individuals are working age adults, and thus vaccinating them first among other working adults is consistent with our uniform and contact-based strategies. For our baseline analysis we assumed the vaccine blocks transmission as well as it prevents COVID-19 disease. But in general, vaccines have differing efficacy in this regard [97]. This can reduce the relative benefits of strategies intended to interrupt transmission. We used a single population model, but inter-population mobility can influence transmission dynamics: a large influx of infectious persons from another population can weaken the indirect protection afforded by vaccines.

We used changes to baseline time spent at retail and recreational outlets to represent population adherence to NPIs. Such mobility data is an imperfect proxy for physical distancing and will not capture mask use or hand-washing. We did not have high resolution mobility data on these practices, although in future it may be possible to infer information about these practices by combining information from phone surveys with online social media data. Our simple ascertainment process in the model was designed to implicitly capture the effects of COVID-19 PCR testing, contact tracing and isolation (TTI). But without explicitly representing them, it is impossible for us to study combined strategies of vaccination and TTI, or to anticipate how specific changes to TTI would influence our findings.

Finally, the model was parameterised with data from Ontario, Canada. For instance, the emergence of a more transmissible strain of SARS-CoV-2 would weaken the indirect protection provided by a vaccine that reduces transmission. At the same time, we note that our findings rely upon a robust epidemiological effect that occurs when R_{eff} becomes sufficiently small. Therefore, the only thing that may change in other settings is the timing of the switch to vaccine strategies that interrupt transmission.

We opted for a coupled social-epidemiological model on account of the importance of interactions between population behaviour and disease dynamics for the control of COVID-19 in the absence of preventive pharmaceutical interventions. Our model generated significantly different projections in our sensitivity analysis where population behaviour was assumed constant, which is similar to conventional approaches to transmission modelling. Our social model is less complicated than our epidemiological model and despite this, the coupled social-epidemiological model fitted population-level behaviour as readily as it fitted the epidemic curve. Predicting behaviour is fraught with uncertainty, but so is predicting an epidemic curve. Moreover, digital data on behaviour and sentiment that can be used to model social dynamics is increasingly available [180]. Given this, we suggest a role for

more widespread use of social-epidemiological models during pandemics.

To apply these results to COVID-19 pandemic mitigation, large-scale seroprevalence surveys before the onset of vaccination could ascertain the level of a population's natural immunity. Age-structured compartmental models could be initialized with this information to generate population-specific projections. In populations where SARS-CoV-2 seropositivity is high due to a Fall/Winter 2020 wave, vaccinating to interrupt transmission may reduce COVID-19 mortality more effectively than targeting vulnerable groups.

Chapter 3

Go big or go home: a model-based assessment of general strategies to slow the spread of forest pests via infested firewood

3.1 Abstract

Invasive pests, such as emerald ash borer or Asian longhorn beetle, have been responsible for unprecedented ecological and economic damage in eastern North America. These and other wood-boring invasive insects can spread to new areas through human transport of untreated firewood. Behaviour, such as transport of firewood, is affected not only by immediate material benefits and costs, but also by social forces. Potential approaches to reduce the spread of wood-boring pests through firewood include raising awareness of the problem and increasing the social costs of the damages incurred by transporting

This chapter is based on the paper: Jentsch, Peter C., et al. "Go big or go home: A model-based assessment of general strategies to slow the spread of forest pests via infested firewood." PloS one 15.9 (2020): e0238979.

firewood. In order to evaluate the efficacy of these measures, we create a coupled social-ecological model of firewood transport, pest spread, and social dynamics, on a geographical network of camper travel between recreational destinations. We also evaluate interventions aimed to slow the spread of invasive pests with untreated firewood, such as inspections at checkpoints to stop the movement of transported firewood and quarantine of high-risk locations. We find that public information and awareness programs can be effective only if the rate of spread of the pest between and within forested areas is slow. Direct intervention via inspections at checkpoints can only be successful if a high proportion of the infested firewood is intercepted. Patch quarantine is only effective if sufficiently many locations can be included in the quarantine and if the quarantine begins early. Our results indicate that the current, relatively low levels of public outreach activities and lack of adequate funding are likely to render inspections, quarantine and public outreach efforts ineffective.

3.2 Introduction

Invasive species pose a significant economic and ecological threat to Canada’s forest ecosystems [213, 104]. In North America, significant funding has been allocated by federal, state and provincial agencies for large-scale control programs to prevent or mitigate these damages with mixed success [198, 144]. Controlling the spread of invasive pests can be difficult because the long-distance spread of invasive organisms is often assisted by human activities [115, 213]. For example, introduction and spread of Emerald ash borer, a harmful forest pest in the North America [116, 117, 161] has been attributed to human factors, such as vehicle transport [45] and recreational travel [114].

The growing problem of invasive species is broadly associated with human mobility, including recreational travel [115, 213, 126, 165]. Outdoor recreation is widespread in North America, and the extent of recreational activities is expected to increase [63, 61, 62]. In North America, national, provincial and state parks, national forests, and state and Crown lands are common destinations for recreational activities [69, 188]. In Canada, recreational activities, especially camper travel, often take place in forested areas and may contribute to spread of harmful invasive pests. In particular, the movement of untreated firewood by campers has been widely acknowledged as a potential introduction pathway for invasive forest pests [25, 199, 159, 114, 104]. Movement of untreated firewood has been linked to the spread of two harmful wood-boring pests, the Asian longhorned beetle (*Anoplophora glabripennis* Motschulsky) and the emerald ash borer (*Agrilus planipennis* Fairmaire), in the United States and Canada (USaC) [86, 160].

Firewood is often moved to distant locations by campers for recreational purposes

[104, 205]. For example, Haack et al. (2010) has found live bark- and wood-boring insects in 23% of the firewood pieces, surrendered at the checkpoint station at Mackinac bridge connecting Michigan's Lower and Upper Peninsulas and an additional 41% had signs of prior borer infestation. Jacobi et al. (2011) reported the emergence of live insects from 47% of the firewood bundles purchased from various US retailers. To reduce the risk of future pest infestations, USaC have implemented various regulations on movement of untreated firewood, including bans for out-of-province movement of untreated firewood and restrictions for its transport by short distances [199, 205, 87, 151]. Also a number of public outreach campaigns have been undertaken to educate the general public about the threats associated with the movement of untreated firewood and its potential to spread harmful invasive pests. Several strategies have been developed to prevent (or minimize) the movement of firewood with recreational travel, including outreach campaigns in public media, enforcements with the inspections at check points for transported firewood, and area quarantine with the restrictions on firewood movement from/to the area of concern. In particular, public outreach campaigns have become widespread with significant funding by local, municipal, and provincial governments on measures such as advertisements along major highways and in public media and educational information in websites and printed media. The use of enforcement and quarantine options is less common but is gaining acceptance as a last resort measure and was implemented at least a few times over the past decade, to varying degrees of success [25, 114, 151].

Assessing the efficacy of the measures aimed to prevent the movement of firewood with recreational travel is a daunting task. Outreach campaigns may spread information widely but there is no guarantee that campers will pay attention and comply with the firewood restriction warnings. Many outreach activities (such as posting ads in public media or distributing flyers) are often implemented sporadically at local scales using local municipal and provincial budgets [199], which makes the assessment of their efficiency difficult. These activities may simultaneously occur in different places and times with little or no coordination, and are difficult to track in time and space.

Alternatively, the enforcement options (such as quarantine or checkpoint inspections for illegal movement of firewood) are gaining acceptance and may be perceived as more effective localized means to stop the movement of untreated firewood by campers. Nevertheless, assessing the effectiveness of enforcement actions is challenging due to a very small scale of enforcement actions (often implemented by individual states or provinces at selected locations) and lack of compliance data.

Mechanistic models of forest invasions have been studied for decades [132], but explicit modelling and consideration of human factors, and the feedback between humans and the environment is relatively new. Ali et al. and Barlow et al. [25, 8] proposed two models

of forest pest spread through firewood transport. The first study presented a differential equation model, and the second an agent-based model, both assuming that humans are the primary long-distance movers of forest pests. The models proposed in [25, 8] coupled infestation dynamics with the social dynamics. However both studies considered a small and idealized spatial structure: two patches in Barlow’s et al. [25] study and ten patches in Ali’s et al. model [8]. Often, illegal movement of firewood occurs over large distances and may involve visits to multiple recreational destinations that are connected differently to one another.

In this study we consider movement of infested firewood to multiple recreational destinations over a complex recreational travel network. We explore the efficacy of common measures aimed to stop the movement of untreated firewood by recreational travelers. To accomplish this, we propose a mechanistic differential equation model that combines human-mediated movement of forest pests through a camper travel network that includes nonlinear feedbacks from social factors, such as population response to strategies preventing the movement of untreated firewood. We identify three basic methods to stop or slow the spread of invasive pests by transport of infested firewood: public awareness campaigns, direct interception of transported firewood at checkpoints near recreational destinations, and quarantining recreational destination sites for movement of firewood. While the first option is more common, the latter has been implemented seldom over the past decade due to legal and liability constraints [173, 210, 145, 87]. We implement the options for intercepting the movement of firewood to slow the spread of invasive pests in a mechanistic metapopulation model, and use the replicator equation to represent social learning dynamics (see [91, 25, 27, 98]). We also evaluate local quarantine at recreational destinations as an alternative control method. Quarantine means closing the site to visitors for a length of time, in order to reduce the amount of transported firewood and slow spread of invasive organisms from other infested locations. Our implementation of quarantine measures follow common practices aimed to slow the spread of invasive species (such as the spread of emerald ash borer in USaC [143, 85]). We apply our mechanistic model to explore the effectiveness of these control measures to slow the spread of an idealized wood-boring invasive pest moved to a set of recreational destinations by recreational travelers transporting untreated firewood. We apply the model to a network of provincial parks and campgrounds in three provinces of central Canada - Manitoba, Ontario, and Quebec.

3.3 Materials and methods

We consider a landscape of N patches, where a patch is represented as $i \in [1, N]$. Each patch represents a recreational destination (eg. provincial parks and campgrounds) with associated neighbouring human population centres. Each patch undergoes its own internal pest and social dynamics. We describe the spread of an invasive pest with the movement of firewood through the network of N patches with a mechanistic metapopulation model based on [25] that captures the spread of an infestation between the patches. The advantage to metapopulation models in this context is suitability for capturing dynamics of a highly fragmented population spread over a broad geographic region. Using the data documenting reservations of provincial campgrounds in Ontario, Manitoba and Quebec ([216], we created a graph of camper travels which depicts a spatial travel network between origin locations (which correspond to residential addresses of camper travelers) and recreational destinations (campgrounds in provincial parks and historic sites). The camper travel network is described by a graph with coefficients $P_{i,j}$ denoting the relative frequency of camper movements between origin locations j and recreational destination locations i (see more details on spatial data in section 3.3.4). Specifically, for a given location j , $P_{i,j}$ is the fraction of trips that go from j to i each year, so we have $\sum_{i=1}^N P_{i,j} = 1$. Consider a patch i with an enforcement intervention, such as firewood movement quarantine, or a voluntary firewood surrender checkpoint aimed to stop the flow of untreated firewood from that location. We denote C_e as the percentage of infested firewood that can be intercepted on a route between two locations i and j , $0 \leq C_e \leq 1$. Interception at i may reduce the movement of infested firewood from a patch i to other patches j , so C_e indicates, in relative terms, the magnitude of interception efforts.

We also consider a public outreach campaign that can take place at a patch i . It is common that only a portion of campers visiting a patch i may be aware of and decide to comply with the public outreach message. We model the social awareness campaign as an increase of the net social cost of transporting firewood. We further conduct sensitivity analyses to compare the efficacy of enforcement vs. outreach measures aimed to stop the movement of firewood and reduce the rates of infestation.

3.3.1 Pest Spread Model

We begin with defining the equation for a population of susceptible host trees that may be attacked by an invasive pest. The pest can be introduced through untreated infested firewood. Variables, their interpretations, and corresponding baseline ranges are shown in

Table 3.1. We assume that a tree population that is susceptible to pest attack undergoes logistic growth in the absence of infestation to a carrying capacity K . The population of susceptible trees, $S_i(t)$, at a patch i is being infested from firewood arriving with campers at i at a rate A :

$$\frac{dS_i}{dt} = \underbrace{rS_i \left(1 - \frac{(S_i + I_i)}{K}\right)}_{\text{Logistic Growth Of Forest}} - \underbrace{AS_i(I_i + B_i)\theta_k(I_i - I_a)}_{\text{Infestation term}} \quad (3.1)$$

where $\theta_k(I_i)$ is a sigmoid function such as

$$\theta_k(x) = \frac{1}{1 + e^{-kx}} \quad (3.2)$$

Terms S_i and I_i are the number of susceptible and infected trees, respectively, at patch i . B_i is the quantity of infested firewood in patch i , which we assume has the same probability of pest transmission within patch as infested trees. We choose the carrying capacity K to be the same in each patch for simplicity. The term $AS_iI_i\theta_k(I_i - I_a)$ represents intra-patch infestation with a density dependent population, parameterized by k and I_a , where I_a determines population of infested trees at which transmission is halved, and k is a constant which affects the sharpness of the transition of $\theta_k(x)$ at I_a . We assume that there is an influx of pest organisms entering a patch i with firewood which defines the propagule pressure at i . Infested trees at i are assumed to die at a constant rate γ , giving the following equation for the infested tree population of a patch.

$$\frac{dI_i}{dt} = \underbrace{-\gamma I_i}_{\text{Death of infested trees}} + \underbrace{AS_i(I_i + B_i)\theta_k(I_i - I_a)}_{\text{Susceptible become infested}} \quad (3.3)$$

The patches are spatially coupled through the transport of firewood by recreational travelers. The infestation rate at i depends on the number of visitors transporting infested firewood to i , which is also a function of the social dynamics at i , such as the enforcement, or public outreach measures described by a utility function, presented in [27], and applied to forest modelling in [25, 183]. Let L_i be the proportion of visitors to patch i who do not transport firewood and buy it locally, and d rate of exportation of infested logs. The rate of infested wood coming into patch i can be estimated as:

$$d \sum_{j=1, j \neq i}^N P_{i,j}(1 - C_e)(1 - L_j)I_j$$

The dynamics of L_i (the number of local transporters in patch i), is modelled by a replicator dynamics model that is suitable for describing systems where social learning occurs [27, 98], and is described in the section below.

3.3.2 Social Dynamics Model

We model the proportion of visitors who choose to use local firewood, L_i as a function of both the perceived threat of introduced pests, and the social cost of illegally transporting infested firewood. We refer to visitors who choose to use local firewood as local strategists, and visitors who do not use local firewood as transport strategists hereafter. Let C_t be the cost of transporting firewood and C_l the cost to obtain it locally (and therefore avoid moving invasive pests to a patch i). We adopt the social influence model from [25], which is based on models of [27] and [98], which we will summarize below. We define the social utilities corresponding to the strategies of transporting firewood (P_t) and buying it locally (P_l) as

$$P_t = -C_t + s(0.5 - L_i) - fI_i$$

$$P_l = -C_l + s(L_i - 0.5)$$

Transportation becomes a less attractive strategy if infestation is more prevalent, depending on the size of f . The parameter f controls the extent to which a local infestation causes behaviour change in that population. The parameter s controls the degree to which individuals are influenced by the the majority opinion in their patch (i.e. peer pressure). We assume that both local strategists and transport strategists in a patch i , given by L_i and $1 - L_i$ respectively, decide whether to change their strategy at the same rate, σ . Their decision is made by considering which strategy will maximize their utility $P_l - P_t$ at that point, leading to the following expression for the rate of change of the local strategist population:

$$\frac{dL_i}{dt} = \sigma L_i(1 - L_i)(P_l - P_t)$$

We replace the individual costs of C_t, C_l with the net utility value $U = C_t - C_l$. The cost difference U abstracts from the explicit definition of costs of using firewood [25] and allows including exogenous social incentives and motivation, such as awareness about the problem or any other form of social influence from outside each location i . A term B_i is introduced to represent the amount of local firewood available in patch i . For simplicity,

we assume that the tree mortality rate at a patch i is only caused by infestation, so the mortality rate is the same as the death rate of the infested trees

$$\frac{dB_i}{dt} = \underbrace{-\gamma B_i}_{\text{Decay of fallen wood}} + d \underbrace{\sum_{j=1, j \neq i}^N P_{i,j}(1 - C_e)(1 - L_j)I_j}_{\text{Import of fallen wood}} \quad (3.4)$$

Because the infested wood imported into patch i in Eq 3.4 must come from another patch in the system, we subtract the corresponding term for leaving wood, $d \sum_{j=1, j \neq i}^N P_{j,i}(1 - C_e)(1 - L_i)I_i$ from Eq 3.6 which describes the rate of change of infested population in a patch i . Using the notation in equations (3.5, 3.6, 3.7, 3.8), we formulate the problem of buying firewood locally vs. transporting it from other potentially infested locations as follows:

$$\frac{dS_i}{dt} = \underbrace{rS_i \left(1 - \frac{(S_i + I_i)}{K}\right)}_{\text{Logistic Growth Of Forest}} - \underbrace{AS_i(I_i + B_i)\theta_k(I_i - I_a)}_{\text{Infestation term}} \quad (3.5)$$

$$\frac{dI_i}{dt} = \underbrace{-\gamma I_i}_{\text{Death of infested trees}} + \underbrace{AS_i(I_i + B_i)\theta_k(I_i - I_a)}_{\text{Susceptibles become infested}} - d \underbrace{\sum_{j=1, j \neq i}^N P_{j,i}(1 - C_e)(1 - L_i)I_i}_{\text{Total infested wood leaving due to transport}} \quad (3.6)$$

$$\frac{dB_i}{dt} = \underbrace{-\gamma B_i}_{\text{Decay of firewood}} + d \underbrace{\sum_{j=1, j \neq i}^N P_{i,j}(1 - C_e)(1 - L_j)I_j}_{\text{Import of fallen wood}} \quad (3.7)$$

$$\frac{dL_i}{dt} = \sigma L_i(1 - L_i) \left(\underbrace{U}_{\text{Net cost to transport firewood}} + \underbrace{s(2L_i - 1)}_{\text{Social influence term}} + \underbrace{fI_i}_{\text{Impact of infestation}} \right) \quad (3.8)$$

Table 3.1 lists the model notation.

3.3.3 Patch-quarantine strategies

Let $V \subset [1, N]$ be a set of patches under a quarantine. We use the patches (nodes of the camper travel network) with the largest (shortest-path) betweenness centrality [76, 39],

Name	Default Value, (Range explored)	Units	Interpretation
N	2250	Patches	Number of patches in the network
S_i	Site specific	Trees	Number of susceptible trees in patch i
I_i	Site specific	Trees	Number of infested trees in patch i
B_i	Site specific	Trees	Infested firewood in patch i
L_i	Site specific	Unitless	Fraction of local strategists in patch i
r	0.02, [0.01, 0.06]	New trees per tree per year	Tree growth rate
A	0.001, [0.00065, 0.0014]	Number of infested trees per susceptible-infested contact per year	Transmission rate of pest
γ	1.4, [0.8, 1.8]	Trees per year	Decay rate for infested trees
K	5000	Trees	Carrying capacity of each patch
U	0, [-5, 5]	Utility	Social cost to transport firewood, or incentive to buy locally
C_e	0, [0.0, 1.0]	Unitless	Interception fraction
f	0.1, [0.01, 0.13]	Utility per capita	Impact of local infection on strategy
s	0.1	Utility per capita	Strength of social norms
σ	0.1	Strategy changes per capita per year	Rate of social learning
$P_{i,j}$	See below	Unitless	Fraction of trips that go from j to i each year.
d	0.1 [0.05, 0.3]	Logs per year	Rate of transmission of infested firewood between patches
I_a	1 [0.5, 5]	Trees	Value at which transmission rate of pest is halved due to density dependence
k	1	Unitless	Steepness of sigmoid function
V	Empty, [0 patches, 500 patches]	Patches	Set of patches to be quarantined
Δt	0, [0, 5]	Years	Length of quarantine
t_0	0, [0, 5]	Years	Time between initial infestation and patch quarantine

Table 3.1: Parameters and default values

which is a common approach for selecting quarantine nodes in vaccination studies [208]. Betweenness centrality measures the extent to which a node lies on paths between other nodes and is used to detect the amount of influence a particular node has over the flow of information in a graph. The measure is often used to find nodes that serve as critical links between different parts of a graph. Formally, the shortest-path betweenness centrality of a node $i \in V$ on a weighted graph G is

$$g(i) = \sum_{i \neq s \neq t; s, t \in G} \frac{g_{st}(i)}{g_{st}}$$

where g_{st} is the number of shortest paths between nodes s, t and $g_{st}(i)$ is the number of geodesic paths between nodes s, t that go through node i . Both of these measurements calculate path length with respect to the weights of G . In words, the betweenness centrality

$g(i)$ of a node i is the probability that i lies on a shortest path between some two nodes in G . In our camper travel network, higher weights denote more frequent trips, so for the purposes of determining the betweenness centrality, the weight of each edge (i, j) is $\max_{i,j}(P_{ij}) + 1 - P_{ij}$.

We model the implementation of firewood quarantine strategies at patches V by introducing a time-dependent term in Eqs (3.6),(3.7). Let t_0 , and Δt be the starting time of the quarantine and the length of the quarantine respectively. Let $H_c(x, \Delta t)$, defined as

$$H_c(x, \Delta t) = \begin{cases} 1 & x < 0 \\ 0 & 0 \leq x \leq \Delta t \\ 1 & x > \Delta t \end{cases}$$

be an upside-down boxcar function of length Δt . This function acts as a switch which is "off" whenever $x \in [0, \Delta t]$. With this function, we can modify equations (3.6),3.7 so that patches $i \in V$ do not import or export firewood whenever $x \in [0, \Delta t]$.

If $i \in V$,

$$\frac{dI_i}{dt} = -\gamma I_i + AS_i(I_i + B_i)\theta_k(I_i + B_i) - dH_c(t - t_0, \Delta t) \sum_{j=1, j \neq i}^N P_{j,i}(1 - C_e)(1 - L_j)I_j \quad (3.9)$$

$$\frac{dB_i}{dt} = -\gamma B_i + dH_c(t - t_0, \Delta t) \sum_{j=1, j \neq i}^N P_{i,j}(1 - C_e)(1 - L_j)I_j \quad (3.10)$$

Note that the only difference in the new equations (3.9),(3.10) from (3.6),3.7 is in the last term denoting the interactions with neighbouring nodes. The equations for patches not in under quarantine (i.e., not in V) require us to distinguish arcs that connect to and from nodes under quarantine in V .

If $i \notin V$,

$$\begin{aligned} \frac{dI_i}{dt} = & -\gamma I_i + AS_i(I_i + B_i)\theta_k(I_i + B_i) - \sum_{j=1, j \neq i, j \notin V}^N P_{j,i}(1 - C_e)(1 - L_j)I_j \\ & - dH_c(t - t_0, \Delta t) \sum_{j=1, j \neq i, j \in V}^N P_{j,i}(1 - C_e)(1 - L_j)I_j \end{aligned} \quad (3.11)$$

$$\frac{dB_i}{dt} = -\gamma B_i + \sum_{j=1, j \neq i, j \notin V}^N dP_{i,j}(1 - C_e)(1 - L_j)I_j + dH_c(t - t_0, \Delta t) \sum_{j=1, j \neq i, j \in V}^N P_{i,j}(1 - C_e)(1 - L_j)I_j \quad (3.12)$$

In equations (3.11),(3.12) we split the summation term into two summations, one over all patches which are not under quarantine (i.e., not in the set V) and patches under quarantine in V . The latter summation is multiplied by a term, $H_c(t - t_0, \Delta t)$ which switches on and off the quarantine conditions.

3.3.4 Parameterization

We used data from [114] and [216], to quantify the risk of firewood transport to recreational destinations in Central Canada. The data documented the movements of campers to provincial campgrounds in Ontario, Quebec and Manitoba. Such data are maintained by provincial ministries of natural resources (MNRs). The dataset included a large number of potential origin sites (i.e., approximately 9000 locations). To reduce the computational burden, we reduced the size of the camper travel network by including all recreational destination locations but considering only the origin locations in the Canadian provinces of Ontario, Manitoba, and Quebec. We further reduced the size of the network by selecting most travelled routes. We selected the largest subgraph with a minimum degree of 10 (the 10-core of the graph) which considered only the most connected nodes, with largest impact on pest transmission. We implemented the procedure using the NetworkX library [88]. The final camper travel network included 2250 sites (Fig 3.1).

Because the model uses a large camper travel network it has a very large parameter space, and many of the parameters, especially those in Eq 3.8, are difficult to estimate directly from data. In this study we are exploring the region of parameter space that most closely approximates the dynamics in real infestations, such as the typical size and duration of the recent emerald ash borer outbreak in eastern Canada. To select the most relevant range of the social influence parameters, σ, s, f , which are difficult to estimate from the literature, we did sensitivity analyses over a wide range of these parameters, and identified the parameter space where these parameters had the largest effect on the model dynamics, and where the course of the invasion was realistic. The inter-patch and intra-patch infection rate parameters, d, A , were selected to infest and eventually kill at least 95% of the tree population within 10 to 15 years.

We integrated equations (3.5-3.8) using code written in the Julia language, using the JuliaDiffEq library [169]. The integration was run on the Compute Canada clusters. Our primary focus was to explore the relative impacts of firewood enforcement versus public outreach and their abilities to reduce pest infestation rates across the camper travel network. We consider a hypothetical scenario where a harmful invasive pest is introduced in

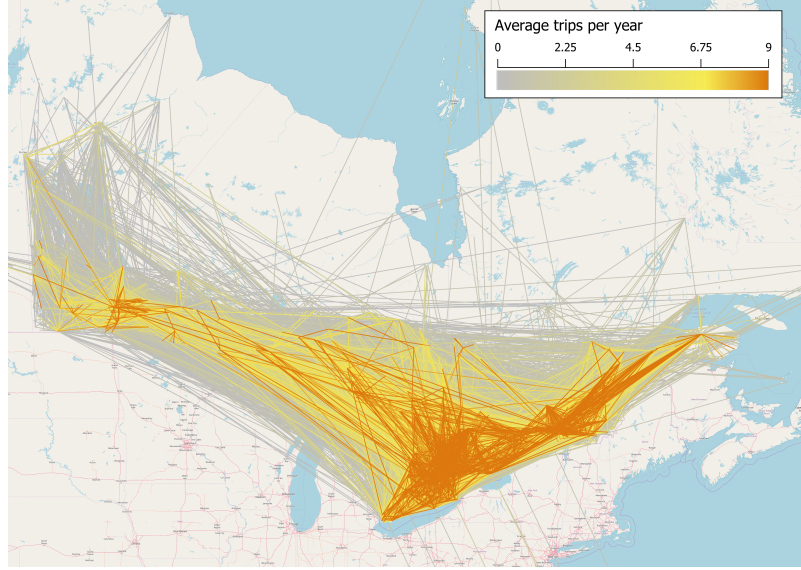


Figure 3.1: **Camper travel network in Ontario, Quebec and Manitoba.** Darker (more orange) lines represent more trips.

the largest urban center in eastern Canada with foreign imports (Greater Toronto Area, GTA) and assume that the bulk host tree population in the GTA is infested. This scenario is based on a history of past entries of invasive wood-boring pests to the GTA with foreign imports (such as introduction of Asian longhorned beetle in Toronto and Mississauga [202]).

3.3.5 Assessing intervention efficacy

The primary statistic we use to assess the total mortality of an infestation after t years is the average cumulative infested population, $\frac{1}{N} \sum_{i=1}^N T_i(t)$. To calculate $T_i(t)$, the cumulative infested population at patch i and time t , we solve the following equation in addition to the model equations.

$$\frac{dT_i}{dt} = AS_i(I_i + B_i)\theta_k(I_i - I_a) \quad (3.13)$$

The right-hand side of equation 3.13 is the only positive term of equation 3.6, so it increases when new infested trees are added to $I_i(t)$, but does not decrease when infested trees die, thereby counting the total number of infestations.

Since it is difficult to determine what utility value U , which defines the social cost of transport, corresponds to the current level of funding, we try to answer whether it would be beneficial to increase the funding, which we call the marginal benefit of increasing U . Given a time \bar{t} , we calculate $T(\bar{t})$ for a set of $U \in [-5, 5]$, then we fit a linear function of U to these points. We find a first-order approximation of $T(\bar{t})$ change per unit U (Fig 3.4) for a given set of parameters and time \bar{t} . A positive slope indicates that total infested tree population increases when U is increased, which means that increasing U does not reduce the impact of the pest (at least, to a first approximation). In figures (3.4) - (3.6) this method is used to show how the total number of infested trees changes with respect to an increase in U , as a function of parameters and time.

3.4 Results

In our baseline scenario (Fig 3.2, parameters as in table 3.1), the model shows a typical pest outbreak originating in the GTA infesting all campgrounds in Ontario, Manitoba and Quebec over 10-20 years. This agrees with the observed timescale of the recent infestation of emerald ash borer (EAB) which entered Ontario in 2002 and now has infested most major populated places in the province [52].

First we discuss the timeseries plot of the baseline parameters (Table 3.1), where the model variables are averaged over all of the patches for easier visualization (Figure 3.2). Accordingly, we define $I(t) = \frac{1}{N} \sum_{i=1}^N I_i(t)$, $B(t) = \frac{1}{N} \sum_{i=1}^N B_i(t)$, $L(t) = \frac{1}{N} \sum_{i=1}^N L_i(t)$, to be the average infested tree population at t , the average quantity of infested logs at t , and the average fraction of local strategists at t , respectively. In figure 3.2, we find that increasing U (the social cost to transport firewood) increases the number of local strategists $L(t)$ (Fig 3.2h)—people who choose not to transport firewood between patches—and also reduces the size of the invasion, (Fig 3.2f) and the average number of infested logs, $B(t)$ (Fig 3.2g). Although the reduction in $B(t)$ is significant (as shown by the large differences in light red and dark red time series in Fig 3.2g), the flattening of the curve for infested trees (Fig 3.2f) is comparatively less significant. We can compare this with the result of increasing the fraction of infested logs intercepted between patches, C_e (3.2a,b,c,d). Increasing C_e decreases the number of infested trees, the delays the peak of the outbreak (Fig 3.2b,c). The delay in the peak of the outbreak also appears to cause the lag in $L(t)$ (Fig 3.2d). Social incentives appear to be very effective at reducing $B(t)$ while being less effective at reducing $I(t)$. This indicates that a shift from transport strategists to local strategists primarily occurs in areas that have already been infested. This effect does not occur with direct interception of infested firewood. Notably, direct interception is difficult

to implement effectively, as even after intercepting high proportions of the infested wood transport, the corresponding decrease in $I(t)$ remains low (Fig 3.2b).

In Fig 3.3 we show the total number of infested trees at time t , $T(t)$, with respect to combinations of U , the social cost to transport firewood, and the fraction of infested firewood intercepted, C_e . If the fraction of intercepted infested firewood, C_e , is greater than 80%, we see a sharp reduction in the total infestation, T , even after 20 years (Fig 3.3 c), but lower interception rates have little effect unless the social cost to transport U is above the threshold seen in panel c) (Fig 3.3). Over a shorter time scale, increasing C_e appears to be effective at all interception rates.

The parameter f controls how the proportion of strategists in a given patch i ($L_i(t)$) responds to the population of infested trees (I_i) in that patch (eqn 3.8). Since social incentives (such as an intervention to human-mediated pest transport) tend to be less effective because they prevent firewood transport mostly in the areas that have already been colonized by pests (as suggested in Fig.3.2), we consider how the parameter f affects the marginal returns on U over time (Fig3.4). The shade of the blue region in Fig.3.4 represents the degree to which increasing U is beneficial, corresponding to a negative slope in the linear approximation of the change in T with respect to U (Fig 3.4 inset). Similarly, a red cell indicates non-negative slope and therefore a neutral or detrimental marginal effect. We begin to see the benefit of increasing U after about 10 years, shown by the transition from lighter blue to dark blue as we move from the bottom of the image to the top (Fig 3.4. This relationship is only affected slightly by altering the impact of local infestation on local strategy, f , where we begin to see slightly detrimental marginal returns after 10 years if $f < 0.04$.

Similarly, we have compared the marginal returns on increasing U with respect to the intra-patch transmission rate A and time t (Fig 3.5). When A is small ($A \leq 0.0009$, beneficial marginal returns on U can be observed over the whole duration of the infestation. We further explore the impact of varying the rate of transmission of infested firewood between patches, d (Fig 3.6). We find a roughly parabola-shaped region in the parameter plane of intra-patch and inter-patch transmission rates (A and d respectively), above which the marginal returns of increasing U are zero or possibly detrimental to the size of the total infested population after 10-20 years. Larger intra-patch transmission rates enable the pest population to establish earlier in a given patch by propagules. We see good marginal return in parameter regimes where few transport strategists (high $L(t)$) would reduce the reproductive ratio of the infection below 1. For instance, at the point $(A, d) = (0.00126, 0.103)$, increasing U is able to delay and eventually prevent a second wave, which decreases the total number of infected trees significantly (SI Fig 1). If the transmission rates A, d are high enough that even with no transport strategists, we get a second wave of

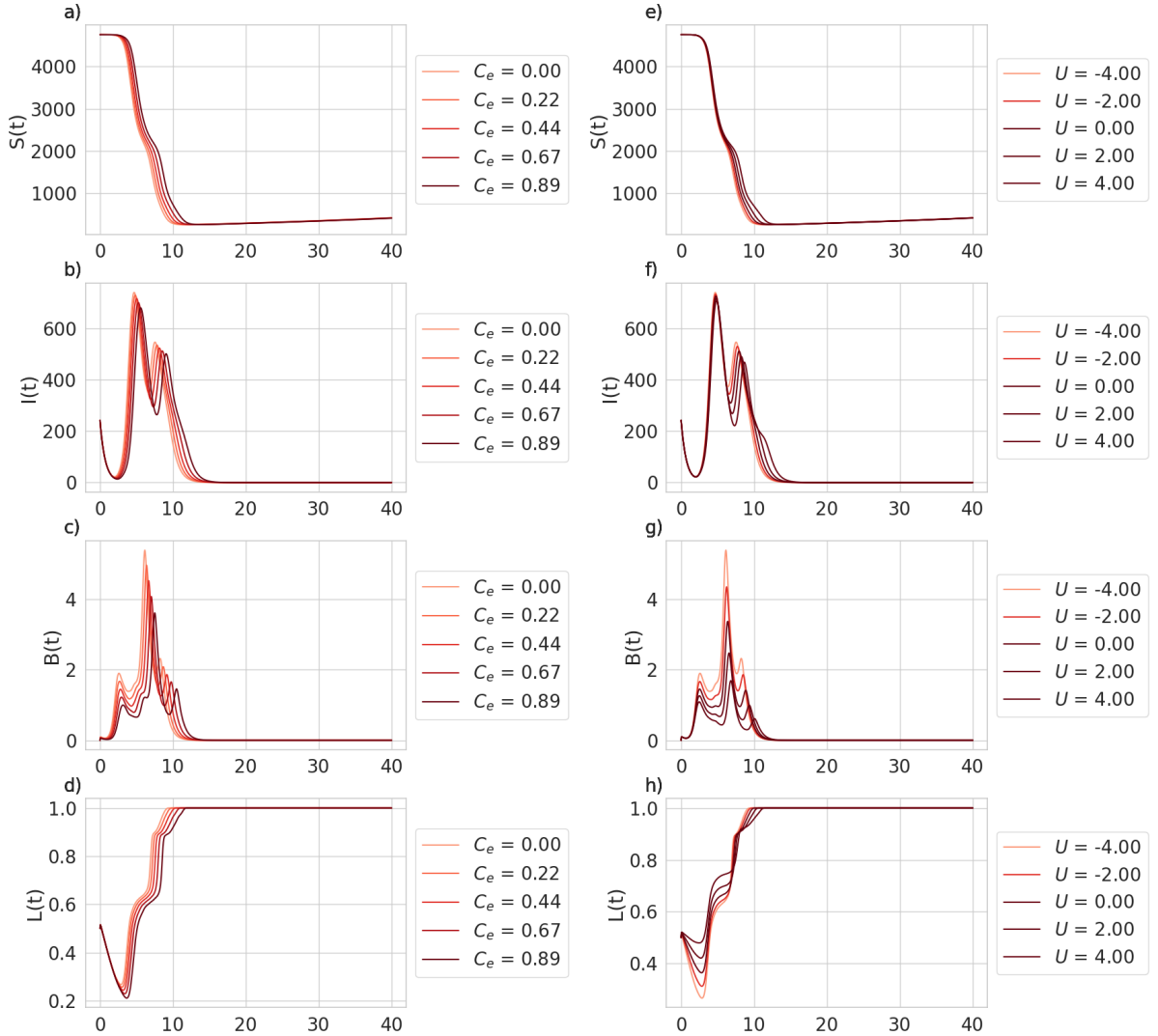


Figure 3.2: **Time series of model variables as a function of interventions, direct (raising C_e , panels a - d) and through social pressure (raising U , panels e - h).** The former intervention, panels a-d, means an increase of social pressure on people who choose to transport firewood (i.e. increasing the U value), and the latter refers to direct interception of firewood (i.e. increasing the C_e value). Terms $L(t) = \frac{1}{N} \sum_{i=1}^N S_i(t)$, $I(t) = \frac{1}{N} \sum_{i=1}^N I_i(t)$, $B(t) = \frac{1}{N} \sum_{i=1}^N B_i(t)$, $L(t) = \frac{1}{N} \sum_{i=1}^N L_i(t)$ are the averages of the state variables over all patches. $S(t)$ has been omitted for brevity.

infection, the effect of increasing U can be slightly detrimental (SI Fig 2). Panel f) of the aforementioned figures plots the number of patches where $I \geq 1$ over time, showing that the detrimental effect is largely due to the infection persisting longer in the network.

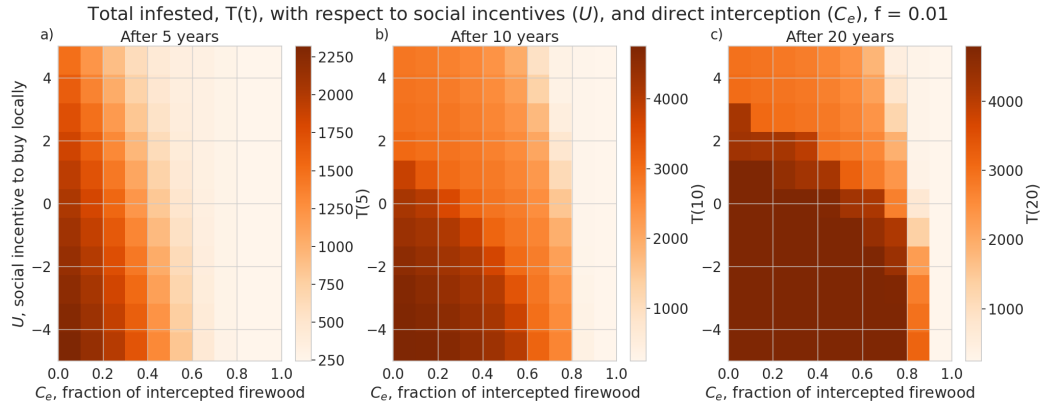


Figure 3.3: **Total infestation per node over 5, 10 and 20 years.** Neither increasing U nor C_e are effective at long time scales.

We also explored the effectiveness of patch quarantine by replacing model equations (3.6) and (3.7) with equations (3.9)-(3.12). This replacement prevents individual patches (nodes in a set V) with the highest betweenness centrality (with respect to the weights P_{ij}) from interacting with their neighbours during the time of the quarantine ($t \in [t_0, t_0 + \Delta t]$). Imposing quarantine on these nodes is expected to have the greatest impact on pest transmission rate. If the quarantine is initiated one year after the pest is introduced into the system (that is, $t_0 = 1.0$) then we find a significant reduction in total infestation even if only 50 patches are quarantined ($|V| = 50$) assuming they are quarantined for more than a year, shown in Fig 3.7. However, in our model, we find that quarantines need to be longer than approximately three years, and involve more than 150 nodes to still be effective in reducing the total infested population after 20 years $T(20)$. An interesting result in our quarantine plots is that we see a slightly larger range of effective parameter values if the quarantine begins after two years, $t_0 = 2.0$ (Fig 3.8), rather than one, $t_0 = 1.0$. This effect is probably due to the delay in infestation after the model is initialized, which can be seen by the local minimum in the infestation timeseries (Fig 3.2b,f).

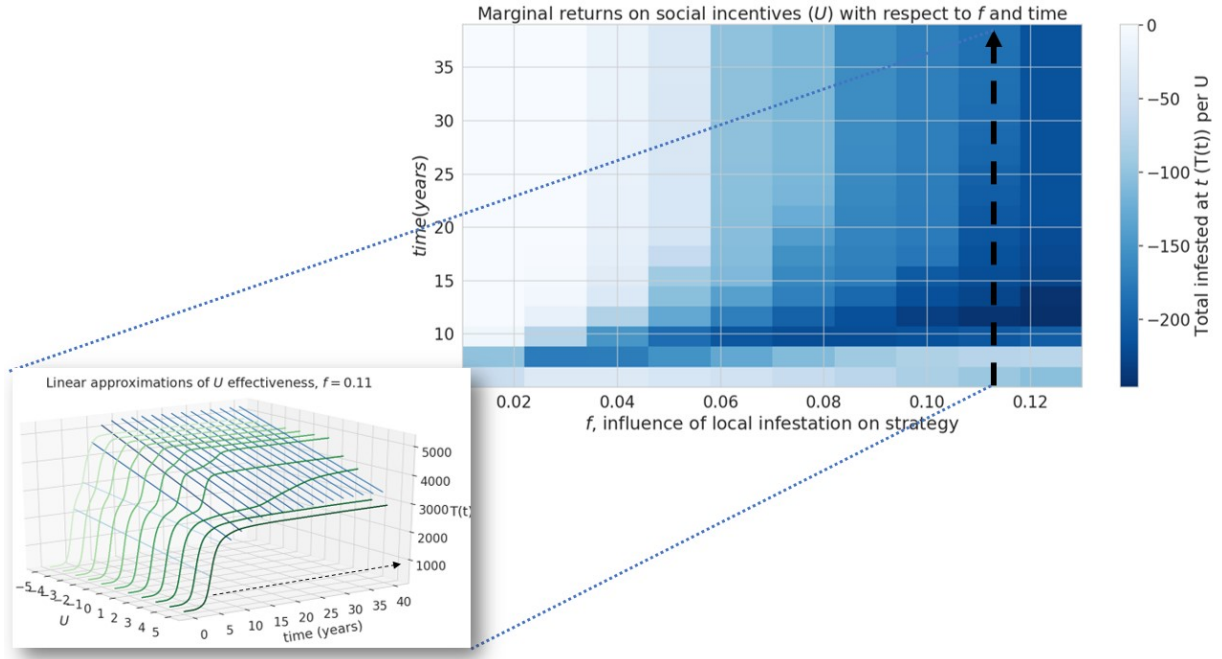


Figure 3.4: **Efficacy of social incentives on infestation after time T .** Inset graph shows an example of cross-section along the line $f = 0.11$. The influence of infestation on transport strategy, f , can hinder the intervention by public outreach, in the long-term (after approximately 20 years). The inset figure illustrates how one column in the heat map, shown by the dotted line, is constructed from the slopes of linear approximations of $T(t)$ over $U \in [-5, 5]$. The blueness of the lines going left to right is a function of their slope, corresponding to the color of the cells in the heatmap.

3.5 Conclusion

We presented a model coupling human social behaviour regarding transport of infested firewood through recreational travel with a model of the spread of an invasive forest pest. Our main focus was to compare, in relative terms, common measures for slowing the spread of invasive species with firewood transport, such as public outreach campaigns aimed to raise awareness about the problem, and enforcement measures, including inspections at checkpoints to control the movement of firewood, and location-specific quarantine. The model is parameterized with campground reservation data for provincial parks and campgrounds in the provinces of Ontario, Manitoba and Quebec, Canada and incorporated

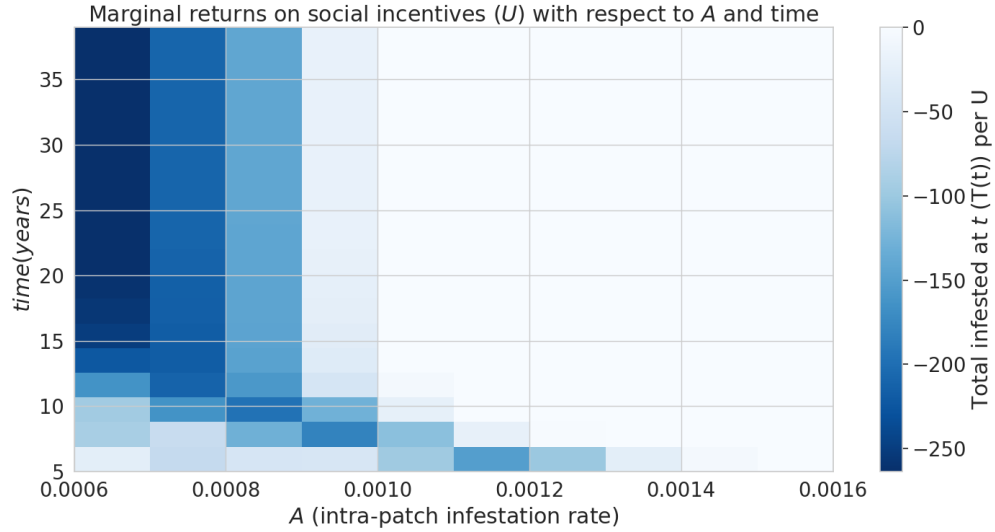


Figure 3.5: **Efficacy of social incentives on infestation after time period T with respect to A , the intra-patch infestation parameter.** This intervention becomes ineffective over time if A is sufficiently large.

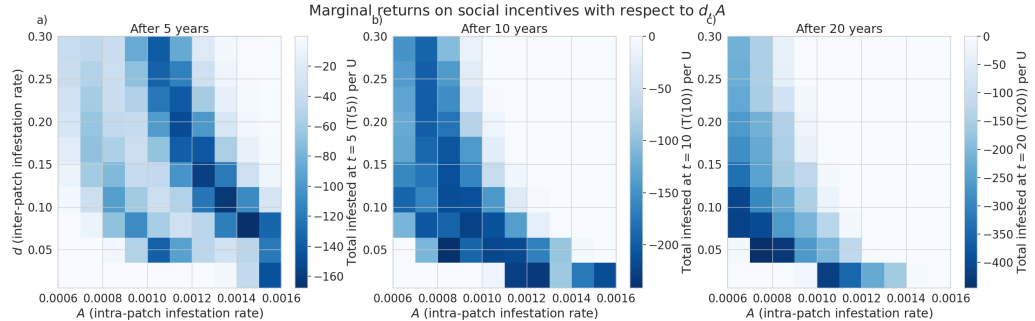


Figure 3.6: **Efficacy of social incentives on infestation after time T intra-patch spreading rate A , affects infestation outcomes.** The social incentive to not transport firewood, U , is more effective with lower pest spread rates.

spatial information on the topology and geographical configuration of the camper travel network.

Under the assumptions of our model and a particular camper travel network configuration used in our model, checkpoints to control the movement of untreated firewood are

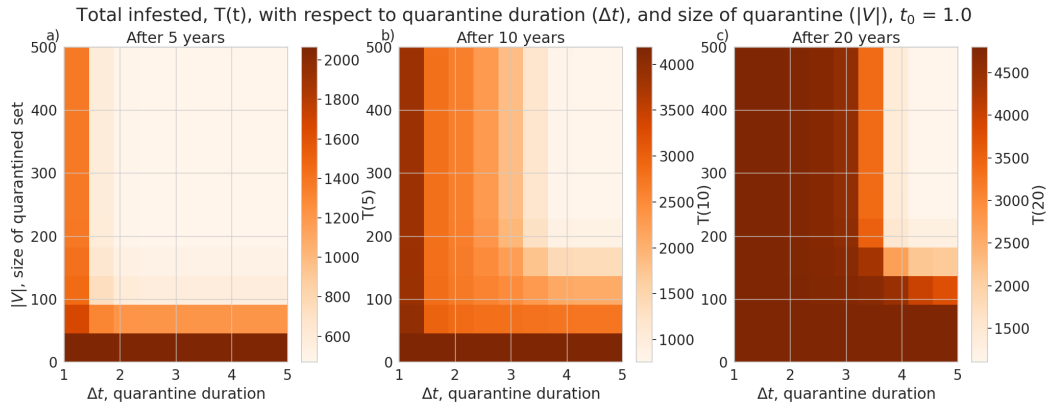


Figure 3.7: **Average total infested trees ($T(t)$) after 5, 10 and 15 years (panels a),b), and c) respectively), assuming the quarantine begins one year after the pest is introduced.** Total infestation plotted with respect to the number of nodes quarantined ($|V|$) and the length of the quarantine (Δt). The quarantine is effective over 5 years with only 50 patches, provided they are closed for over a year.

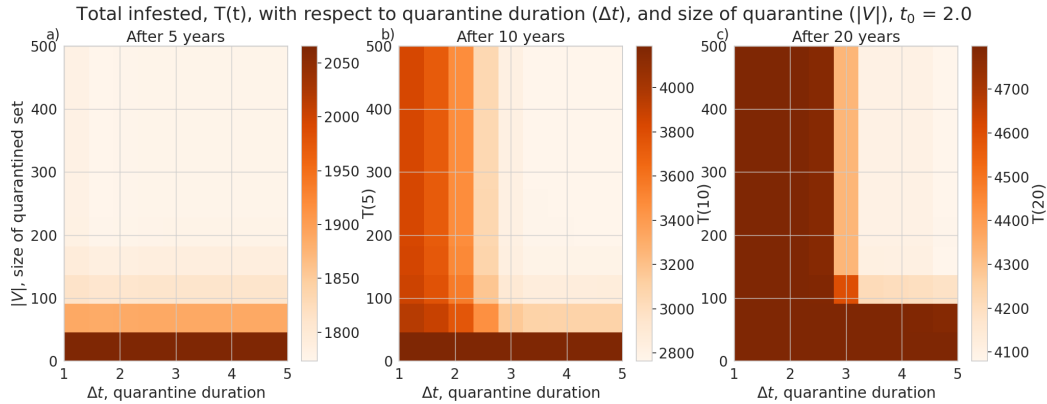


Figure 3.8: **Average total infested trees ($T(t)$) after 5, 10 and 15 years (panels a),b), and c) respectively), assuming the quarantine begins two years after the pest is introduced.** Total infestation plotted with respect to the number of nodes quarantined ($|V|$) and the length of the quarantine (Δt).

unlikely to be effective at slowing the spread of invasive forest pests with firewood transport given typical moderate levels of funding and long delays in the response measures. We find the rate of interception to halve the total infested tree population after 5 years

is about 30% (Fig 3.3), which is unlikely to be achieved in practice given typical limited budgets and personnel constraints in present-day firewood control programs. Given that our model uses somewhat simplified assumptions and does not account for fine-scale logistical constraints (which are inspectors may face in various spatial locations) the actual rate of interception is likely to be lower in practical conditions. While a previous study [25] that used a similar model has demonstrated that social incentives may improve outcomes in a two-patch model under equilibrium conditions, we have found that in our complex landscape network, the outcomes of infestation and invasion control measures are highly dependent on the time scale and the characteristics of the invaders, such as the inter-patch and intra-patch infestation rate. Social incentives (which aim to decrease the transport of firewood, U), are generally able to reduce the infestation rate in the short term but its effectiveness is highly dependent on the ability of the pest to spread and infest other locations (Fig 3.6,3.5) under the conditions we have explored. Humans in our model tend to reduce their transport of firewood between patches in already infested areas, which causes the pest to persist longer in the network (Fig 3.2). Our results show that there could exist a threshold in the pest transmission rate A and the proportion of the infested wood which is turned into firewood, d (Fig 3.6). Below this threshold, it would not be beneficial to increase social outreach (i.e., increase U). This insight could be helpful in determining the spatial allocation of firewood movement control efforts for a particular pest species. We have also found that the location-specific quarantines that aim to restrict the movement of firewood to/from a particular location, might only be effective at slowing the invasion spread if a sufficiently large number (at least 140 in our case) of highly connected locations is quarantined, and the quarantine is established at early stages of infestation (Fig 3.7,3.8).

Given the typical cost limitations and logistics constraints faced by today's firewood control programs, and the assumptions made in our modeling framework, it is unlikely that local quarantine measures could significantly slow the spread of invasive pests through firewood unless drastic control and quarantine measures are undertaken. Public outreach campaigns, while helping increasing awareness of problem, cannot reliably slow the spread of pests within the parameter values tested, when the invasion spreads through a network based on camper travel data in Manitoba, Ontario and Quebec. Within our model, public outreach could be more effective for slow-spreading pests when the organism is able to kill host trees quickly but does not have significant spread capacity (that is, the inter-patch and intra-patch infestation rates are sufficiently small). Direct intervention, such as checkpoint inspections for illegally transported firewood, is also not an option, because meaningful outcomes can only be achieved if significant fractions of firewood transports can be intercepted. We find that patch quarantine is effective at slowing, or even stopping, the spread of an invasive forest pest when a large number of highly-connected patches are

quarantined, for a long enough period. Our results in general terms agree with a present-day situation when numerous outreach and local quarantine measures had limited impact on illegal transport of firewood by campers and failed to slow the spread of wood-boring pests transported with untreated firewood. Our results also indicate that the enforcement campaigns aimed to intercept illegal movement of untreated firewood can only be effective if implemented at very large spatial scales in timely fashion (which, in turn, would require massive amounts of funding and personnel support).

There are some shortcomings to our model that could be addressed in future work. The interventions we study do not have spatial or time specifications for individual locations in the camper travel network. Deciding where and when, to deploy the outreach and enforcement measures in a particular location would be a major enhancement of the model. Second, our model depicted a general problem of an invasive pest spreading with untreated firewood moved by recreational travelers. To adapt the problem to a particular pest species, a more specialized spread model will be required. We simplified the model by assuming that each infested patch provides similar propagule pressure to recreational travellers leaving the infested site. This assumption was made because no data about the actual proportions of infested wood carried by recreational travellers leaving the infested sites were available. Also, our analysis did not offer much insight at the level of individual spatial locations in a camper travel network. A simpler mechanistic model that applies unique pest control decisions at individual spatial locations could potentially address that aspect. Another possible way to simplify the model would be to remove the tree growth dynamics—since it operates on a longer time scale than the infestation spread—and so an invasion model without the forest growth component could be a reasonable approximation for short-term planning horizons. This will be the focus of future efforts.

3.6 Acknowledgements

The authors would like to thank Dr. Hanno Seebens and an anonymous reviewer for their contributions. Their detailed and thorough suggestions have significantly improved the quality of our paper.

Chapter 4

Fire Mitigates Bark Beetle Outbreaks in Serotinous Forests

Bark beetle outbreaks and forest fires have imposed severe ecological damage and caused billions of dollars in lost resources in recent decades. The impact of such combined disturbances is projected to become more severe, especially as climate change takes its toll on forest ecosystems in the coming years. Here, we investigate the impact of multiple disturbances in a demographically heterogeneous tree population, using an age-structured difference equation model of bark beetle outbreaks and forest fires. We identify two dynamical regimes for beetle and fire dynamics. The model predicts that fire helps dampen beetle outbreaks not only by removing host trees but also by altering the demographic structure of forest stands. We show that a stand thinning protocol, which reduces the population size of the largest few juvenile classes by a small percentage, is able to significantly reduce beetle-induced tree mortality. Our research demonstrates one approach to capturing compound disturbances in a mathematical model.

4.1 Introduction

Ecosystems have long been characterized by resilience in the face of large disturbances such as fire, storms, pathogens, and drought, which are often interacting. For example, the pine forests of western North America are highly adapted to both wildfires and bark beetle infestations. Many pine species, including lodgepole (*Pinus contorta*) and ponderosa

This chapter is based on a paper accepted for publication in *Theoretical Ecology*

(*Pinus ponderosa*) pine, depend on stand replacing fires to maintain healthy populations in their endemic range [33].

Of the major natural processes influencing lodgepole pine forests, the two with the greatest potential for large scale disturbance are mountain pine beetle (MPB, *Dendroctonus ponderosae*) and fire [112]. It has been noted that "In western North America, insect outbreaks and wildfires are the two most ecologically and economically significant natural forest disturbances" [138]. The MPB is a small insect endemic to the pine forests of western North America. MPB has recently attained previously unrecorded outbreak levels, probably due to anthropogenic factors [33, 179]. British Columbia's Ministry of Forests estimates that British Columbia contains roughly 35 million acres of lodgepole pine forest (about 23%), and slightly less ponderosa pine forest. They estimate that over the past 20 years, MPB has affected approximately 1.6 million acres of forest annually in British Columbia, more than forest fire and logging combined [30].

Ecological studies examining the relationship between MPB and wildfire damage are numerous, but have not reached a strong consensus in all aspects [21, 134, 189, 38, 112, 138, 5, 185, 107]. Lynch et al. [134] used remote sensing data associated with the 1988 Yellowstone National Park fires to investigate the link between fire prevalence and beetle attack. They found that beetle attack initially lowered the probability of crown fire in a patch, but bark beetle activity significantly increases fire risk 13-16 years in the future. On the other hand, Siedl et al. [185] find that wildfire increases spatial variability in stands, and therefore reduces the susceptibility of the stand to beetle outbreak. To make things more complicated, some studies have found that measures of burn severity are positively correlated with beetle damage[189, 38], although the results of Simard et al. [189] have been disputed by others [142].

MPB, and forest pests more generally, have attracted the attention of mathematical biologists since the 1970s due to importance of the problem and the dynamical complexity of outbreaks. The dynamical model of a full forest ecosystem would be intractable, necessitating simplifying assumptions. An early model of forest-pest dynamics by Ludwig and Holling [132] is a 3-dimensional differential equation model derived from simple population dynamics principles by separating fast (pest dynamics) and slow (forest dynamics). Powell, Logan and Bentz [164], derive a 7-dimensional nonlinear partial differential equation model, incorporating beetle pheromone dynamics, which they then integrate to a local ordinary differential equation model. Others look at just one facet of the forest ecosystem. For instance, since beetle lifecycle depends heavily on temperature, Gilbert and Powell [80] discussed three models which incorporate temperature-dependent emergence and attack. Tree mortality also exhibits sharp transitions as a function of tree vigor. Duncan et al.[67] incorporated a Leslie matrix to explicitly model multiple vigor categories in a

discrete time dynamical model, while Lewis, Nelson, and Xu [124] developed an infinite-dimensional model which accounts for arbitrary vigor distributions. Some recent research also considers dynamic interactions between forest pest outbreaks and human population decision-making regarding transport of infested campfire wood [25, 8].

Whether fire suppression changes stand structure in a way that alters susceptibility to beetle attack is a current topic of research. It has been hypothesized that wildfire encourages variability in spatial structure[185], which inhibits the ability of the bark beetle to find hosts and therefore dampens outbreak dynamics. We hypothesize that demographic variability (in the age structure of tree populations) can have a similar effect on MPB outbreaks. Age structure is pertinent because MPB mortality is much higher among larger, and therefore older, trees [22, 177]. This aspect has been studied in at least two previous models of MPB [124, 67] and has been found to affect system dynamics, although the additional role of fire was not considered in these models. Our objective is to characterize the model dynamics of an age-structured tree stand subject to disturbance from both fire and bark beetles, and to understand how changes in stand age structure due to wildfire or control measures can influence bark beetle outbreaks.

4.2 Methods

4.2.1 Model Description

Our model is based on a discrete-time model developed by Duncan et al.[67], describing beetle-tree dynamics in a well-mixed, sufficiently large, single-species stand. We expand their model to include fire dynamics by introducing a category for burned trees, implemented as a Kermack-McKendrick-style contagious process[70]. We also add stochastic forcing to both the infested category and the burned category. The discrete-time dynamics are defined in terms of population size in the spring of year n . Trees killed by beetle infestation die over the course of a few years, becoming a snag (a dead or dying tree that remains standing), until they decompose enough that they no longer shade the forest floor. If a tree is infested in the summer of year n , its needles will turn red and it will be a "red snag" in the spring of year $n + 1$. Then, in the spring of year $n + 2$, a "grey snag" with grey needles. After this it will decay sufficiently that new juvenile trees can grow up in its place, in year $n + 3$. Wildfire also produces snags: a tree that is standing and shading the forest floor but no longer alive. We assume that wildfire clears the forest faster than MPB infections, so a tree that has been sufficiently affected by fire in the summer of year n becomes a snag in the spring of year $n + 1$, and then the following spring, new juvenile

trees come up in its place. We assume that the forest is at carrying capacity, so new trees can only come up at the locations where trees have died. The forest is assumed to be a monospecies lodgepole pine stand, which are common hosts of MPB in western Canada and the USA.

Age structure is incorporated because beetles cannot effectively infest trees less than a certain diameter in size [177, 7]. Juveniles grow through the K age categories, at a rate of one age class per year, with a probability $(1 - d)$ of surviving until the next year. Figure 4.2.1 illustrates the cycle each category should move through in any particular year. We define the following state variables: $j_{n,k}$ is the population of juvenile trees of age k at year n , $J_n = \sum_{k=0}^K j_{n,k}$, the total number of trees in the Juvenile class, S_n is the population of susceptible trees at year n , I_n is the population of infested trees at year n , and F_n is the population of burned trees at year n .

$$j_{n+1,1} = dJ_n + I_{n-2} + F_n \quad (4.1)$$

New juvenile trees are created each year according to equation 4.1. The number of juveniles of age 1 is equal to the total number of juveniles that died last year, $dJ_n = d \sum_{k=1}^N j_{n,k}$, plus the number of grey snags I_{-2} , plus the number of burnt snags (trees that burned the previous summer) F_n .

The severity of forest fire in year n in the stand as a function of the previously unburned area is

$$P_n = T - \sum_{i=1}^n F_i e^{-\kappa(n-i)} \quad (4.2)$$

where the variable κ determines the half-life of decaying fuel. In other words, we define the severity or size of a fire in the year n as inversely proportional to the amount of land burned in recent seasons.

The growth of juvenile trees is defined by equation 4.3. A fraction $1 - d$ of juveniles from class $k - 1$ grows into class k juveniles, minus the trees in this class that burn, proportional to P_n .

$$j_{n+1,k} = (1 - d)j_{n,k-1} - \frac{\alpha_1}{T} P_n j_{n,k-1}, k = 2 \dots K - 1, K \quad (4.3)$$

The number of susceptibles in the spring of year $n + 1$ is equal to the number of susceptibles in the spring of year n , plus the number of juveniles growing into mature trees $((1 - d)j_n, K)$. We subtract the trees that were infested in the summer of year n , I_n , the

infested *and* burnt trees, $\frac{\alpha_3}{T}P_nI_n$, the trees that were only burnt, $\frac{\alpha_2}{T}P_nS_n$, and the juveniles from class K that would have become mature if they had not caught fire, $(\frac{\alpha_2}{T}P_n(1-d)j_{n,K})$.

$$S_{n+1} = S_n + (1-d)j_{n,K} - \left(I_n + \frac{\alpha_3}{T}P_nI_n\right) - \frac{\alpha_2}{T}P_n(S_n + (1-d)j_{n,K}) \quad (4.4)$$

$$I_{n+1} = r_1 I_n e^{-\beta_1(T-S_n-(1-d)j_{n,K}+(I_n+\frac{\alpha_2}{T}P_nI_n)+\frac{\alpha_2}{T}P_n(S_n+(1-d)j_{n,K}))} - \frac{\alpha_3}{T}P_nI_n \quad (4.5)$$

The model for infested trees is based on ricker-style dynamics, where r_1 is the reproduction rate of beetles, and the exponential term denotes the probability that each individual will find a susceptible tree. The number of infested trees burned is subtracted after reproduction, for simplicity. As in Duncan et al., we have $I_{n+1} = r_1 I_n e^{I_n+I_{n-1}+F_n+J_{n+1}}$, where the exponent is the number of current non-susceptible trees. From the conservation of tree-equivalents $T = I_n + I_{n-1} + F_n + J_{n+1} + S_{n+1}$, so the exponent is just $T - S_{n+1}$.

$$F_{n+1} = P_n \left[\frac{\alpha_1}{T} \sum_{k=1}^{K-1} j_{n,k} + \frac{\alpha_2}{T}(S_n + (1-d)j_{n,K}) + \frac{\alpha_3}{T}I_n \right] + \sigma_F \gamma_n \quad (4.6)$$

The burnt snags in the spring of year $n+1$ is equal to the sum of the number of burnt juveniles ($\frac{\alpha_1}{T}P_n \sum_i^K j_{n,K}$), susceptibles ($\frac{\alpha_2}{T}P_n(S_n + (1-d)j_{n,K})$), and infested ($\frac{\alpha_3}{T}I_nP_n$).

Then, our model is defined by:

$$j_{n+1,1} = dJ_n + I_{n-2} + F_n \quad (4.7a)$$

$$j_{n+1,k} = (1-d)j_{n,k-1} - \frac{\alpha_1}{T}P_n j_{n,k-1}, \quad k = 2 \dots K-1, K \quad (4.7b)$$

$$S_{n+1} = S_n + (1-d)j_{n,K} - \left(I_n + \frac{\alpha_2}{T}P_nI_n\right) - \frac{\alpha_2}{T}P_n(S_n + (1-d)j_{n,K}) - \sigma_F \gamma_n \quad (4.7c)$$

$$I_{n+1} = r_1 I_n e^{-\beta_1(T-S_{n+1})} - \frac{\alpha_2}{T}P_nI_n + \sigma_I \xi_n \quad (4.7d)$$

$$F_{n+1} = P_n \left[\frac{\alpha_1}{T} \sum_{k=1}^{K-1} j_{n,k} + \frac{\alpha_2}{T}(S_n + (1-d)j_{n,K}) + \frac{\alpha_2}{T}I_n \right] + \sigma_F \gamma_n \quad (4.7e)$$

$$P_n = T - \sum_{i=1}^n F_i e^{-\kappa(n-i)} \quad (4.7f)$$

ξ_n and γ_n are normal random variates with zero mean and unit variance, drawn independently in year n . The model conserves the total number of tree-equivalents, which is a

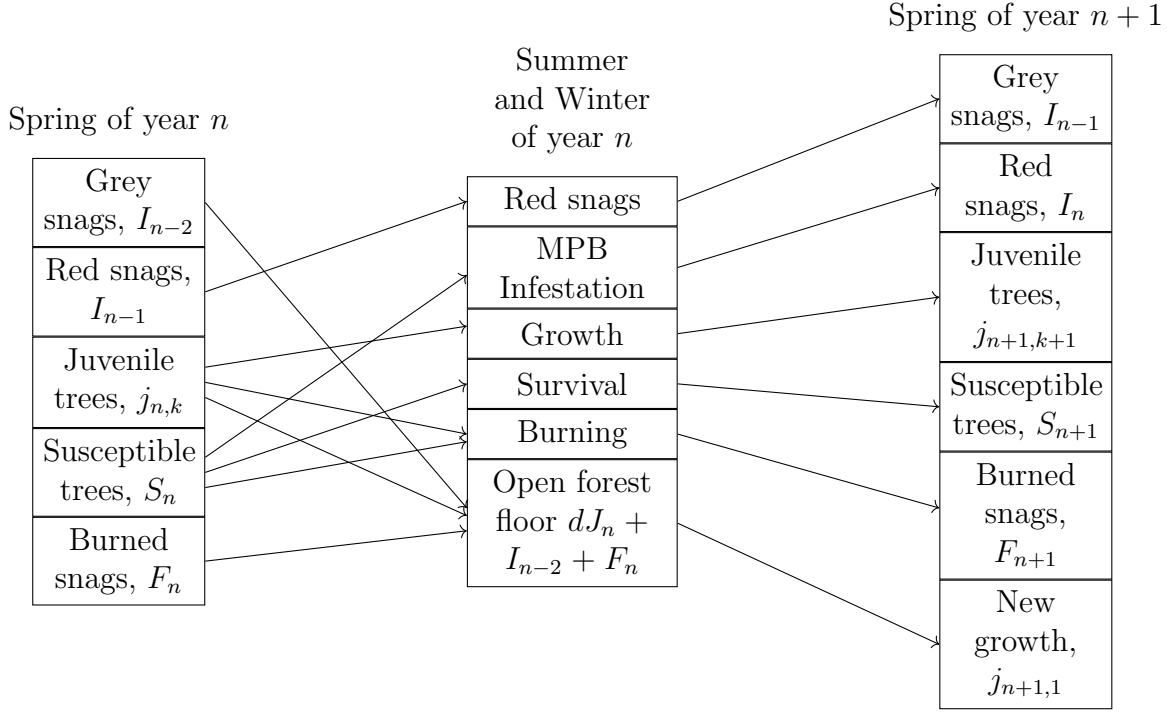


Figure 4.1: Conceptual diagram of compartments (state variables) and transitions between compartments across seasons. See main text and Table 4.1 for definitions of variables and parameters.

tree, a snag, or an open space in the canopy where a tree will grow the next season. The conservation equation is $T = I_{n-1} + I_{n-2} + F_n + J_n + S_n$, which can also be seen as the left or right column in figure 4.2.1. Descriptions of the variables can be found in Table 4.1. Fire could have been modelled in a more complex way using a different timescale than seasonal beetle outbreaks, but we chose to simplify the modelling by matching the timestep of the pest outbreak cycles instead. Fire prevalence is also dependent on precipitation patterns, temperature, human activity, and other factors which operate on different time and spatial scales than our model. We assume this risk is roughly constant each year, and that it contributes to the environmental noise experienced by the system denoted by σ_F .

The following lemma demonstrates that the model equations preserve the total tree equivalent population present in the initial conditions.

Lemma 1. *Let $I_{-1} + I_{-2} + F_0 + J_0 + S_0 = T$. The equation $I_{n-1} + I_{n-2} + F_n + J_n + S_n = T$ is true for all $n \geq 0$ under the evolution equations 4.7a-4.7f.*

Proof. First, notice that the only individuals leaving the Juvenile compartment J_n are the surviving oldest juvenile age class $(1 - d)j_{n,K}$ and the sum of the trees burned from each juvenile age class (except the oldest), $\frac{\alpha_1}{T}P_n \sum_{k=1}^{K-1} j_{n,k}$. The individuals entering the Juvenile compartment are the seedlings germinating in the canopy gaps created by the gray snags I_{n-2} and the trees burned the previous summer, F_n . Therefore we have the following equation for the total number of juvenile trees J_{n+1} .

$$J_{n+1} = J_n - (1 - d)j_{n,K} + I_{n-2} + F_n - \frac{\alpha_1}{T}P_n \sum_{k=1}^{K-1} j_{n,k} \quad (4.8)$$

Then, proceed by induction. The base case, $I_{-1} + I_{-2} + F_0 + J_0 + S_0 = T$, is true by definition. For the inductive step, assume that $I_{n-1} + I_{n-2} + F_n + J_n + S_n = T$ is true, then we have:

$$I_{n-1} + I_{n-2} + F_n + J_n + S_n + (1 - d)j_{n,K} - (1 - d)j_{n,K} = T \quad (4.9a)$$

$$\begin{aligned} &\implies J_n + I_{n-2} + F_n - (1 - d)j_{n,K} + I_{n-1} + S_n + (1 - d)j_{n,K} \\ &\quad + F_{n+1} - \frac{\alpha_1}{T}P_n \sum_{k=1}^{K-1} j_{n,k} - \frac{\alpha_2}{T}(S_n + (1 - d)j_{n,K})P_n \\ &\quad - \frac{\alpha_2}{T}I_n P_n - \sigma_F \gamma_n = T \end{aligned} \quad (4.9b)$$

where we use the definition of F_{n+1} .

$$\begin{aligned} &\implies J_{n+1} + I_{n-1} + S_n + (1 - d)j_{n,K} + F_{n+1} - \frac{\alpha_2}{T}(S_n + (1 - d)j_{n,K})P_n \\ &\quad - \frac{\alpha_2}{T}I_n P_n - \sigma_F \gamma_n = T \end{aligned} \quad (4.9c)$$

(4.9d)

by definition of J_{n+1} .

$$\begin{aligned} &\implies J_{n+1} + I_{n-1} + S_n + (1 - d)j_{n,K} + F_{n+1} \\ &\quad - \frac{\alpha_2}{T}(S_n + (1 - d)j_{n,K})P_n - \frac{\alpha_2}{T}I_n P_n - \sigma_F \gamma_n + I_n - I_n = T \end{aligned} \quad (4.9e)$$

(4.9f)

$$\implies J_{n+1} + S_{n+1} + F_{n+1} + I_n + I_{n-1} = T \quad (4.9g)$$

where we obtain the conservation equation for the spring of year $n + 1$ by definition of S_{n+1} . Therefore the inductive step is true, and the model equations conserve tree equivalents. \square

\square

4.3 Initial conditions

The initial conditions we use in the model are defined as follows.

$$I_0 = 2000 \quad (4.10a)$$

$$I_{-1} = 1000 \quad (4.10b)$$

$$I_{-2} = 0 \quad (4.10c)$$

$$S_0 = 108000 \quad (4.10d)$$

$$F_0 = 1000 \quad (4.10e)$$

$$j_{0,k} = 0, \quad k = 1 \dots K \quad (4.10f)$$

$$(4.10g)$$

These conditions were chosen to provide reasonable representations of the system being modeled. The model appears to be robust to the choice of initial conditions and so the observations in the main text hold for any reasonable set of initial conditions. Note that $I_{-1} + I_{-2} + F_0 + J_0 + S_0 = 110000 = T$, where T is the parameter that determines the total number of stems, from the main text.

4.3.1 Forest thinning protocol (FTP) and controlled burning protocol (CBP)

One of the MPB control methods is to thin the forest, or conduct controlled burns, to increase the overall resilience of the forest to outbreaks or wildfire.[178, 182, 11]. In this section we modify our discrete process to include a control protocol, which is a simplified description of altering the structure of a growing stand to limit susceptibility to MPB. Define τ as the fraction of juvenile trees removed from the m oldest juvenile age classes,

each year. The removed trees are added to the youngest juvenile class, to model trees replaced by seedlings. Since it is not realistic to perform this every year, we also investigate the effect of performing this protocol every 5 years. We will refer to the preceding protocol as the *forest thinning protocol (FTP)*.

$$X_n = \arg \max_{S \subset [1, 50]: |S|=m} \sum_{k \in S} j_{n,k} \quad (4.11)$$

Let X_n be the set of m largest juvenile age classes defined as in equation 4.11. Mathematically, for all age classes $k' \in X_n$, we change equation 4.7b to equation 4.12b. In order to thin the fraction τ of trees from each age class in X_n , we add the corresponding population to $j_{n,0}$.

$$\begin{aligned} j_{n+1,1} &= dJ_n + I_{n-2} + F_n + \sigma_F \gamma_n \\ &+ \tau \sum_{k' \in X_n} \left((1-d)j_{n,k'-1} - \frac{\alpha_1}{T} P_n j_{n,k'} \right) \end{aligned} \quad (4.12a)$$

$$j_{n+1,k'} = (1-\tau) \left((1-d)j_{n,k'-1} - \frac{\alpha_1}{T} P_n j_{n,k'-1} \right), \quad k' \in X_n \quad (4.12b)$$

$$\begin{aligned} F_{n+1} &= P_n \left[\frac{\alpha_1}{T} \sum_{i=1}^{K-1} j_{n,k} + \frac{\alpha_2}{T} (S_n + (1-d)j_{n,K}) + \frac{\alpha_2}{T} I_n \right] + \sigma_F \gamma_n \\ &+ \tau \sum_{k' \in X_n} \left((1-d)j_{n,k'-1} - \frac{\alpha_1}{T} P_n j_{n,k'-1} \right) \end{aligned} \quad (4.12c)$$

Controlled burning is modelled similarly, but instead we add the reduced age compartments to the F compartment as shown in equation 4.12c. We will refer to this modification as the controlled burning protocol (CBP) in the text from here on. We only consider removing juvenile trees because a tree removed before it is susceptible to MPB has the most potential effect on reducing MPB infestation size.

4.3.2 Parameters and simulation design

Table 4.1 contains a list of the parameters used in the model, their interpretation, and their baseline values. Duncan et al. used a similar model with parameters fitted to data as in [5]. We performed sensitivity analysis on all other parameters (including all fire-related parameters) as shown in the Results section.

Table 4.1: Parameters and baseline values of compound fire and pest model. Except for α_i and the noise magnitude, all parameters were obtained from Duncan et al. [67]

Parameter name	Default value	Interpretation	Source
r_1	1.8	yearly fecundity of beetles	[163]
β_1	10.8×10^{-6}	search failure rate of MPB	[163]
d	0.01	annual mortality rate of juveniles	[67]
α_1	-	burning rate of juveniles	-
α_2	-	burning rate of adult trees	-
κ	0.1	decay rate of fuel	-
T	110,000	total number of trees in stand	[163]
K	50	number of juvenile generations	[67]
σ_F	20	noise in burned tree	
σ_I	20	noise in infested tree	
m	0	number of age classes considered by FTP and CBP	
τ	0	fraction of juvenile trees removed from the m age classes with FTP and CBP	

To generate parameter planes, we simulated equations 4.7a-4.7f across a grid of parameter values. We conducted 100 simulations for each point on the parameter grid and computed the average outcome for that grid point. We also recorded a representative sample of the resulting time series. We found the dominant period of the outbreaks by finding the frequency with maximum modulus via the discrete Fourier transform of the time series. In the deterministic case (with no noise), this frequency is the period of the periodic solution. When noise is added and the system becomes stochastic, there is no longer a clear periodic solution, but it is possible to estimate the mean of the distribution of the period by averaging the dominant frequency of the system at equilibrium. The period is assumed to be 1, corresponding to a (stochastic) steady state, if the smallest and largest values of the susceptible timeseries were sufficiently close together. The model and analysis of model output were coded in Julia. Throughout the results section, we mostly focus on the α_1, α_2 plane. We kept the remainder of the parameters constant as it was possible to set their values from empirical literature as described above.

4.4 Results

We first characterize the dynamical regimes of the model as a function of the burning rates α_1, α_2 , and the decay rate κ . Then, we describe how the forest responds to the FTP and CBP described previously. Note that the susceptible class refers to mature trees, i.e., those large enough to be susceptible to infestation by MPB. Maximum outbreak sizes and fire season sizes are taken over a 500 year period.

4.4.1 Dynamical regimes

There are roughly two equilibrium dynamical regimes in the α_1, α_2 parameter plane, although the sizes of the equilibrium populations varies continuously with the parameters inside each dynamical regime. The shapes of these dynamical regimes are affected by the rate of fuel decay, κ .

As α_1, α_2 increase, the model displays larger, and more frequent fires, and smaller MPB outbreaks (Figure 4.2). When α_1, α_2 are small and not equal, years with severe fire seasons roughly follow the same period as MPB outbreaks (Figure 4.2b,d). The variation in fire season size is more pronounced when α_1 is either much larger or smaller than α_2 . This is shown in by the unit period in Figure 4.2d which signifies that the burned tree population is roughly constant and therefore recurs with period one. The presence of large stands

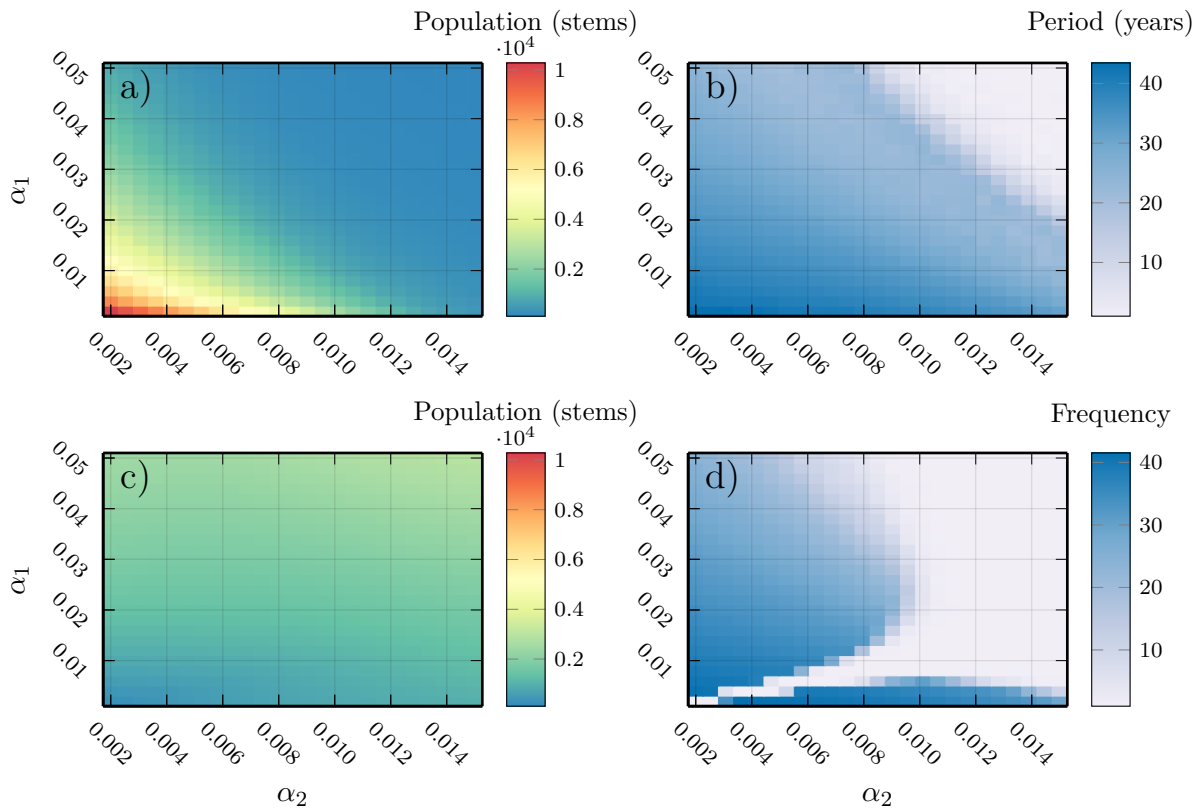


Figure 4.2: Approximate dynamical regimes of the system, where α_1 is the burning rate of juvenile trees, and α_2 is the burning rate of susceptible (mature) trees. a) Average size of largest MPB population (over 500 years at equilibrium) b) Average frequency of MPB outbreaks at equilibrium c) Average size of largest fire season (over 500 years at equilibrium) d) Average frequency of severe fire seasons at equilibrium. The juvenile burning rate (α_1) and susceptible burning rate (α_2) control fire and MPB prevalence. Large α_1, α_2 implies low infestation and also more regularity in the fire regime. All other parameters were set to baseline values (Table 4.1).

with similar ages is determined by the size of the MPB outbreaks, since they mostly affect sufficiently old (susceptible) trees (Figure 4.3a,b). This can be seen in the bump at $k = 40$, which will age out of the juvenile age classes and become a large concentration of susceptible trees, triggering an mpb outbreak. Dead trees from this MPB outbreak clear canopy space for seedlings, which causes another large even-aged stand to arise, and the cycle repeats.

4.4.2 Impact of forest thinning protocol (FTP) and controlled burning protocol (CBP)

The model predicts that the FTP described in section 2.2 (remove a fraction τ of trees in the m oldest juvenile age classes each year) is an effective way to control MPB outbreaks, as long as control intensity parameters are sufficiently large. We consider trimming fractions τ up to 0.15, and the number of age classes trimmed m up to 8.

The FTP reduces the size of MPB outbreaks differently depending on the values of α_1, α_2 (Figure 4.6). The parts of the parameter regime where thinning is most effective at reducing MPB outbreak sizes occur when α_1 is small, where we see approximately 70% smaller MPB outbreaks (Figure 4.6a) for all considered values of α_2 . Generally, parameter ranges where MPB is more prevalent experience the largest reductions. With $\alpha_1 = 0.02, \alpha_2 = 0.0025$, there is a reduction in maximum outbreak population of about 30% when thinning the largest 8 stands by 15% each year (Appendix, figure 28a). With $\alpha_1 = 0.01, \alpha_2 = 0.006$, MPB populations are already damped by the fire regime, but MPB outbreak peak population sizes are reduced from roughly 1600 infested trees to 800 infested (Appendix, figure 28b). A similar practice conducted every five years is almost as effective as the yearly trimming (Figure 4.6b). Maximum MPB infestation sizes for FTP every 5 years and CBP are in the Appendix, figures 28-30. Increasing the heterogeneity of the age distribution in this way always reduces MPB populations by some amount. If we apply the CBP instead (see Equation 4.12c), then controlled burns are largely effective with significant MPB populations, but can worsen outbreaks by up to 80% in regions were the MPB outbreak size is already small (Figure 4.6c).

FTP, and to a lesser extent CBP, does not simply indirectly reduce the number of susceptible trees (and therefore available MPB hosts) but rather flattens the age distribution better to reduce the occurrence of large, even aged, stands. We compare the average susceptible population (Figure 4.5) with and without FTP/CBP and find that in large parts of the parameter regime, the susceptible population is unchanged or increased, despite MPB outbreak sizes being reduced in most areas. Figure 4.4 shows a time-series at the

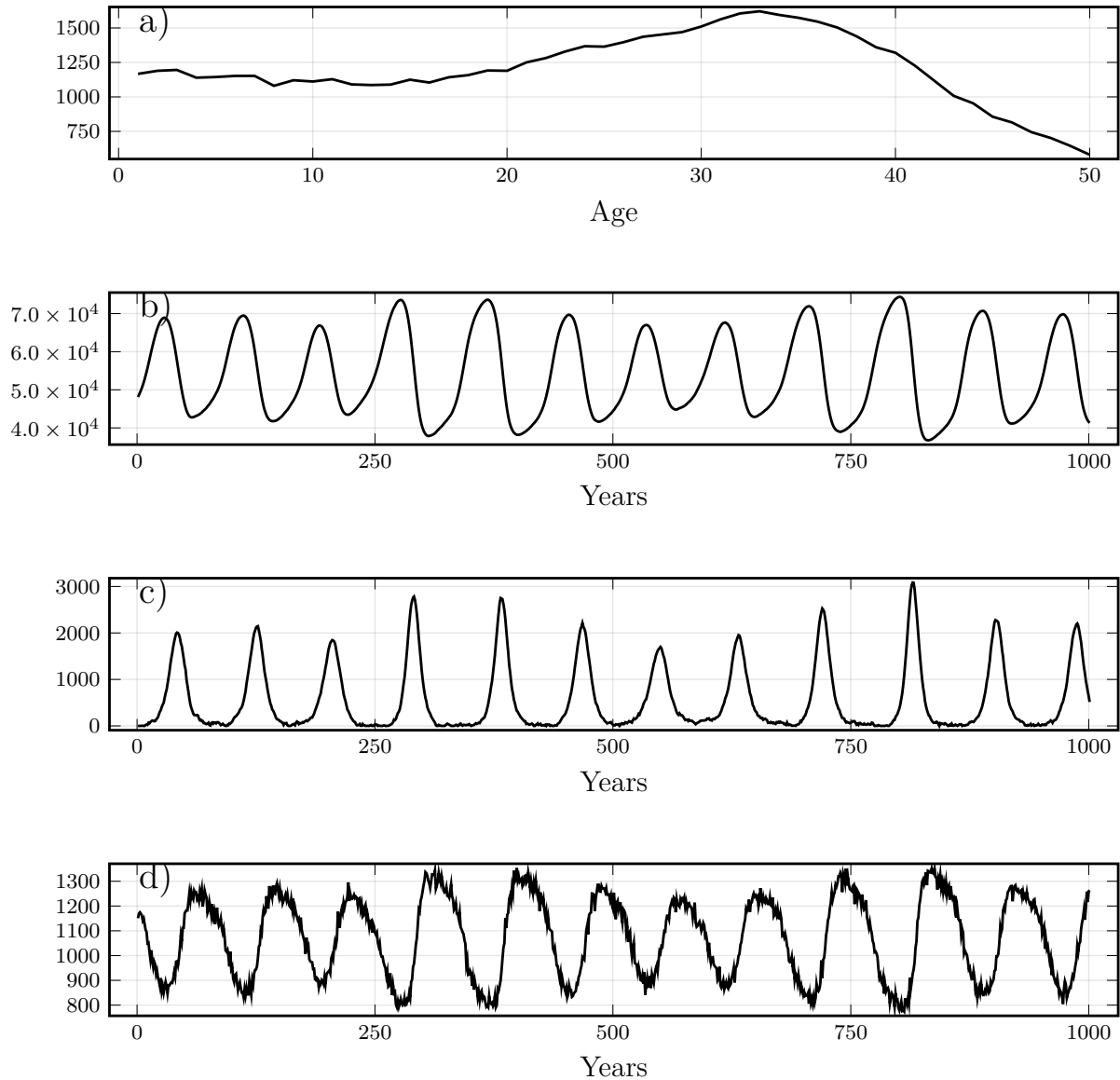


Figure 4.3: Time series of each state variable of a single realization where $\alpha_1 = 0.02$, $\alpha_2 = 0.0025$, showing the regular outbreaks of pests, periodic shifts in fire prevalence, and uneven age distribution generated by MPB outbreaks. a) juvenile distribution at time $t = 2050$ (note different x-axis), b) susceptible population after year t , c) infested tree population after year t , d) number of burned trees after year t . All other parameters were set to baseline values (Table 4.1).

same parameters as Figure 4.3, except with FTP flattening, to show the flattening of the age distribution.

4.5 Discussion

In this paper we used a mathematical model of pest and fire dynamics in pine forests to show how fire can suppress beetle outbreaks. The effect is related not only to the assumption of competition between fire and beetles in the model, but also due to the impact of fire on the age structure of stands: fires remove many large, mature trees and make space for rapidly growing juvenile populations that are not susceptible to forest pest outbreaks. The behaviour of the fire-beetle system is due to the fact that susceptibility to fire cuts across all age classes, compared to beetle outbreaks that affect mostly mature age classes. We show that large outbreaks of wildfires and beetle outbreaks inhabit the same dynamical regime, and that very small beetle populations are consistent with a regular fire regime. These results echo ecological evidence from Kaufmann et al.[112] and Seidl et al.[185] showing that a consistent fire regime can dampen outbreaks of bark beetle in a serotinous forest stand. Furthermore, we showed how a stand thinning protocol can significantly reduce tree mortality due to MPB outbreaks in forests prone to both fire and beetle outbreaks. Only a small intensity of thinning is required to see significant results. Prescribed burning has a similar, although less significant, effect on the age structure of the forest, and therefore similarly dampens MPB outbreaks. Prior to the arrival of European colonists, indigenous americans routinely burned areas in western North America [26], these practices were not recognized as beneficial by colonial governments, and were outlawed [37].

Implications for Fire/beetle management

Our work provides support for the practice of thinning forest stands to create more heterogeneity in age structure [108, 146], despite the absence of spatially explicit dynamics in our model. We show that even small changes to the demographics of forest stands can result in large shifts in forest dynamics, dampening out oscillating disturbance patterns and thereby increasing stand resilience. Using an abstract model for this purpose hopefully allows the evidence to generalize better over the wide range of possible ecosystem parameters.

Evidence in literature for dynamical regimes described

Broadly, our model can describe the current dynamical regime of stands of pine forests in the western interior with low fire susceptibility parameters α_1, α_2 (the bottom right-hand corner of Figure 4.2a) depending on the location and time. Our model represents a

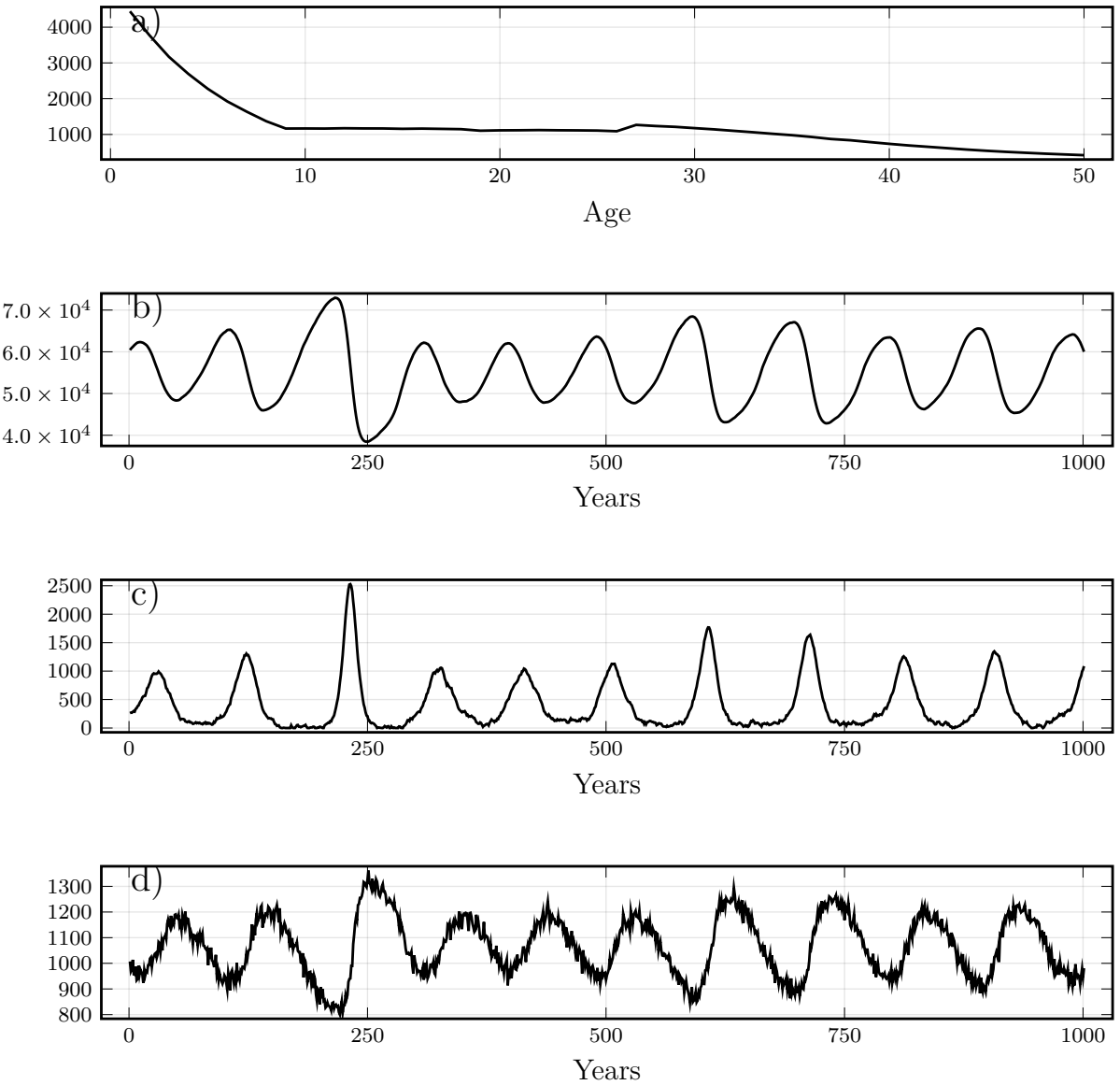


Figure 4.4: Time series showing realization of model under FTP with $\tau = 0.15$ fraction of $m = 8$ juvenile stands cleared, conducted each year, where $\alpha_1 = 0.02$, $\alpha_2 = 0.0025$. a) juvenile distribution at time $t = 2050$ (note different x-axis), b) susceptible population after year t , c) infested tree population after year t , d) burned forest after year t . Notice the flattening of the age distribution compared to the same parameters with no FTP (Figure 4.3)

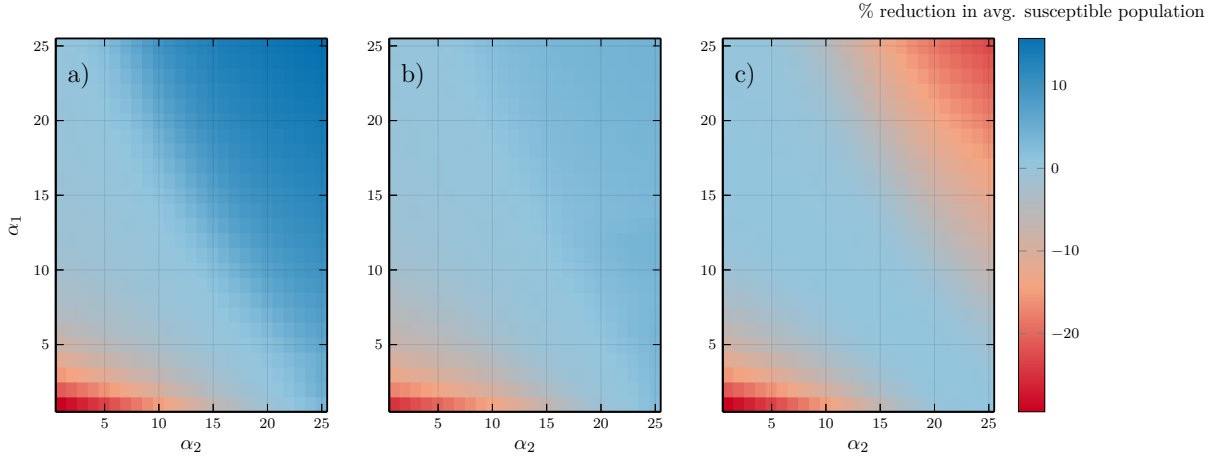


Figure 4.5: Percentage change in average susceptible (mature) forest population compared to no FTP with a) $\tau = 0.15, m = 8$, b) with $\tau = 0.15, m = 8$ applied every 5 years, c) controlled burning with $\tau = 0.15, m = 8$, with respect to burning rates α_1, α_2 . FTP and CBP increase the average population of mature trees in many cases, in addition to reducing outbreak sizes.

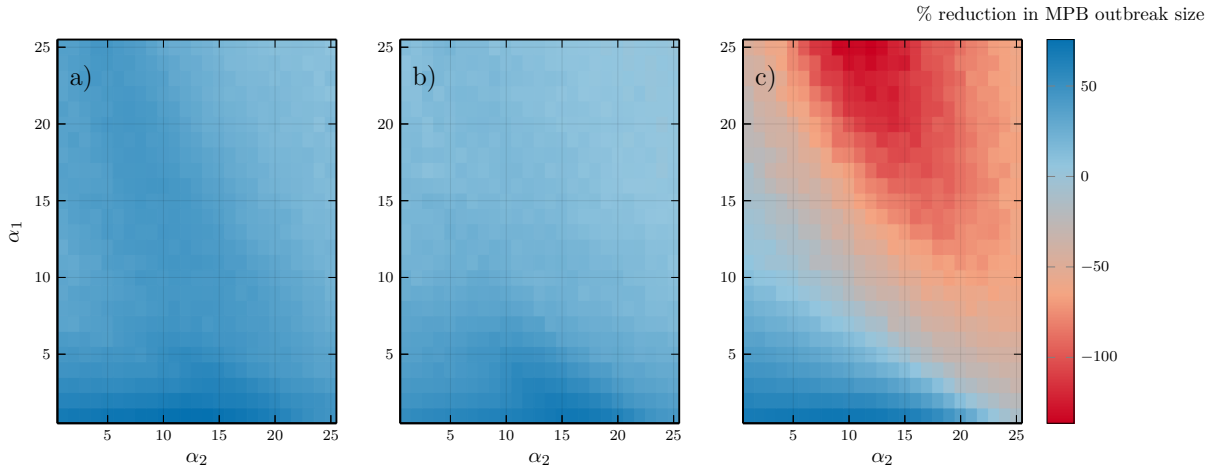


Figure 4.6: Percentage change in maximum MPB infestation size within 500 year period under FTP with a) $\tau = 0.15, m = 8$, b) with $\tau = 0.15, m = 8$ applied every 5 years, c) controlled burning with $\tau = 0.15, m = 8$, with respect to burning rates α_1, α_2 . FTP is always effective at reducing MPB outbreaks, and CBP worsens them if the population of MPB is already low.

single stand with autonomous parameters, and in reality, there are probably many possible dynamical regimes coexisting across the landscape and through time. Taylor and Carroll [194] studied the wildfire and MPB history of interior British Columbia, and also found this dynamic regime, albeit with decreasing prevalence of wildfire and increasing MPB outbreaks through the 20th century. They find that the low frequency and severity of wildfire has increased the percentage of pine in susceptible age classes to 55%, consistent with our estimate for low α_1, α_2 (see Figure 4.3a for an example of the large susceptible stands in this dynamical regime). Axelson et al. [21] records that, for their study area in southern interior British Columbia, there has been a fire-free interval of over 100 years. While this period is much longer than in our model, a trend towards higher variance in fire periods does match our model for the aforementioned parameter range, and a more complex fire model could potentially capture this additional complexity. They also record an average return time of 36 years for MPB in their area, consistent with our estimate for sufficiently low burning parameters. Kulakowski et al. [118] records a similar dynamic regime as [21] for the 20th century, but more frequent fire outbreaks, more closely matching this model.

Implications for Forest Ecosystems

The dry pine forest ecosystem that we model in this paper is home to many vertebrates who react to disturbance, biotic and otherwise, in different ways. Many wood-boring birds use MPB as a food source [148, 162]. Of these bird species, the three-toed woodpecker (*Picoides dorsalis*) and hairy woodpecker (*Leuconotopicus villosus*) depend significantly on bark beetles as a source of food [121]. Accounts estimate that they make up about 23% of the woodpeckers diet on an average year [31], although during outbreak years the fraction could be much larger [121]. Woodpeckers increase their reproduction rate during outbreak years of MPB [72], so dampening MPB outbreaks could be detrimental to bird populations, although there are feedbacks here that warrant further study. At least one predator of MPB, the black-backed woodpecker (*Picoides arcticus*), is heavily dependent on wildfires for habitat. Therefore, improving forest heterogeneity would likely also improve resilience in woodpecker populations which depend on these disturbances for habitat. Small mammals that inhabit western pine forests differ on their preference for burn-cleared habitat [220]. Mammals such as the deer mouse (*Peromyscus maniculatus*) strongly prefer burn clearing [221], while the red backed-vole (*Myodes gapperi*) favors undisturbed stands [220]. Increasing heterogeneity would improve the availability of both open stands for species which prefer the former habitat and closed, undisturbed stands for species which favor the latter. The impact of our results for these ecosystems are likely to be significant, but due to the complex feedbacks mentioned in these relationships, it is difficult to know without extending the model and further empirical data on the strength

of these feedbacks.

The primary goal of this paper was to build on work on the age structured models of beetle-infested stands[67] to a dynamical situation with a more complex disturbance regime that includes wildfire, a common feature of the forests inhabited by MPB. The modelling of fire spread is a very complex problem which is dependent on many variables which are not modelled here. Moreover, the beetle infestation model we used was relatively simple, necessitating use of a simple fire model as well in order to retain tractability of the model. We opted for a simple approach derived from the compartmental modelling literature. The dynamics we see here are an average case, so a more sophisticated fire model would yield more detailed results. The assumed impact of fire on all age classes, and the mechanism through which we model fire spread could also be refined in future work. Snags are also not considered burnable material, which may have an effect on some of the dynamics. We chose not to include these to reduce the number of parameters, especially parameters for which we don't have empirically-derived values. Lastly, the parameters which we drew from Duncan et al. [67] were not tested for sensitivity, and therefore our findings could be affected by these values.

A number of other approaches that relax our simplifying assumptions could be explored in future research. Other models combine annual difference equations with continuous time intra-year equations [193, 134, 53]. A continuous time summer phase is one way we could more accurately explicitly model a wildfire season. The FTP is straightforward and corroborates the findings of similar work with more complex mechanisms [193]. Nevertheless, our control strategies could be significantly more detailed and take into account fire-regimes and current susceptible population. Our goal was to illustrate that we can take advantage of the system dynamics by flattening the age distribution through burning a small percentage of juvenile trees, but more complex strategies might be more efficient. Spatial models would provide even more possibilities for control options. We did not explore the complex relationship between bark beetle emergence and temperature. MPB life-cycles are heavily regulated by temperature: warm years can cause more than one generation to emerge in a season, and severe cold can wipe out large populations. The higher precipitation and temperatures predicted by models of climate change imply conditions more conducive to MPB reproduction and therefore MPB outbreaks. Fire season intensity is also affected by temperature, and some evidence suggests that increasing temperatures and earlier snowmelts are probably creating worse fire seasons in this area [211].

Serotinous forests will be subject to very different environmental regimes in coming decades that involve multiple stressors. We have demonstrated how a model can explore the impact of fire and control protocols on tree stand age structure and thus MPB outbreaks. Future models that account for multiple disturbance mechanisms could be useful

for anticipating how forests will respond to novel environmental regimes in the rest of the twenty-first century.

Funding

This research was supported by an NSERC discovery grant to Chris T. Bauch and Madhur Anand.

Conflicts of interest/Competing interests

The authors declare no competing interests.

Availability of data and material

Not Applicable.

Code availability

The source code for this work can be found at the author's public git repository: <https://git.uwaterloo.ca/pjentsch/fire-mitigates-bark-beetle-outbreaks-in-serotinous-forests>

Authors' contributions

All authors conceived ideas for the study. PCJ designed and coded the model, performed analyses, created figures, and drafted the manuscript. All authors revised the manuscript

Chapter 5

Conclusion

5.1 Summary of findings

I have presented three projects that exhibit extensions of models of complex infectious systems. The technique used in each chapter was to project the time-evolution of a particular population with age or spatial structure into the language of dynamical systems and use the tools we have in that realm to hopefully provide insight about the corresponding natural system. It is common to imagine complex systems in nature, such as a population undergoing a pandemic, as a dynamical system with an enormous but finite number of dimensions. Understanding of such a massive system can be at least partially achieved by projecting down to the low-dimensional space which preserves the most significant features.

The first chapter presented a model of Sars-CoV-2 spreading throughout a population, coupled to population opinion dynamics on the use of NPIs. The mortality rate after Covid-19 diagnosis varies significantly based on age, therefore our research questions for this model regarded age-based vaccination strategies. We used an age-structured compartmental model to represent the population for this reason. Availability of vaccines, lockdown timing, distancing and the effect of these factors on vaccination planning were explored in the analysis. Age-specific transmission is proportional to empirically-derived location specific contact rates given by Prem et al [166]. The contribution of the contact rates for a given location to the overall contact rate is determined by the fraction of people using NPIs at that point, and the government lockdown policy. The fraction of people using NPIs is also treated as a dynamic variable. The evolution over time of NPI use is determined by a replicator equation where the payoff for using NPIs depends on the current ascertained case level, and the current population sentiment towards NPIs. We fit

all parameters, using both case and mobility data from the beginning of the pandemic in Ontario, until November 12th, 2020. A fraction of the vaccines available in a given day are allocated to each age group according to a vaccination strategy. Vaccines leftover from the age groups specified in the strategy are distributed uniformly to the remaining age groups. The four vaccination strategies considered are: oldest first, youngest first, uniform, and contact-based. The contact-based strategy determines proportions based upon the groups most likely to be infected, according to the contact matrices. In contrast, the oldest-first strategy represents vaccination of groups most vulnerable to Sars-CoV-2 infection. Our model shows that under some conditions, such as a low vaccination supply, and an early vaccination begin date, the contact-based vaccination strategy is most effective at reducing mortality in the long term. Otherwise, it is best to vaccinate the oldest (most vulnerable) populations first.

In the second chapter, we extended a model of forest pest spread via firewood transport of [25] to a network, and analysed the efficacy of various prevention mechanisms. Compartmental models are designed to represent populations that are approximately well-mixed, that is each member of a compartment has the same statistical properties as any other member. In the case of the forest pest model, we assume that each patch of forest is homogenous, but that these homogenous patches are connected via human transport of trees as firewood. It is common in eastern North America to see individuals selling wood from trees on their property, and this is often more convenient than wood from inside the park area. Research has shown that at least a few invasive insects harmful to forest ecosystems in North America are transported this way [114, 199, 87]. Barlow et al. [25] therefore couple the infection dynamics of the forest pest to the social dynamics of firewood transport. Their models coupled only a few patches of forest, and only considered altering the price of firewood as a countermeasure. Our extension of their model to an empirical network of several thousand patches [114] incorporated other methods of slowing the spread, such as direct interception, broader information campaigns, and patch quarantine, in order to inform policy. Our analysis consisted of evaluating these countermeasures over realistic parameter ranges to determine the conditions under which each is a feasible approach to slow the spread of invasive species. We found that extraordinary measures are needed to demonstrably reduce total attack rates of a pest over 20 years from detection, over most parameter values.

The third chapter of this thesis covered our investigation of a simple fire model coupled to the MPB model of Duncan et al [67]. As discussion in the introduction, wildfire is a crucial part of the ecosystem where MPB is native. The host species that MPB prefers most are highly adapted to frequent wildfires, and depend on these disturbances to out-compete other tree species and maintain the large monospecific stands that we observe.

The model we present and analyze is a discrete-time compartmental model, where the host population is age structured. A discrete-time model is used because MPB lifecycles can be approximated well as discrete generations. The host population is age-structured because the susceptibility of a tree to MPB increases sharply at a certain DBH (diameter at breast height), which we assume to be achieved once a host tree reaches 50 years old. To match the discrete yearly approximation of forest dynamics, we also use a dynamical model for the yearly fire burn area. We find that, despite the simplicity of the model, the interaction of these two processes arrives at useful insights. We show that wildfire can increase heterogeneity of stand structure such that MPB outbreak sizes are small. Specifically, increase the susceptibility of a stand to stand-clearing fires provides a regular disturbance, which flattens the age structure of the stand. This confirms old observations made by forest ecologists [112, 185], but in a very general model. To this end, we show that even small adjustments to the age structure of juvenile trees in a stand can have large effects in increasing the resilience of a stand against MPB outbreaks.

These chapters are novel in their application of existing human-environment modeling ideas to questions pertinent to disease and forest pest dynamics. As discussed in the introduction, individual participation is critical to the effectiveness of many NPIs against Covid-19. Age-structure vaccine prioritization has been modelled elsewhere [44, 46], but not coupled to behavioural dynamics. Chapter 2 addresses this gap in the literature. Chapter 3 expands upon Barlow et al. [25] to use a large real world network, and introduces further interventions. Chapter 4 sheds light on the function of stand structure in wildfire-MPB dynamics. To our knowledge, it is the first analysis of a mechanistic model of stand dynamics subject to these coupled disturbances. The human aspect of this system is the form of the control mechanism we suggest. This research addresses the dearth of models coupling wildfire and MPB in a dynamical system, despite the importance of these disturbances.

5.2 Discussion

Throughout this thesis we have discussed infections in human-environment systems, represented with compartmental systems of differential or difference equations. We use this framework as a way to homogenize attributes of the population for a particular application. Assuming that there is some spatial or age structure on the hosts lets us further subdivide the population. Analysis of disease models can be focused on the dynamics of a particular outbreak, or set of outbreaks, represented by the transient behavior of the underlying dynamical system. These are generally characteristics of the model output immediately after

the introduction of a small number of infected hosts into the population, until the outbreak has ended because the infection has reached an equilibrium. Our model of Covid-19 (Chapter 2) follows the outbreak transient from the first day with more than 50 cases until mid-november when the manuscript was submitted for publication. Similarly, our model for forest pest transport (Chapter 3) considers the outbreak transients arising from the introduction of a new invasive forest pest into the Greater Toronto Area, and minimizing the length of these transients with a few methods. In contrast, Chapter 4 covered a model of an endemic forest pest. MPB has been a naturally occurring part of the ecosystem it resides in for many thousands of years, and therefore we assume it has reached an equilibrium solution. Analysis for a disease endemic to humans could follow a similar pattern. For instance, Chitnis et al. studied conditions for the stability of endemic malaria [58]. Even with systems considering an endemic infection, we can look at transients following some perturbation to the system, such as outcomes following vaccination against human papillomavirus [122].

Indirect protection from infection is a consistent theme throughout this thesis. In an otherwise homogenous model, indirect protection is representable through additional age structure (chapters 2, 4) or spatial structure (chapter 3) in the host population of an infectious process. We explicitly discuss indirect protection frequently in the context of disease models and immunization, but it is also present under the concept of heterogeneity in ecological systems. Chapter 4 studies the indirect protection created by heterogeneous age structure, and shows that it can be maintained by wildfire disturbances in a specific forest ecosystem. Chapter 3 discusses indirect protection, in the form of patch quarantine. In that chapter we conclude that adequate indirect protection is difficult to achieve in a model with many perfectly well-mixed pockets (the individual forest patches). Although, it should be noted that patch quarantine in the forest-pest model context is necessarily a much weaker form of indirect protection than, for example, vaccination in a disease model.

In all three chapters, methods for increasing resilience of host populations to infectious agents are compared. Age-based vaccination strategies (chapter 2), forest pest mitigation strategies (chapter 3), and forest thinning protocols (chapter 4) are evaluated in terms of their host mortality reduction. We test each strategy over a large range of the parameter space to understand when each strategy works and why. Furthermore, strategies are often learned from the structure of the model itself. The contact-based vaccination strategy in chapter 2, for instance, is derived from the model for contact patterns. Similarly, the stand thinning protocol (FTP in chapter 4) was created to use features of the stand dynamics present in the MPB-fire model.

5.3 Limitations and future work

The work in this thesis is focused on models to understand how dynamics act upon major features of a given system. Our model of Covid-19 was designed to provide guidance on the broad strokes of a vaccination response, and since its publication there has been some work confirming our findings in other settings [56, 99]. There are still some areas where we could have improved the model, and opportunities for modeling responses to future pandemics. The vaccination response in our paper is defined by a fraction of vaccines allocated to each age group, if there are fewer people in that age group than vaccines available for that day, these vaccines are allocated uniformly over the remaining age groups. A more intuitive way to allocate available vaccines, and the way that this has been implemented in many jurisdictions, would be with a priority list. In Ontario, Canada, for instance, vaccines were made available first to healthcare workers and the very old, and then those with high risk health conditions. We assume, for simplicity, that the vaccination rate is constant, but vaccination availability usually ramps up as supply chains are developed. Since the results of the paper are dependent on the vaccination rate, a non-constant vaccination rate would improve predictions. An extension of the model that includes vaccine hesitancy is considered in this chapter, where there is room for additional research. As vaccination against Covid-19 comes underway in 2021, there have been many more cases of hesitancy than we initially considered [184, 191, 49].

Socio-epidemic models, particularly those based upon game theoretic assumptions about belief formation, usually do not account for structural inequalities present in the study population. We refer to inequality as structural when properties inherent to the construction of health institutions, economic systems, social organizations, and governments result in worse outcomes for certain groups of people living within these systems [90, 170, 175]. The Covid-19 pandemic has magnified and exacerbated many of these structural inequalities [18, 215, 54, 55, 36, 204, 100, 207]. Our model in chapter 2 assumes that NPI usage is based on a combination of state policy and individual perception of the severity of the pandemic. While NPI protocols in reality are implemented jurisdiction-wide, actually following these protocols is often a privilege for the wealthy and white for reasons such as access to transportation, housing conditions, and food insecurity [106, 136]. While we incorporate essential work in chapter 2, we do not incorporate the fact that essential workers are overwhelmingly marginalized groups [119]. In Ontario, paid sick leave was only granted to workers on April 29th, 2021, over one year after the beginning of the pandemic [12]. Behavioral models of vaccination hesitancy are subject to similar criticism. For marginalized groups, there are reasons to distrust a vaccine that should not be described as defecting from the co-operative strategy. Among others, black and indigenous people

in North America have survived many centuries of medical experimentation by European colonists [155, 209] which could contribute to vaccine hesitancy [105, 35]. A lack of vaccine uptake could also be due to the significant inequities in vaccine distribution, which we ignore by focusing on vaccine hesitancy [103, 154, 60]. In short, game theoretic models generally assume that decisions are based firmly in individual choice, an assumption which does not accurately describe the social and material landscape many people exist within. Nevertheless, population behaviour is an important and often neglected aspect of disease spread. Further research should explore frameworks of behavioural modeling that are able to incorporate these issues.

Chapter 3 attempts to generally address invasive forest pests in Ontario, Manitoba and Quebec in a network of well-mixed patches of forest. The model in this section uses available traffic data to parameterize the relative magnitude of pest spread between patches, but data on spatial spread of forest pests would be greatly beneficial to calibrate the model for particular species. The complexity and scale of the patch quarantine in the model could be increased further. Our model considered closure of a set number of patches for a fixed time, where patches were closed based upon network centrality. More complex methods could be implemented where patches are closed partially and reactively, based on detected pest locations. Given more data, we could use information about specific pests to better inform patch closure. Beliefs about firewood transport are probably less susceptible to the limitations of behavioural models mentioned in the previous paragraph. Our assumption that each patch has its own independent beliefs about firewood transport was not explored in the chapter. It is likely that the behavioural dynamics are strongly coupled, and that urban centres are more susceptible to messaging about the dangers of firewood transport than rural areas. The assumption of well-mixed patches aligning with campsites could also be relaxed. One approach would be an agent-based model of the real forested patches in eastern Canada overtop the same campsite network. This method adds orders of magnitude to the dimensionality of the problem, which would be difficult to understand without additional data on pest spread.

The core idea of chapter 4 is that age structure in ecosystems, and the way that disturbances interact within an age structured population, is a useful perspective in understanding them. Rather than adding complexity to our model of MPB and wildfire, an approach that has been explored in many detailed agent-based simulations [48, 158, 4, 129], it would be interesting to explore similar disturbances which might have interactions on a structured population. For example, periodical cicada populations exhibit different predators depending on their life stage [128], which can be longer than the life stage of their predators.

5.4 Concluding comments

We presented three models aiming to understand the effects of infectious agents within complex human-environment systems. These approaches are novel in their treatment of coupled interactions between these infectious agents, and other significant aspects of their respective systems. Through their application we have gained new insight into the dynamics of such systems, provided actionable policy recommendations, and confirmed patterns observed in empirical research. We hope that future work will be able to extend our methodology to address new problems in these areas.

References

- [1] Impact of covid-19 on people's livelihoods, their health and our food systems. <https://www.who.int/news/item/13-10-2020-impact-of-covid-19-on-people%27s-livelihoods-their-health-and-our-food-systems>, October 2020.
- [2] WHO announces COVID-19 outbreak a pandemic. <https://www.euro.who.int/en/health-topics/health-emergencies/coronavirus-covid-19/news/news/2020/3/who-announces-covid-19-outbreak-a-pandemic>, December 2020.
- [3] James K Agee. *Fire ecology of Pacific Northwest forests*. Island press, 1996.
- [4] Alan A Ager, Andrew McMahan, Jane L Hayes, and Eric L Smith. Modeling the effects of thinning on bark beetle impacts and wildfire potential in the blue mountains of eastern oregon. *Landscape and Urban Planning*, 80(3):301–311, 2007.
- [5] Michelle C Agne, Travis Woolley, and Stephen Fitzgerald. Fire severity and cumulative disturbance effects in the post-mountain pine beetle lodgepole pine forests of the pole creek fire. *Forest Ecology and Management*, 366:73–86, 2016.
- [6] Muntasir Alam, KM Ariful Kabir, and Jun Tanimoto. Based on mathematical epidemiology and evolutionary game theory, which is more effective: quarantine or isolation policy? *Journal of Statistical Mechanics: Theory and Experiment*, 2020(3):033502, 2020.
- [7] René I Alfaro, Rochelle Campbell, Paula Vera, Brad Hawkes, Terry L Shore, et al. Dendroecological reconstruction of mountain pine beetle outbreaks in the chilcotin plateau of british columbia. In *Mountain Pine Beetle Symposium: Challenges and solutions*. TL Shore, JE Brooks, and JE Stone (editors). Kelowna, BC, pages 245–256, 2003.

- [8] Qasim Ali, Chris T Bauch, and Madhur Anand. Coupled human-environment dynamics of forest pest spread and control in a multi-patch, stochastic setting. *PLoS one*, 10(10):e0139353, 2015.
- [9] Francesco Allemano. Kissabc.jl. <https://github.com/JuliaApproxInference/KissABC.jl>, 2020.
- [10] Marco A Amaral, Marcelo M de Oliveira, and Marco A Javarone. An epidemiological model with voluntary quarantine strategies governed by evolutionary game dynamics. *arXiv preprint arXiv:2008.05979*, 2020.
- [11] GD Amman and JA Logan. Silvicultural control of mountain pine beetle: prescriptions and the influence of microclimate. *American Entomologist*, 44(3):166–178, 1998.
- [12] Alexandra Anadarajah, Fusco Alessandra, and Andrew Shaw. Paid sick leave in ontario for reasons related to COVID-19, 2021.
- [13] Kristian G Andersen, Andrew Rambaut, W Ian Lipkin, Edward C Holmes, and Robert F Garry. The proximal origin of sars-cov-2. *Nature medicine*, 26(4):450–452, 2020.
- [14] Roy M Anderson, B Anderson, and Robert M May. *Infectious diseases of humans: dynamics and control*. Oxford university press, 1992.
- [15] Roy M Anderson and Robert M May. Vaccination and herd immunity to infectious diseases. *Nature*, 318(6044):323–329, 1985.
- [16] Sean C Anderson, Andrew M Edwards, Madi Yerlanov, Nicola Mulberry, Jessica Stockdale, Sarafa A Iyaniwura, Rebeca C Falcao, Michael C Otterstatter, Michael A Irvine, Naveed Z Janjua, et al. Estimating the impact of COVID-19 control measures using a bayesian model of physical distancing. *medRxiv*, 2020.
- [17] Michael A Andrews and Chris T Bauch. Disease interventions can interfere with one another through disease-behaviour interactions. *PLoS computational biology*, 11(6):e1004291, 2015.
- [18] Adjoa Anyane-Yeboa, Toshiro Sato, and Atsushi Sakuraba. Racial disparities in covid-19 deaths reveal harsh truths about structural inequality in america. *Journal of internal medicine*, 288(4):479–480, 2020.

- [19] Stephen F Arno. Forest fire history in the northern rockies. *Journal of Forestry*, 78(8):460–465, 1980.
- [20] Australian Government, Department of Health. Australian influenza surveillance report. 2(20 April to 3 May 2020), 2020.
- [21] Jodi N Axelson, René I Alfaro, and Brad C Hawkes. Influence of fire and mountain pine beetle on the dynamics of lodgepole pine stands in british columbia, canada. *Forest Ecology and Management*, 257(9):1874–1882, 2009.
- [22] Jodi N Axelson, René I Alfaro, and Brad C Hawkes. Changes in stand structure in uneven-aged lodgepole pine stands impacted by mountain pine beetle epidemics and fires in central british columbia. *The Forestry Chronicle*, 86(1):87–99, 2010.
- [23] Atoossa Bakhshaii and Edward A Johnson. A review of a new generation of wildfire–atmosphere modeling. *Canadian Journal of Forest Research*, 49(6):565–574, 2019.
- [24] Frank Ball, Tom Britton, Thomas House, Valerie Isham, Denis Mollison, Lorenzo Pellis, and Gianpaolo Scalia Tomba. Seven challenges for metapopulation models of epidemics, including households models. *Epidemics*, 10:63–67, 2015.
- [25] Lee-Ann Barlow, Jacob Cecile, Chris T Bauch, and Madhur Anand. Modelling interactions between forest pest invasions and human decisions regarding firewood transport restrictions. *PloS one*, 9(4):e90511, 2014.
- [26] Stephen W Barrett and Stephen F Arno. Indian fires as an ecological influence in the northern rockies. *Journal of Forestry*, 80(10):647–651, 1982.
- [27] Chris T Bauch. Imitation dynamics predict vaccinating behaviour. *Proceedings of the Royal Society B: Biological Sciences*, 272(1573):1669–1675, 2005.
- [28] Chris T Bauch and Samit Bhattacharyya. Evolutionary game theory and social learning can determine how vaccine scares unfold. *PLoS Comput Biol*, 8(4):e1002452, 2012.
- [29] Chris T Bauch and David JD Earn. Vaccination and the theory of games. *Proceedings of the National Academy of Sciences*, 101(36):13391–13394, 2004.
- [30] BC Ministry of Forests, Mines and Lands. The state of british columbia’s forests, 3rd ed., 2010.

- [31] Foster Ellenborough Lascelles Beal. *Food of the woodpeckers of the United States*. Number 37. US Department of Agriculture, Biological Survey, 1911.
- [32] Barbara Bentz, James Vandygriff, Camille Jensen, Tom Coleman, Patricia Maloney, Sheri Smith, Amanda Grady, and Greta Schen-Langenheim. Mountain pine beetle voltinism and life history characteristics across latitudinal and elevational gradients in the western united states. *Forest Science*, 60(3):434–449, 2014.
- [33] Barbara J Bentz, Jacques Régnière, Christopher J Fettig, E Matthew Hansen, Jane L Hayes, Jeffrey A Hicke, Rick G Kelsey, Jose F Negrón, and Steven J Seybold. Climate change and bark beetles of the western united states and canada: direct and indirect effects. *BioScience*, 60(8):602–613, 2010.
- [34] Alan A Berryman, Nils Chr Stenseth, and David J Wollkind. Metastability of forest ecosystems infested by bark beetles. *Population Ecology*, 26(1):13–29, 1984.
- [35] Laura M Bogart, Bisola O Ojikutu, Keshav Tyagi, David J Klein, Matt G Mutchler, Lu Dong, Sean J Lawrence, Damone R Thomas, and Sarah Kellman. Covid-19 related medical mistrust, health impacts, and potential vaccine hesitancy among black americans living with hiv. *Journal of acquired immune deficiency syndromes (1999)*, 86(2):200, 2021.
- [36] Lisa Bowleg. We're not all in this together: on covid-19, intersectionality, and structural inequality, 2020.
- [37] Robert Boyd. Indians, fire and the land.
- [38] Tim Bradley and Paul Tueller. Effects of fire on bark beetle presence on jeffrey pine in the lake tahoe basin. *Forest Ecology and Management*, 142(1):205–214, 2001.
- [39] Ulrik Brandes. On variants of shortest-path betweenness centrality and their generic computation. *Social Networks*, 30(2):136–145, 2008.
- [40] Fred Brauer. Compartmental models in epidemiology. In *Mathematical epidemiology*, pages 19–79. Springer, 2008.
- [41] Fred Brauer, Carlos Castillo-Chavez, and Zhilan Feng. *Mathematical models in epidemiology*, volume 32. Springer, 2019.
- [42] EG Brockerhoff and AM Liebhold. Ecology of forest insect invasions. *Biological Invasions*, 19(11):3141–3159, 2017.

- [43] M Brown, TA Black, Z Nesic, VN Foord, DL Spittlehouse, AL Fredeen, NJ Grant, PJ Burton, and JA Trofymow. Impact of mountain pine beetle on the net ecosystem production of lodgepole pine stands in british columbia. *Agricultural and Forest Meteorology*, 150(2):254–264, 2010.
- [44] Kate M Bubar, Stephen M Kissler, Marc Lipsitch, Sarah Cobey, Yonatan Grad, and Daniel B Larremore. Model-informed COVID-19 vaccine prioritization strategies by age and serostatus. *medRxiv*, 2020.
- [45] James H Buck and Jordan M Marshall. Hitchhiking as a secondary dispersal pathway for adult emerald ash borer, agrilus planipennis. *Gt Lakes Entomol*, 41:197–199, 2009.
- [46] Jack H Buckner, Gerardo H Chowell, and Michael R Springborn. Optimal dynamic prioritization of scarce COVID-19 vaccines. *medRxiv*, 2020.
- [47] Thomas M Bury, Chris T Bauch, and Madhur Anand. Charting pathways to climate change mitigation in a coupled socio-climate model. *PLoS computational biology*, 15(6):e1007000, 2019.
- [48] Megan K Caldwell, Todd J Hawbaker, Jenny S Briggs, PW Cigan, and Susan Stitt. Simulated impacts of mountain pine beetle and wildfire disturbances on forest vegetation composition and carbon stocks in the southern rocky mountains. *Biogeosciences*, 10(12):8203–8222, 2013.
- [49] Timothy Callaghan, Ali Moghtaderi, Jennifer A Lueck, Peter J Hotez, Ulrich Strych, Avi Dor, Erika Franklin Fowler, and Matt Motta. Correlates and disparities of covid-19 vaccine hesitancy. Available at SSRN 3667971, 2020.
- [50] Natural Resources Canada. Emerald ash borer. <https://www.nrcan.gc.ca/our-natural-resources/forests/wildland-fires-insects-disturbances/top-forest-insects-and-diseases-canada/emerald-ash-borer/13377>.
- [51] Natural Resources Canada. Mountain pine beetle (factsheet). <http://www.nrcan.gc.ca/forests/fire-insects-disturbances/top-insects/13397>, Feb 2017.
- [52] Canadian Food Inspection Agency (CFIA). <https://www.inspection.gc.ca/plants/plant-pests-invasive-species/insects/emerald-ash-borer/areas-regulated/eng/1347625322705/1367860339942>, 2019.
- [53] Renato Casagrandi and Sergio Rinaldi. A minimal model for forest fire regimes. *The American Naturalist*, 153(5):527–539, 1999.

- [54] Jarvis T Chen and Nancy Krieger. Revealing the unequal burden of covid-19 by income, race/ethnicity, and household crowding: Us county versus zip code analyses. *Journal of Public Health Management and Practice*, 27(1):S43–S56, 2021.
- [55] Jarvis T Chen, Pamela D Waterman, and Nancy Krieger. Covid-19 and the unequal surge in mortality rates in massachusetts, by city/town and zip code measures of poverty, household crowding, race/ethnicity, and racialized economic segregation. In *Harvard Center for Population and Development Studies*. Harvard Center for Population and Development Studies, 2020.
- [56] Xianhao Chen, Guangyu Zhu, Lan Zhang, Yuguang Fang, Linke Guo, and Xinguang Chen. Age-stratified covid-19 spread analysis and vaccination: A multitype random network approach. *IEEE Transactions on Network Science and Engineering*, 2021.
- [57] B Chen-Charpentier and Maria Conceição A Leite. A model for coupling fire and insect outbreak in forests. *Ecological modelling*, 286:26–36, 2014.
- [58] Nakul Chitnis, Jim M Cushing, and JM Hyman. Bifurcation analysis of a mathematical model for malaria transmission. *SIAM Journal on Applied Mathematics*, 67(1):24–45, 2006.
- [59] Vittoria Colizza and Alessandro Vespignani. Invasion threshold in heterogeneous metapopulation networks. *Physical review letters*, 99(14):148701, 2007.
- [60] Giselle Corbie-Smith. Vaccine hesitancy is a scapegoat for structural racism. In *JAMA Health Forum*, volume 2, pages e210434–e210434. American Medical Association, 2021.
- [61] H Ken Cordell. The latest trends in nature-based outdoor recreation. *Forest History Today, Spring 2008*, 2008.
- [62] H Ken Cordell. Outdoor recreation trends and futures: a technical document supporting the forest service 2010 rpa assessment. *Gen. Tech. Rep. SRS-150. Asheville, NC: US Department of Agriculture Forest Service, Southern Research Station*, 167 p., 150:1–167, 2012.
- [63] H Ken Cordell, Carter Betz, and Gary T Green. Nature-based outdoor recreation trends and wilderness. *International Journal of Wilderness, August 2008, Volume 14, Number 2, Page 7-13*, 2008.

- [64] Timothy J Cudmore, Niklas Björklund, Allan L Carroll, and B Staffan Lindgren. Climate change and range expansion of an aggressive bark beetle: evidence of higher beetle reproduction in naïve host tree populations. *Journal of Applied Ecology*, 47(5):1036–1043, 2010.
- [65] Asli Demircue-Kunt, Michael Lokshin, and Ivan Torre. The sooner, the better: The early economic impact of non-pharmaceutical interventions during the covid-19 pandemic. *World Bank Policy Research Working Paper*, (9257), 2020.
- [66] Odo Diekmann, JAP Heesterbeek, and Michael G Roberts. The construction of next-generation matrices for compartmental epidemic models. *Journal of the Royal Society Interface*, 7(47):873–885, 2010.
- [67] Jacob P Duncan, James A Powell, Luis F Gordillo, and Joseph Eason. A model for mountain pine beetle outbreaks in an age-structured forest: Predicting severity and outbreak-recovery cycle period. *Bulletin of mathematical biology*, 77(7):1256–1284, 2015.
- [68] Jonathan Dushoff, Joshua B Plotkin, Cecile Viboud, Lone Simonsen, Mark Miller, Mark Loeb, and JD David. Vaccinating to protect a vulnerable subpopulation. *PLoS Med*, 4(5):e174, 2007.
- [69] Paul FJ Eagles. Trends in park tourism: Economics, finance and management. *Journal of sustainable tourism*, 10(2):132–153, 2002.
- [70] Leah Edelstein-Keshet. *Mathematical models in biology*, volume 46. SIAM, 1988.
- [71] Leah Edelstein-Keshet. *Mathematical models in biology*. SIAM, 2005.
- [72] Amanda B Edworthy, Mark C Drever, and Kathy Martin. Woodpeckers increase in abundance but maintain fecundity in response to an outbreak of mountain pine bark beetles. *Forest Ecology and Management*, 261(2):203–210, 2011.
- [73] Songlin Fei, Randall S Morin, Christopher M Oswalt, and Andrew M Liebhold. Biomass losses resulting from insect and disease invasions in us forests. *Proceedings of the National Academy of Sciences*, 116(35):17371–17376, 2019.
- [74] Neil Ferguson, Daniel Laydon, Gemma Nedjati Gilani, Natsuko Imai, Kylie Ainslie, Marc Baguelin, Sangeeta Bhatia, Adhiratha Boonyasiri, ZULMA Cucunuba Perez, Gina Cuomo-Dannenburg, et al. Report 9: Impact of non-pharmaceutical interventions (npis) to reduce covid19 mortality and healthcare demand. 2020.

- [75] Seth Flaxman, Swapnil Mishra, Axel Gandy, H Juliette T Unwin, Thomas A Mellan, Helen Coupland, Charles Whittaker, Harrison Zhu, Tresnia Berah, Jeffrey W Eaton, et al. Estimating the effects of non-pharmaceutical interventions on covid-19 in europe. *Nature*, 584(7820):257–261, 2020.
- [76] Linton C Freeman. A set of measures of centrality based on betweenness. *Sociometry*, pages 35–41, 1977.
- [77] Sebastian Funk, Erez Gilad, Chris Watkins, and Vincent AA Jansen. The spread of awareness and its impact on epidemic outbreaks. *Proceedings of the National Academy of Sciences*, 106(16):6872–6877, 2009.
- [78] Sebastian Funk, Marcel Salathé, and Vincent AA Jansen. Modelling the influence of human behaviour on the spread of infectious diseases: a review. *Journal of the Royal Society Interface*, 7(50):1247–1256, 2010.
- [79] Ken Gibson, Sandy Kegley, and Barbara Bentz. Mountain pine beetle. *Forest Insect and Disease Leaflet No. 2. FS-R6-RO-FIDL# 2/002-2009. Portland, OR: US Department of Agriculture, Forest Service, Pacific Northwest Region. 12 p.*, 2009.
- [80] Estella Gilbert, James A Powell, Jesse A Logan, and Barbara J Bentz. Comparison of three models predicting developmental milestones given environmental and individual variation. *Bulletin of Mathematical Biology*, 66(6):1821, 2004.
- [81] Globalnews. The dates and staggered starts for all GTA schools. September 2020. <https://globalnews.ca/news/6668240/coronavirus-ontario-schools-closed/>.
- [82] Globalnews Canada. Coronavirus: All publicly funded schools in ontario closing for 2 weeks due to COVID-19. March 2020. <https://globalnews.ca/news/6668240/coronavirus-ontario-schools-closed/>.
- [83] Robert Gooding-Townsend. The forest transition and ecological thresholds: resilience, recovery, and predictions. Master’s thesis, University of Waterloo, 2018.
- [84] Google, Inc. COVID-19 community mobility reports, September 2020. Available at <https://www.google.com/{COVID}19/mobility/>.
- [85] Tim R Gottwald, Gareth Hughes, James H Graham, Xiaoan Sun, and Tim Riley. The citrus canker epidemic in florida: the scientific basis of regulatory eradication policy for an invasive species. *Phytopathology*, 91(1):30–34, 2001.

- [86] Robert A Haack, Kenneth R Law, Victor C Mastro, H Sharon Ossenburghen, and Bernard J Raimo. New york's battle with the asian long-horned beetle. *Journal of Forestry*. 95 (12): 11-15., 2(12), 1997.
- [87] Robert A Haack, Toby R Petrice, and Alex C Wiedenhoeft. Incidence of bark-and wood-boring insects in firewood: a survey at michigan's mackinac bridge. *Journal of Economic Entomology*, 103(5):1682–1692, 2010.
- [88] Aric Hagberg, Pieter Swart, and Daniel S Chult. Exploring network structure, dynamics, and function using networkx. Technical report, Los Alamos National Lab.(LANL), Los Alamos, NM (United States), 2008.
- [89] WILLIAM HEATON Hamer. *Epidemic disease in England: the evidence of variability and of persistency of type*. Bedford Press, 1906.
- [90] Angela P Harris and Aysha Pamukcu. The civil rights of health: A new approach to challenging structural inequality. *UCLA L. Rev.*, 67:758, 2020.
- [91] Kirsten A Henderson, Madhur Anand, and Chris T Bauch. Carrot or stick? modelling how landowner behavioural responses can cause incentive-based forest governance to backfire. *PloS one*, 8(10):e77735, 2013.
- [92] Kirsten A Henderson, Chris T Bauch, and Madhur Anand. Alternative stable states and the sustainability of forests, grasslands, and agriculture. *Proceedings of the National Academy of Sciences*, 113(51):14552–14559, 2016.
- [93] Daniel A Herms and Deborah G McCullough. Emerald ash borer invasion of north america: history, biology, ecology, impacts, and management. *Annual review of entomology*, 59:13–30, 2014.
- [94] Herbert W Hethcote. An age-structured model for pertussis transmission. *Mathematical biosciences*, 145(2):89–136, 1997.
- [95] Herbert W Hethcote. The mathematics of infectious diseases. *SIAM review*, 42(4):599–653, 2000.
- [96] Joe Hilton and Matt J Keeling. Estimation of country-level basic reproductive ratios for novel coronavirus (COVID-19) using synthetic contact matrices. *medRxiv*, 2020.
- [97] Susanne H Hodgson, Kushal Mansatta, Garry Mallett, Victoria Harris, Katherine RW Emary, and Andrew J Pollard. What defines an efficacious covid-19 vaccine?

a review of the challenges assessing the clinical efficacy of vaccines against sars-cov-2. *The lancet infectious diseases*, 2020.

- [98] Josef Hofbauer, Karl Sigmund, et al. *Evolutionary games and population dynamics*. Cambridge university press, 1998.
- [99] Alexandra B Hogan, Peter Winskill, Oliver J Watson, Patrick GT Walker, Charles Whittaker, Marc Baguelin, Nicholas F Brazeau, Giovanni D Charles, Katy AM Gaythorpe, Arran Hamlet, et al. Within-country age-based prioritisation, global allocation, and public health impact of a vaccine against sars-cov-2: a mathematical modelling analysis. *Vaccine*, 2021.
- [100] Aggie J Yellow Horse, Tse-Chuan Yang, and Kimberly R Huyser. Structural inequalities established the architecture for covid-19 pandemic among native americans in arizona: a geographically weighted regression perspective. *Journal of Racial and Ethnic Health Disparities*, pages 1–11, 2021.
- [101] Thomas House and Matt J Keeling. Deterministic epidemic models with explicit household structure. *Mathematical biosciences*, 213(1):29–39, 2008.
- [102] Clinton Innes, Madhur Anand, and Chris T Bauch. The impact of human-environment interactions on the stability of forest-grassland mosaic ecosystems. *Scientific reports*, 3(1):1–10, 2013.
- [103] James Iveniuk and Scott Leon. An uneven recovery: Measuring covid-19 vaccine equity in ontario, 2021.
- [104] WR Jacobi, BA Goodrich, CM Cleaver, et al. Firewood transport by national and state park campers: a risk for native or exotic tree pest movement. *Arboriculture and Urban Forestry*, 37(3):126, 2011.
- [105] Amelia M Jamison, Sandra Crouse Quinn, and Vicki S Freimuth. “you don’t trust a government vaccine”: Narratives of institutional trust and influenza vaccination among african american and white adults. *Social Science & Medicine*, 221:87–94, 2019.
- [106] Jonathan Jay, Jacob Bor, Elaine O Nsoesie, Sarah K Lipson, David K Jones, Sandro Galea, and Julia Raifman. Neighbourhood income and physical distancing during the covid-19 pandemic in the united states. *Nature human behaviour*, 4(12):1294–1302, 2020.

- [107] Michael J. Jenkins, Elizabeth Hebertson, Wesley Page, and C. Arik Jorgensen. Bark beetles, fuels, fires and implications for forest management in the intermountain west. *Forest Ecology and Management*, 254(1):16–34, 2008.
- [108] Michael J Jenkins, Wesley G Page, Elizabeth G Hebertson, and Martin E Alexander. Fuels and fire behavior dynamics in bark beetle-attacked forests in western north america and implications for fire management. *Forest Ecology and Management*, 275:23–34, 2012.
- [109] Peter C Jentsch, Madhur Anand, and Chris T Bauch. Spatial correlation as an early warning signal of regime shifts in a multiplex disease-behaviour network. *Journal of theoretical biology*, 448:17–25, 2018.
- [110] Peter C Jentsch, Madhur Anand, and Chris T Bauch. Prioritising covid-19 vaccination in changing social and epidemiological landscapes: a mathematical modelling study. *The Lancet Infectious Diseases*, 2021.
- [111] Peter C Jentsch, Chris T Bauch, Denys Yemshanov, and Madhur Anand. Go big or go home: A model-based assessment of general strategies to slow the spread of forest pests via infested firewood. *PloS one*, 15(9):e0238979, 2020.
- [112] Merrill R Kaufmann et al. The status of our scientific understanding of lodgepole pine and mountain pine beetles: a focus on forest ecology and fire behavior. 2008.
- [113] William Ogilvy Kermack and Anderson G McKendrick. A contribution to the mathematical theory of epidemics. *Proceedings of the royal society of london. Series A, Containing papers of a mathematical and physical character*, 115(772):700–721, 1927.
- [114] Frank H Koch, Denys Yemshanov, Robert A Haack, and Roger D Magarey. Using a network model to assess risk of forest pest spread via recreational travel. *PloS one*, 9(7):e102105, 2014.
- [115] Cynthia S Kolar and David M Lodge. Progress in invasion biology: predicting invaders. *Trends in ecology & evolution*, 16(4):199–204, 2001.
- [116] Kent F Kovacs, Robert G Haight, Deborah G McCullough, Rodrigo J Mercader, Nathan W Siegert, and Andrew M Liebhold. Cost of potential emerald ash borer damage in us communities, 2009–2019. *Ecological Economics*, 69(3):569–578, 2010.
- [117] Kent F Kovacs, Robert G Haight, Rodrigo J Mercader, and Deborah G McCullough. A bioeconomic analysis of an emerald ash borer invasion of an urban forest with multiple jurisdictions. *Resource and Energy Economics*, 36(1):270–289, 2014.

- [118] Dominik Kulakowski, Daniel Jarvis, Thomas T Veblen, and Jeremy Smith. Stand-replacing fires reduce susceptibility of lodgepole pine to mountain pine beetle outbreaks in colorado. *Journal of Biogeography*, 39(11):2052–2060, 2012.
- [119] The Lancet. The plight of essential workers during the covid-19 pandemic. *Lancet (London, England)*, 395(10237):1587, 2020.
- [120] Stephen A Lauer, Kyra H Grantz, Qifang Bi, Forrest K Jones, Qulu Zheng, Hannah R Meredith, Andrew S Azman, Nicholas G Reich, and Justin Lessler. The incubation period of coronavirus disease 2019 (COVID-19) from publicly reported confirmed cases: estimation and application. *Annals of internal medicine*, 2020.
- [121] Dave Leatherman, I Aguayo, and TM Mehall. Mountain pine beetle. *Colorado Birds*, page 33, 2012.
- [122] Shernita L Lee and Ana M Tameru. A mathematical model of human papillomavirus (hpv) in the united states and its impact on cervical cancer. *Journal of Cancer*, 3:262, 2012.
- [123] Richard Levins. Some demographic and genetic consequences of environmental heterogeneity for biological control. *American Entomologist*, 15(3):237–240, 1969.
- [124] Mark A Lewis, William Nelson, and Cailin Xu. A structured threshold model for mountain pine beetle outbreak. *Bulletin of mathematical biology*, 72(3):565–589, 2010.
- [125] You Li, Harry Campbell, Durga Kulkarni, Alice Harpur, Madhurima Nundy, Xin Wang, Harish Nair, Usher Network for COVID, et al. The temporal association of introducing and lifting non-pharmaceutical interventions with the time-varying reproduction number (r) of sars-cov-2: a modelling study across 131 countries. *The Lancet Infectious Diseases*, 2020.
- [126] Andrew M Liebhold and Patrick C Tobin. Population ecology of insect invasions and their management. *Annu. Rev. Entomol.*, 53:387–408, 2008.
- [127] Rodman Linn, Jon Reisner, Jonah J Colman, and Judith Winterkamp. Studying wildfire behavior using firetec. *International journal of wildland fire*, 11(4):233–246, 2002.
- [128] Monte Lloyd and Henry S Dybas. The periodical cicada problem. i. population ecology. *Evolution*, 20(2):133–149, 1966.

- [129] Rachel A Loehman, Robert E Keane, Lisa M Holsinger, and Zhiwei Wu. Interactions of landscape disturbances and climate change dictate ecological pattern and process: spatial modeling of wildfire, insect, and disease dynamics under future climates. *Landscape Ecology*, 32(7):1447–1459, 2017.
- [130] James E Lotan. Cone serotiny-fire relationships in lodgepole pine. *The Bark Beetles, Fuels, and Fire Bibliography*, page 8, 1976.
- [131] James E Lotan, James K Brown, and Leon F Neuenschwander. Role of fire in lodgepole pine forests. In *Lodgepole pine: the species and its management symposium proceedings’.(Eds D Baumgartner et al.) pp*, pages 133–152, 1985.
- [132] Donald Ludwig, Dixon D Jones, Crawford S Holling, et al. Qualitative analysis of insect outbreak systems: the spruce budworm and forest. *Journal of animal ecology*, 47(1):315–332, 1978.
- [133] Nicole Lurie, Melanie Saville, Richard Hatchett, and Jane Halton. Developing COVID-19 vaccines at pandemic speed. *New England Journal of Medicine*, 382(21):1969–1973, 2020.
- [134] Heather J Lynch, Roy A Renkin, Robert L Crabtree, and Paul R Moorcroft. The influence of previous mountain pine beetle (*dendroctonus ponderosae*) activity on the 1988 yellowstone fires. *Ecosystems*, 9(8):1318–1327, 2006.
- [135] Amyn A. Malik, SarahAnn M. McFadden, Jad Elharake, and Saad B. Omer. Determinants of covid-19 vaccine acceptance in the us. *EClinicalMedicine*, 26:100495, 2020.
- [136] Svenn-Erik Mamelund, Jessica Dimka, and Nan Zou Bakkeli. Social disparities in adopting non-pharmaceutical interventions during covid-19. *Journal of Developing Societies*, page 0169796X21996858, 2021.
- [137] Laura Matrajt, Julie Eaton, Tiffany Leung, and Elizabeth R Brown. Vaccine optimization for COVID-19, who to vaccinate first? *medRxiv*, 2020.
- [138] Garrett W Meigs, Harold SJ Zald, John L Campbell, William S Keeton, and Robert E Kennedy. Do insect outbreaks reduce the severity of subsequent forest fires? *Environmental Research Letters*, 11(4):045008, 2016.
- [139] William Mell, Mary Ann Jenkins, Jim Gould, and Phil Cheney. A physics-based approach to modelling grassland fires. *International Journal of Wildland Fire*, 16(1):1–22, 2007.

- [140] Ian F Miller, Alexander D Becker, Bryan T Grenfell, and C Jessica E Metcalf. Disease and healthcare burden of COVID-19 in the United States. *Nature Medicine*, 26(8):1212–1217, 2020.
- [141] Kenji Mizumoto, Katsushi Kagaya, Alexander Zarebski, and Gerardo Chowell. Estimating the asymptomatic proportion of coronavirus disease 2019 (COVID-19) cases on board the diamond princess cruise ship, yokohama, japan, 2020. *Eurosurveillance*, 25(10):2000180, 2020.
- [142] Christopher J Moran and Mark A Cochrane. Do mountain pine beetle outbreaks change the probability of active crown fire in lodgepole pine forests? comment. *Ecology*, 93(4):939–941, 2012.
- [143] Jim R Muirhead, Brian Leung, Colin van Overdijk, David W Kelly, Kanavillil Nandakumar, Kenneth R Marchant, and Hugh J MacIsaac. Modelling local and long-distance dispersal of invasive emerald ash borer *agrilus planipennis* (coleoptera) in north america. *Diversity and Distributions*, 12(1):71–79, 2006.
- [144] National Invasive Species Council (NISC). Fiscal year 2007 interagency invasive species performance budget. Online source, 2007.
- [145] Brian Nearing. Checkpoint tries to halt wood traffic. *timesunion*, 2012.
- [146] José F Negrón, Kurt K Allen, Angie Ambourn, Blaine Cook, and Kenneth Marchand. Large-scale thinnings, ponderosa pine, and mountain pine beetle in the black hills, usa. *Forest Science*, 63(5):529–536, 2017.
- [147] Hiroshi Nishiura, Natalie M Linton, and Andrei R Akhmetzhanov. Serial interval of novel coronavirus (COVID-19) infections. *International journal of infectious diseases*, 2020.
- [148] Andrea R Norris and Kathy Martin. Mountain pine beetle presence affects nest patch choice of red-breasted nuthatches. *The Journal of Wildlife Management*, 72(3):733–737, 2008.
- [149] Cameron Nowzari, Victor M Preciado, and George J Pappas. Analysis and control of epidemics: A survey of spreading processes on complex networks. *IEEE Control Systems Magazine*, 36(1):26–46, 2016.
- [150] Ontario Agency for Health Protection and Promotion (Public Health Ontario). COVID-19 case fatality, case identification,

and attack rates in ontario. <https://www.publichealthontario.ca/-/media/documents/ncov/epi/2020/06/COVID19-epi-case-identification-age-only-template.pdf?la=en>, 2020.

- [151] Ontario Ministry of Natural Resources. Are you moving firewood? important information you should read, 2011.
- [152] Tamer Oraby, Vivek Thampi, and Chris T Bauch. The influence of social norms on the dynamics of vaccinating behaviour for paediatric infectious diseases. *Proceedings of the Royal Society B: Biological Sciences*, 281(1780):20133172, 2014.
- [153] World Health Organization. Who target product profiles for COVID-19 vaccines, [https://www.who.int/who-documents-detailredirect/ who-target-product-profiles-for-COVID-19-vaccines](https://www.who.int/who-documents-detailredirect/who-target-product-profiles-for-COVID-19-vaccines), accessed 25 september 2020, 2020.
- [154] Tasnime Osama, Mohammad S Razai, and Azeem Majeed. Covid-19 vaccine allocation: addressing the united kingdom's colour-blind strategy. *Journal of the Royal Society of Medicine*, page 01410768211001581, 2021.
- [155] Christina M Pacheco, Sean M Daley, Travis Brown, Melissa Filippi, K Allen Greiner, and Christine M Daley. Moving forward: breaking the cycle of mistrust between american indians and researchers. *American journal of public health*, 103(12):2152–2159, 2013.
- [156] Corey M Peak, Rebecca Kahn, Yonatan H Grad, Lauren M Childs, Ruoran Li, Marc Lipsitch, and Caroline O Buckee. Individual quarantine versus active monitoring of contacts for the mitigation of COVID-19: a modelling study. *The Lancet Infectious Diseases*, 2020.
- [157] Sansao A Pedro, Frank T Ndjomatchoua, Peter Jentsch, Jean M Tcheunche, Madhur Anand, and Chris T Bauch. Conditions for a second wave of COVID-19 due to interactions between disease dynamics and social processes. *medRxiv*, 2020.
- [158] Daniel DB Perrakis, Rick A Lanoville, Stephen W Taylor, and Dana Hicks. Modeling wildfire spread in mountain pine beetle-affected forest stands, british columbia, canada. *Fire Ecology*, 10(2):10–35, 2014.
- [159] Kim Peterson and Andrea Diss-Torrance. Motivation for compliance with environmental regulations related to forest health. *Journal of environmental management*, 112:104–119, 2012.

- [160] Toby R Petrice and Robert A Haack. Effects of cutting date, outdoor storage conditions, and splitting on survival of *agrilus planipennis* (coleoptera: Buprestidae) in firewood logs. *Journal of Economic Entomology*, 99(3):790–796, 2006.
- [161] Therese M Poland and Deborah G McCullough. Emerald ash borer: invasion of the urban forest and the threat to north america’s ash resource. *Journal of Forestry*, 104(3):118–124, 2006.
- [162] Hugh DW Powell, Sallie J Hejl, and Diana L Six. Measuring woodpecker food: a simple method for comparing wood-boring beetle abundance among fire-killed trees. *Journal of Field Ornithology*, 73(2):130–140, 2002.
- [163] James A Powell and Barbara J Bentz. Connecting phenological predictions with population growth rates for mountain pine beetle, an outbreak insect. *Landscape Ecology*, 24(5):657–672, 2009.
- [164] James A Powell, Jesse A Logan, and Barbara J Bentz. Local projections for a global model of mountain pine beetle attacks. *Journal of Theoretical Biology*, 179(3):243–260, 1996.
- [165] Anantha M Prasad, Louis R Iverson, Matthew P Peters, Jonathan M Bossenbroek, Stephen N Matthews, T Davis Sydnor, and Mark W Schwartz. Modeling the invasive emerald ash borer risk of spread using a spatially explicit cellular model. *Landscape ecology*, 25(3):353–369, 2010.
- [166] Kiesha Prem, Kevin van Zandvoort, Petra Klepac, Rosalind M Eggo, Nicholas G Davies, Alex R Cook, Mark Jit, et al. Projecting contact matrices in 177 geographical regions: an update and comparison with empirical data for the COVID-19 era. *medRxiv*, 2020.
- [167] Provincial government of Ontario, Canada. Reopening ontario in stages, 2020. Available at <https://www.ontario.ca/page/reopening-ontario-stages>.
- [168] Public Health Ontario. Covid-19 serosurveillance summary: Covid-19 seroprevalence in ontario: March 27, 2020 to june 30, 2020, 2020.
- [169] Christopher Rackauckas and Qing Nie. Differentialequations. jl—a performant and feature-rich ecosystem for solving differential equations in julia. *Journal of Open Research Software*, 5(1), 2017.

- [170] K Sabeel Rahman. Constructing and contesting structural inequality. *Critical Analysis of Law*, 5, 2018.
- [171] Angela L Rasmussen. On the origins of sars-cov-2. *Nature Medicine*, 27(1):9–9, 2021.
- [172] Linda Rass, MA Lifshits, and John Radcliffe. *Spatial deterministic epidemics*. American Mathematical Soc., 2003.
- [173] Nick Reid. Roadside checkpoints to monitor illegal firewood transport in new hampshire. *Concord Monitor*, 2017.
- [174] Timothy C Reluga. Game theory of social distancing in response to an epidemic. *PLoS Comput Biol*, 6(5):e1000793, 2010.
- [175] Edward Royce. *Poverty and power: The problem of structural inequality*. Rowman & Littlefield, 2018.
- [176] Howard Russell. Emerald ash borer (*agrilus planipennis*) on a penny. accessed June 10, 2021.
- [177] Les Safranyik et al. Mountain pine beetle epidemiology in lodgepole pine. In *Mountain pine beetle symposium: Challenges and solutions*, pages 33–40, 2003.
- [178] Les Safranyik, Douglas A Linton, Terry L Shore, BC Hawkes, et al. *The effects of prescribed burning on mountain pine beetle in lodgepole pine*, volume 391. 2001.
- [179] Les Safranyik, Bill Wilson, et al. *The mountain pine beetle: a synthesis of biology, management and impacts on lodgepole pine*. Canadian Forest Service, 2007.
- [180] Marcel Salathe, Linus Bengtsson, Todd J Bodnar, Devon D Brewer, John S Brownstein, Caroline Buckee, Ellsworth M Campbell, Ciro Cattuto, Shashank Khandelwal, Patricia L Mabry, et al. Digital epidemiology. *PLoS Comput Biol*, 8(7):e1002616, 2012.
- [181] Marcel Salathé and Sebastian Bonhoeffer. The effect of opinion clustering on disease outbreaks. *Journal of The Royal Society Interface*, 5(29):1505–1508, 2008.
- [182] Charles Sartwell and Robert E. Stevens. Mountain pine beetle in ponderosa pine—prospects for silvicultural control in second-growth stands. *Journal of Forestry*, 73(3):136–140, 1975.

- [183] Akiko Satake, Heather M Leslie, Yoh Iwasa, and Simon A Levin. Coupled ecological–social dynamics in a forested landscape: Spatial interactions and information flow. *Journal of theoretical biology*, 246(4):695–707, 2007.
- [184] Michaël Schwarzinger, Verity Watson, Pierre Arwidson, François Alla, and Stéphane Luchini. Covid-19 vaccine hesitancy in a representative working-age population in france: a survey experiment based on vaccine characteristics. *The Lancet Public Health*, 6(4):e210–e221, 2021.
- [185] Rupert Seidl, Daniel C Donato, Kenneth F Raffa, and Monica G Turner. Spatial variability in tree regeneration after wildfire delays and dampens future bark beetle outbreaks. *Proceedings of the National Academy of Sciences*, page 201615263, 2016.
- [186] Victor A Shegelski, Maya L Evenden, and Felix AH Sperling. Morphological variation associated with dispersal capacity in a tree-killing bark beetle *dendroctonus ponderosae* hopkins. *Agricultural and Forest Entomology*, 21(1):79–87, 2019.
- [187] Ram Sigdel, Madhur Anand, and Chris T Bauch. Convergence of socio-ecological dynamics in disparate ecological systems under strong coupling to human social systems. *Theoretical Ecology*, 12(3):285–296, 2019.
- [188] Juha Siikamäki. Contributions of the us state park system to nature recreation. *Proceedings of the National Academy of Sciences*, 108(34):14031–14036, 2011.
- [189] Martin Simard, William H Romme, Jacob M Griffin, and Monica G Turner. Do mountain pine beetle outbreaks change the probability of active crown fire in lodgepole pine forests? *Ecological Monographs*, 81(1):3–24, 2011.
- [190] John Snow. *On the mode of communication of cholera*. John Churchill, 1855.
- [191] Patricia Soares, João Victor Rocha, Marta Moniz, Ana Gama, Pedro Almeida Laires, Ana Rita Pedro, Sónia Dias, Andreia Leite, and Carla Nunes. Factors associated with covid-19 vaccine hesitancy. *Vaccines*, 9(3):300, 2021.
- [192] Statistics Canada. Census profile, 2016 census, <https://www12.statcan.gc.ca/>, accessed 25 september 2020, 2020.
- [193] S Strohm, ML Reid, and RC Tyson. Impacts of management on mountain pine beetle spread and damage: A process-rich model. *Ecological Modelling*, 337:241–252, 2016.

- [194] Stephen W Taylor, Allan L Carroll, et al. Disturbance, forest age, and mountain pine beetle outbreak dynamics in bc: A historical perspective. In *Mountain pine beetle symposium: Challenges and solutions*, volume 3031. Natural Resources Canada, Canadian Forest Service, Pacific Forestry Centre . . . , 2003.
- [195] Vivek A Thampi, Madhur Anand, and Chris T Bauch. Socio-ecological dynamics of caribbean coral reef ecosystems and conservation opinion propagation. *Scientific reports*, 8(1):1–11, 2018.
- [196] Robin N Thompson. Epidemiological models are important tools for guiding covid-19 interventions. *BMC medicine*, 18(1):1–4, 2020.
- [197] Lauren Tindale, Michelle Coombe, Jessica E Stockdale, Emma Garlock, Wing Yin Venus Lau, Manu Saraswat, Yen-Hsiang Brian Lee, Louxin Zhang, Dongxuan Chen, Jacco Wallinga, et al. Transmission interval estimates suggest pre-symptomatic spread of COVID-19. *medRxiv*, 2020.
- [198] Patrick C Tobin. Cost analysis and biological ramifications for implementing the gypsy moth slow the spread program. *Gen. Tech. Rep. NRS-37. Newtown Square, PA: US Department of Agriculture, Forest Service, Northern Research Station.* 21 p., 37, 2008.
- [199] Patrick C Tobin, Andrea Diss-Torrance, Laura M Blackburn, and Brian D Brown. What does “local” firewood buy you? managing the risk of invasive species introduction. *Journal of economic entomology*, 103(5):1569–1576, 2010.
- [200] Treasury Board Secretariat of Ontario. Confirmed positive cases of COVID-19 in Ontario, September 2020. Available at <https://data.ontario.ca/dataset/confirmed-positive-cases-of-{COVID}-19-in-ontario/resource/455fd63b-603d-4608-8216-7d8647f43350>.
- [201] Ashleigh R Tuite, David N Fisman, and Amy L Greer. Mathematical modelling of COVID-19 transmission and mitigation strategies in the population of ontario, canada. *CMAJ*, 192(19):E497–E505, 2020.
- [202] Jean J Turgeon, Mary Orr, Cara Grant, Yunke Wu, and Ben Gasman. Decade-old satellite infestation of anoplophora glabripennis motschulsky (coleoptera: Cerambycidae) found in ontario, canada outside regulated area of founder population. *The Coleopterists Bulletin*, 69(4):674–679, 2015.

- [203] Brandon M Turner and Per B Sederberg. Approximate Bayesian computation with differential evolution. *Journal of Mathematical Psychology*, 56(5):375–385, 2012.
- [204] Germaine Tuyisenge and Shira M Goldenberg. Covid-19, structural racism, and migrant health in canada. *The Lancet*, 397(10275):650–652, 2021.
- [205] United States Department of Agriculture Animal and Plant Health Inspection Service. Risk assessment of the movement of firewood within the united states, 2011.
- [206] Frederik Verelst, Lander Willem, and Philippe Beutels. Behavioural change models for infectious disease transmission: a systematic review (2010–2015). *Journal of The Royal Society Interface*, 13(125):20160820, 2016.
- [207] Yuanyuan Wang, Bailin Pan, Ye Liu, Amanda Wilson, Jianjun Ou, and Runsen Chen. Health care and mental health challenges for transgender individuals during the covid-19 pandemic. *The Lancet Diabetes & Endocrinology*, 8(7):564–565, 2020.
- [208] Zhen Wang, Chris T Bauch, Samit Bhattacharyya, Alberto d’Onofrio, Piero Manfredi, Matjaž Perc, Nicola Perra, Marcel Salathe, and Dawei Zhao. Statistical physics of vaccination. *Physics Reports*, 664:1–113, 2016.
- [209] Harriet A Washington. *Medical apartheid: The dark history of medical experimentation on Black Americans from colonial times to the present*. Doubleday Books, 2006.
- [210] Laren Weber. Checkpoint tries to halt wood traffic. *The Toledo Blade*, 2006.
- [211] Anthony L Westerling, Hugo G Hidalgo, Daniel R Cayan, and Thomas W Swetnam. Warming and earlier spring increase western us forest wildfire activity. *science*, 313(5789):940–943, 2006.
- [212] Wikimedia user Jonhall. Pine beetle in manning park photo. accessed June 10, 2021.
- [213] John RU Wilson, Eleanor E Dormontt, Peter J Prentis, Andrew J Lowe, and David M Richardson. Something in the way you move: dispersal pathways affect invasion success. *Trends in ecology & evolution*, 24(3):136–144, 2009.
- [214] Toby Wise, Tomislav Damir Zbozinek, Giorgia Michelini, Cindy C Hagan, et al. Changes in risk perception and protective behavior during the first week of the COVID-19 pandemic in the united states. 2020.

- [215] Sanni Yaya, Helena Yeboah, Carlo Handy Charles, Akaninyene Otu, and Ronald Labonte. Ethnic and racial disparities in covid-19-related deaths: counting the trees, hiding the forest. *BMJ Global Health*, 5(6):e002913, 2020.
- [216] Denys Yemshanov, Robert G Haight, Frank H Koch, Bo Lu, Robert Venette, D Barry Lyons, Taylor Scarr, and Krista Ryall. Optimal allocation of invasive species surveillance with the maximum expected coverage concept. *Diversity and Distributions*, 21(11):1349–1359, 2015.
- [217] Emilio Zagheni, Francesco C Billari, Piero Manfredi, Alessia Melegaro, Joel Mossong, and W John Edmunds. Using time-use data to parameterize models for the spread of close-contact infectious diseases. *American journal of epidemiology*, 168(9):1082–1090, 2008.
- [218] Shi Zhao, Lewi Stone, Daozhou Gao, Salihu S Musa, Marc KC Chong, Daihai He, and Maggie H Wang. Imitation dynamics in the mitigation of the novel coronavirus disease (COVID-19) outbreak in wuhan, china from 2019 to 2020. *Annals of Translational Medicine*, 8(7), 2020.
- [219] Na Zhu, Dingyu Zhang, Wenling Wang, Xingwang Li, Bo Yang, Jingdong Song, Xiang Zhao, Baoying Huang, Weifeng Shi, Roujian Lu, et al. A novel coronavirus from patients with pneumonia in china, 2019. *New England journal of medicine*, 2020.
- [220] Rafał Zwolak. A meta-analysis of the effects of wildfire, clearcutting, and partial harvest on the abundance of north american small mammals. *Forest Ecology and Management*, 258(5):539–545, 2009.
- [221] Rafał Zwolak and Kerry R Foresman. Deer mouse demography in burned and unburned forest: no evidence for source–sink dynamics. *Canadian Journal of Zoology*, 86(2):83–91, 2008.

Appendix

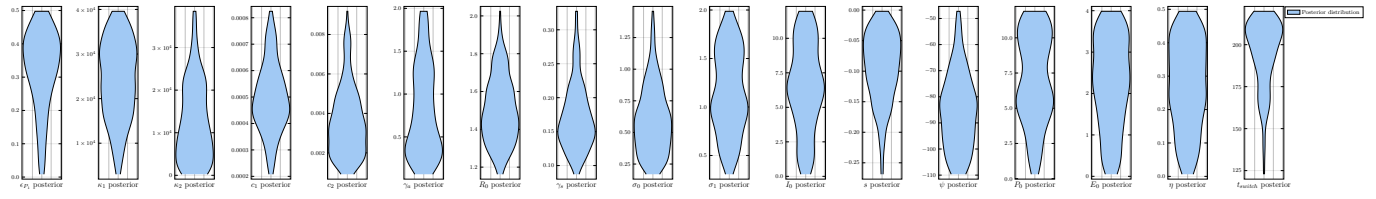


Figure 1: Posterior distributions on inferred non-age structured model parameters for baseline model. Posteriors are composed of 200 candidate parameter sets from the particle filtering, the model was evaluated at these points for all future runs.

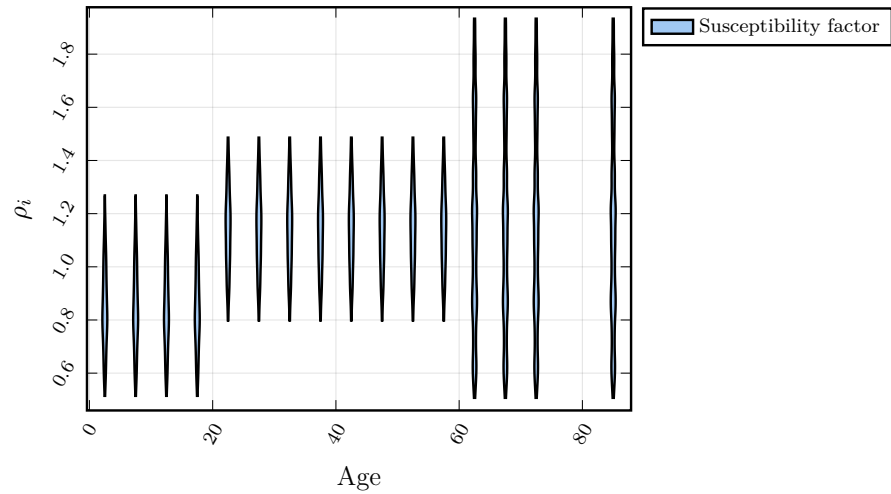


Figure 2: Posterior distributions on inferred age-specific susceptibility modifier parameter ρ_i for baseline model. Three age-specific susceptibility parameters shown here, ρ_1, ρ_2, ρ_3 , were also inferred from particle filtering on the case and mobility data, corresponding to the age brackets 0-20, 20-60, 60+.

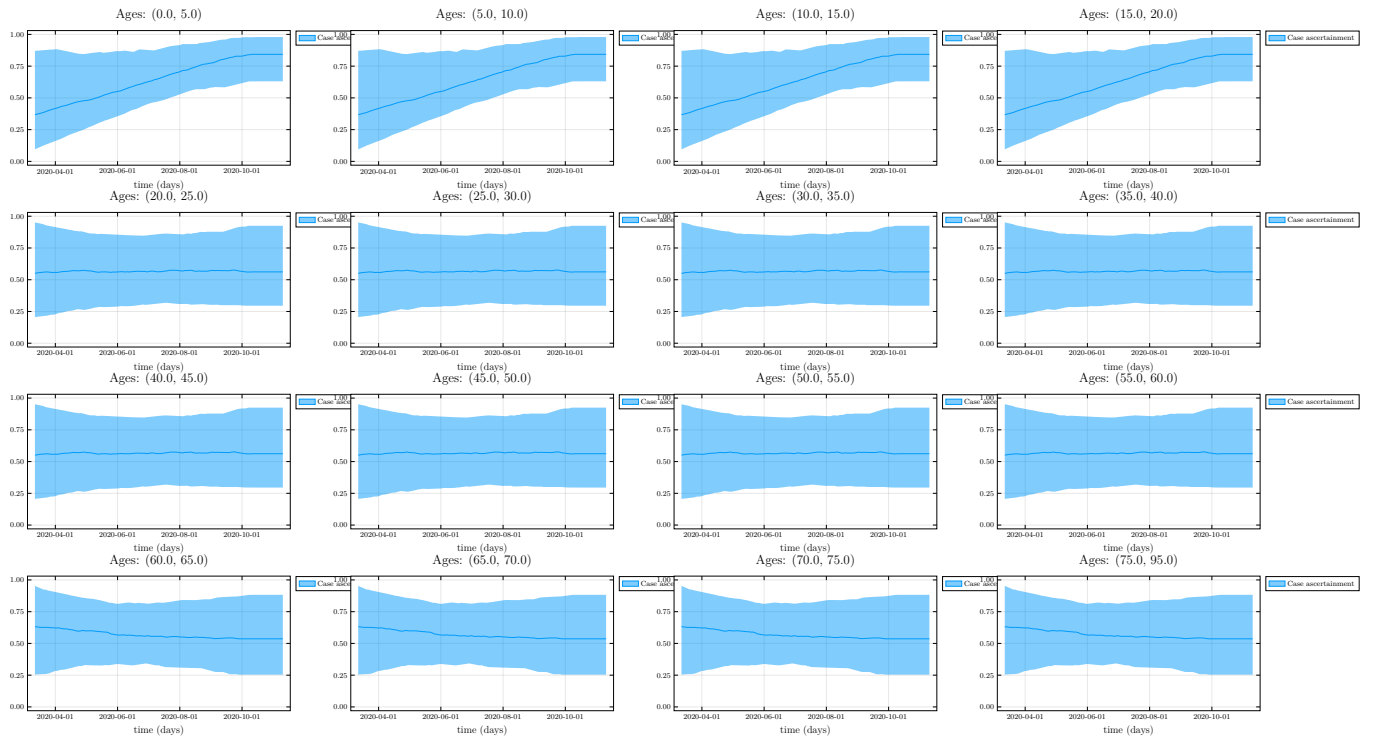


Figure 3: Posterior distributions on inferred age-specific ascertainment rate over time for baseline model. Time dependent ascertainment rates inferred from the data, corresponding to the fraction of actual cases detected by the Ontario testing system.

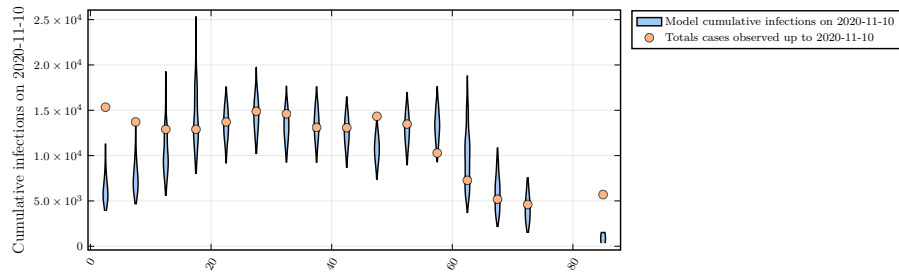


Figure 4: Empirical data of cumulative infections due to COVID-19 by age and model posterior predictions. The age-specific total cases at the end of the fitting window, were used to calibrate the model, in an age dependent way. We used only three parameters to capture age specific effects and therefore trade-off some accuracy in the youngest and oldest age groups.

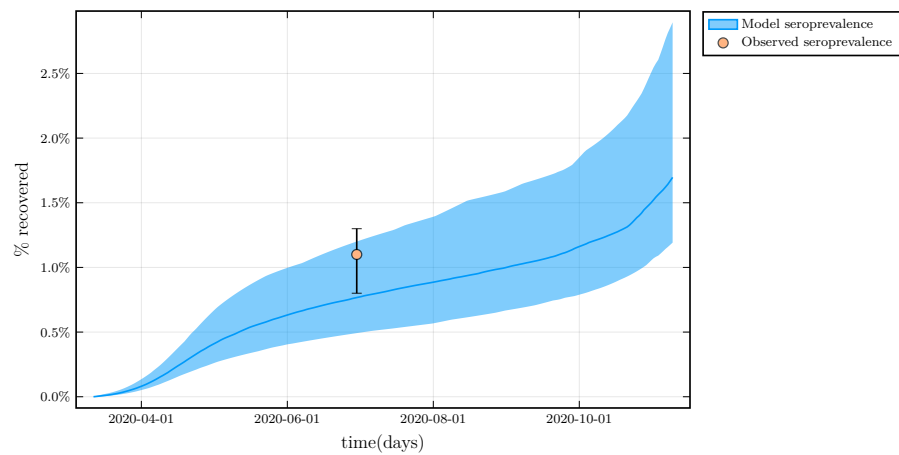


Figure 5: **Average of model posterior population seropositivity over time, compared to empirical data.** Total seroprevalence in Ontario was assessed during the month of June. We used this value to calibrate the model further.

Contact-based vaccination strategy

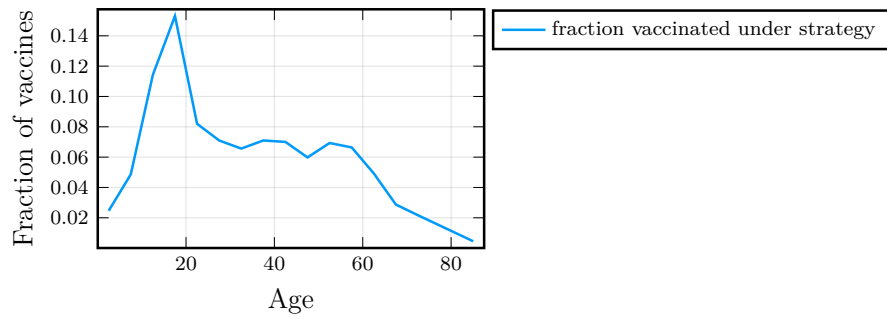


Figure 6: **Age distribution of vaccination under the contact-based strategy.** This strategy vaccinates proportionally to the leading eigenvector of the full contact matrix, $C(0)$, to vaccinate people who will, approximately, produce the most secondary infections in a linearized regime.

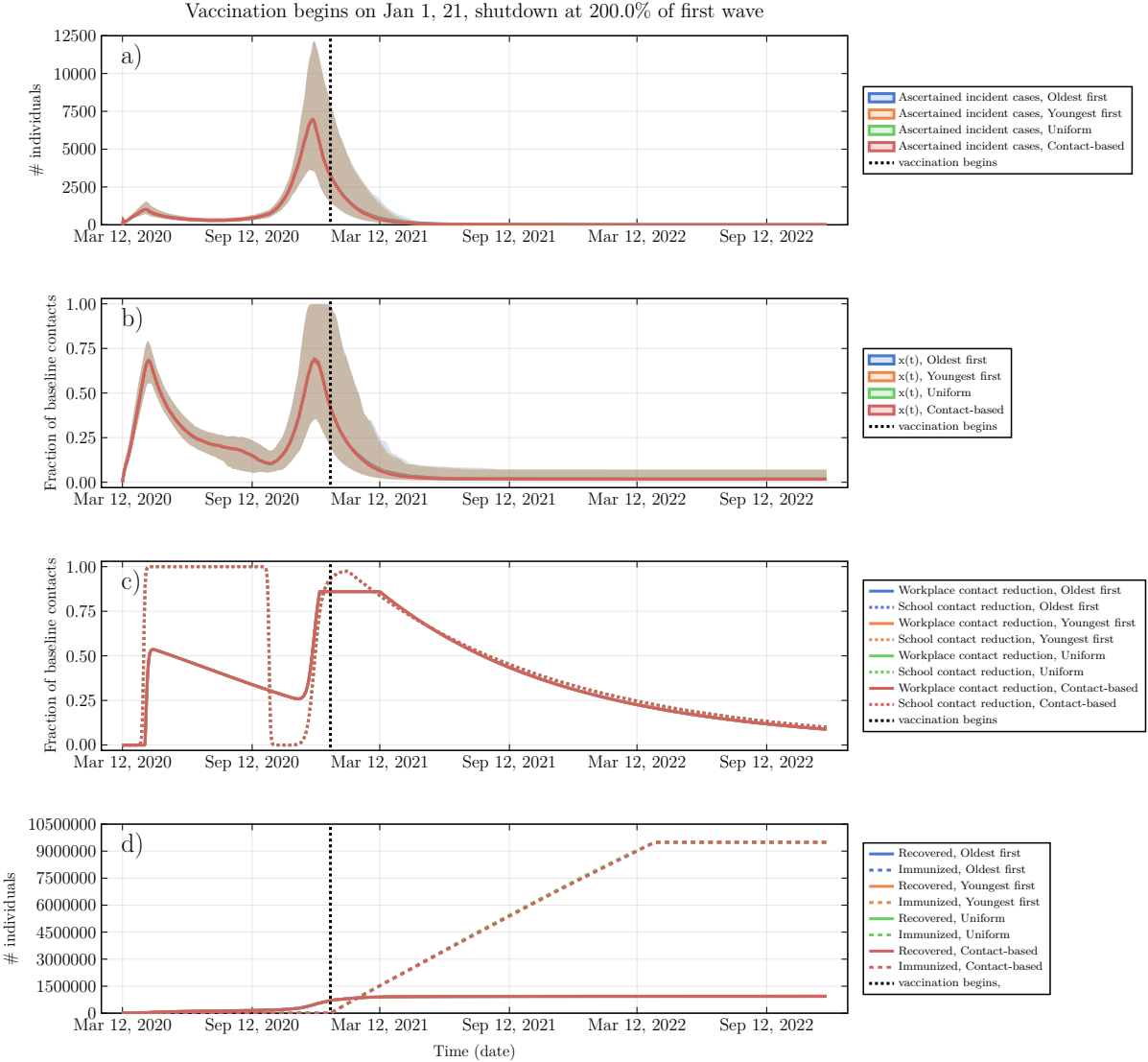


Figure 7: Social and epidemic dynamics for early vaccine availability and high vaccination rate. (a) Ascertained incident COVID-19 cases, (b) proportion x of the population practicing NPIs, (c) Intensity of school and workplace closure, (d) percentage of population with natural or vaccine-derived immunity versus time. $T = 200\%$, $\psi_0 = 1.5\%$ per week, vaccine available in January 2021. Other parameters are in Table 2.1.

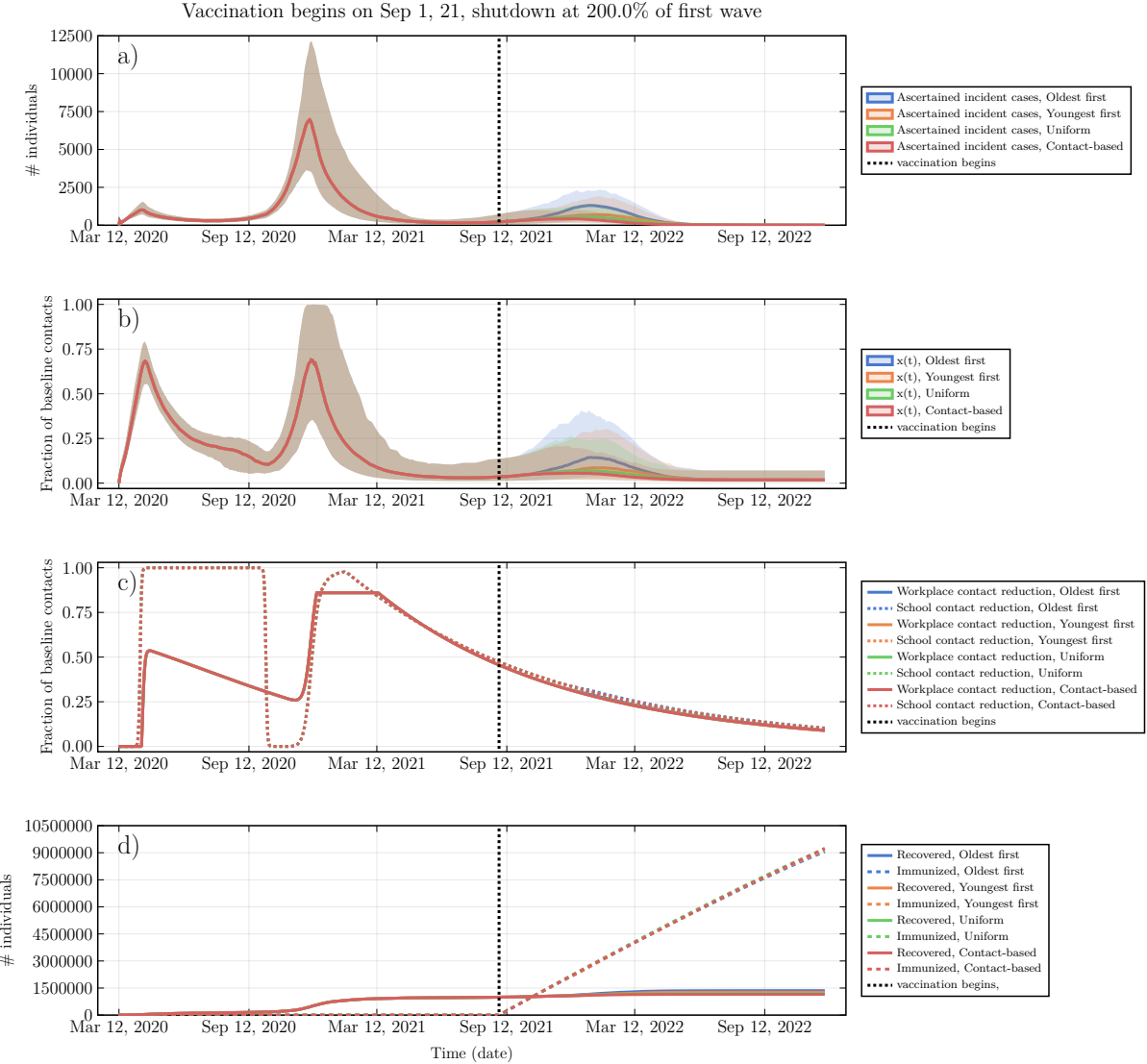


Figure 8: Social and epidemic dynamics for late vaccine availability and high vaccination rate. (a) Ascertained incident COVID-19 cases, (b) proportion x of the population practicing NPIs, (c) Intensity of school and workplace closure, (d) percentage of population with natural or vaccine-derived immunity versus time. $T = 200\%$, $\psi_0 = 1.5\%$ per week, vaccine available in September 2021. Other parameters are in Table 2.1.

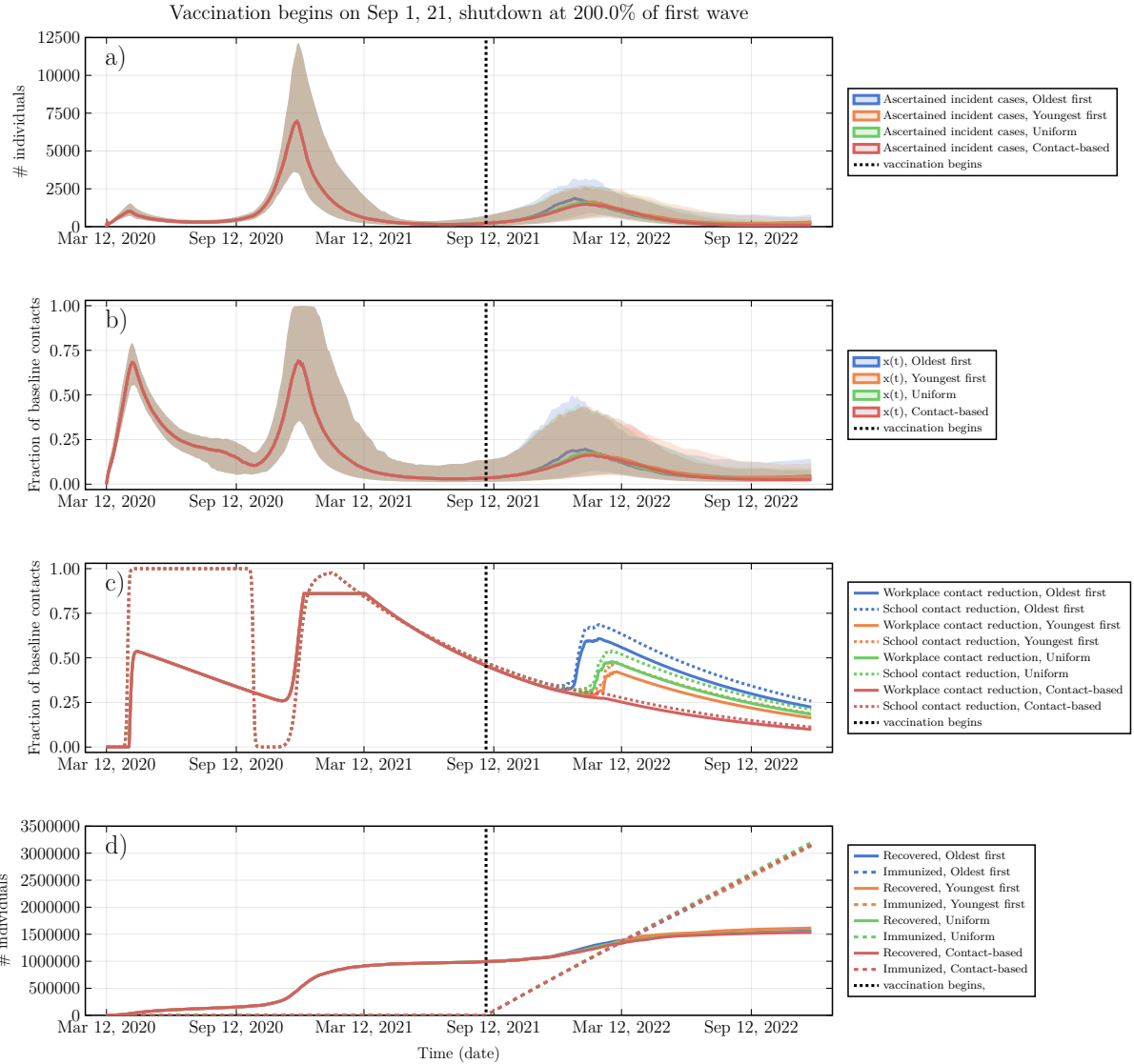


Figure 9: Social and epidemic dynamics for late vaccine availability and low vaccination rate. (a) Ascertained incident COVID-19 cases, (b) proportion x of the population practicing NPIs, (c) Intensity of school and workplace closure, (d) percentage of population with natural or vaccine-derived immunity versus time. $T = 200\%$, $\psi_0 = 0.5\%$ per week, vaccine available in September 2021. Other parameters are in Table 2.1.

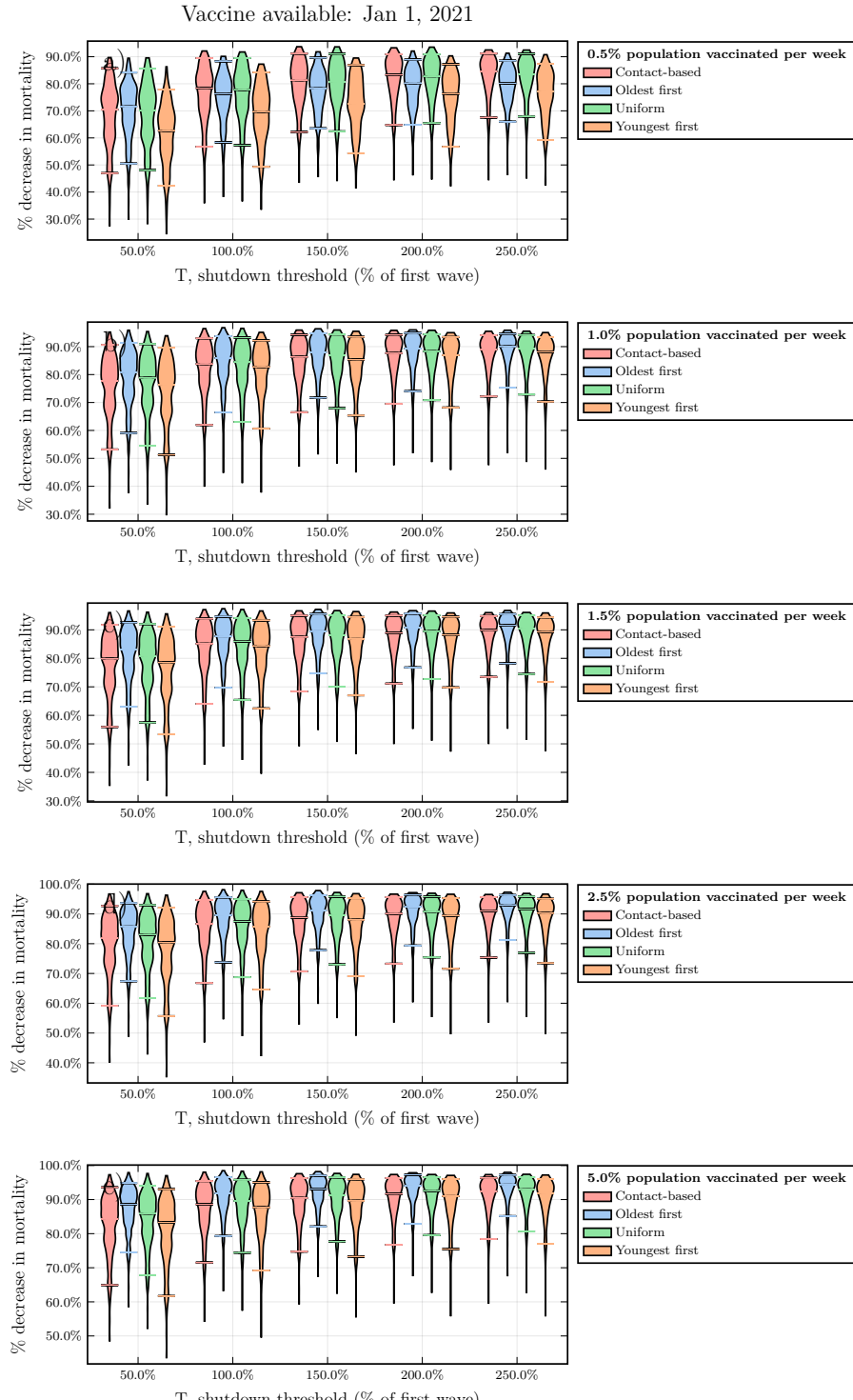


Figure 10: Mortality reductions under various values of T and ψ_0 , early vaccine availability. Violin plots of the percent reduction in mortality under the four vaccine strategies, relative to no vaccination, as a function of the vaccination rate ψ_0 , for January 2021 availability. Horizontal lines represent median values of posterior model projections. Other parameter values in Table S1. Percentage reductions are relative to no vaccination. Projected number of deaths in the absence of vaccination were 35597.2 (CI: 57465.9–19507.9), 48518.8 (CI: 26252.9–22225.7), 61320.1 (CI: 196622.9–24612.5), 72007.3

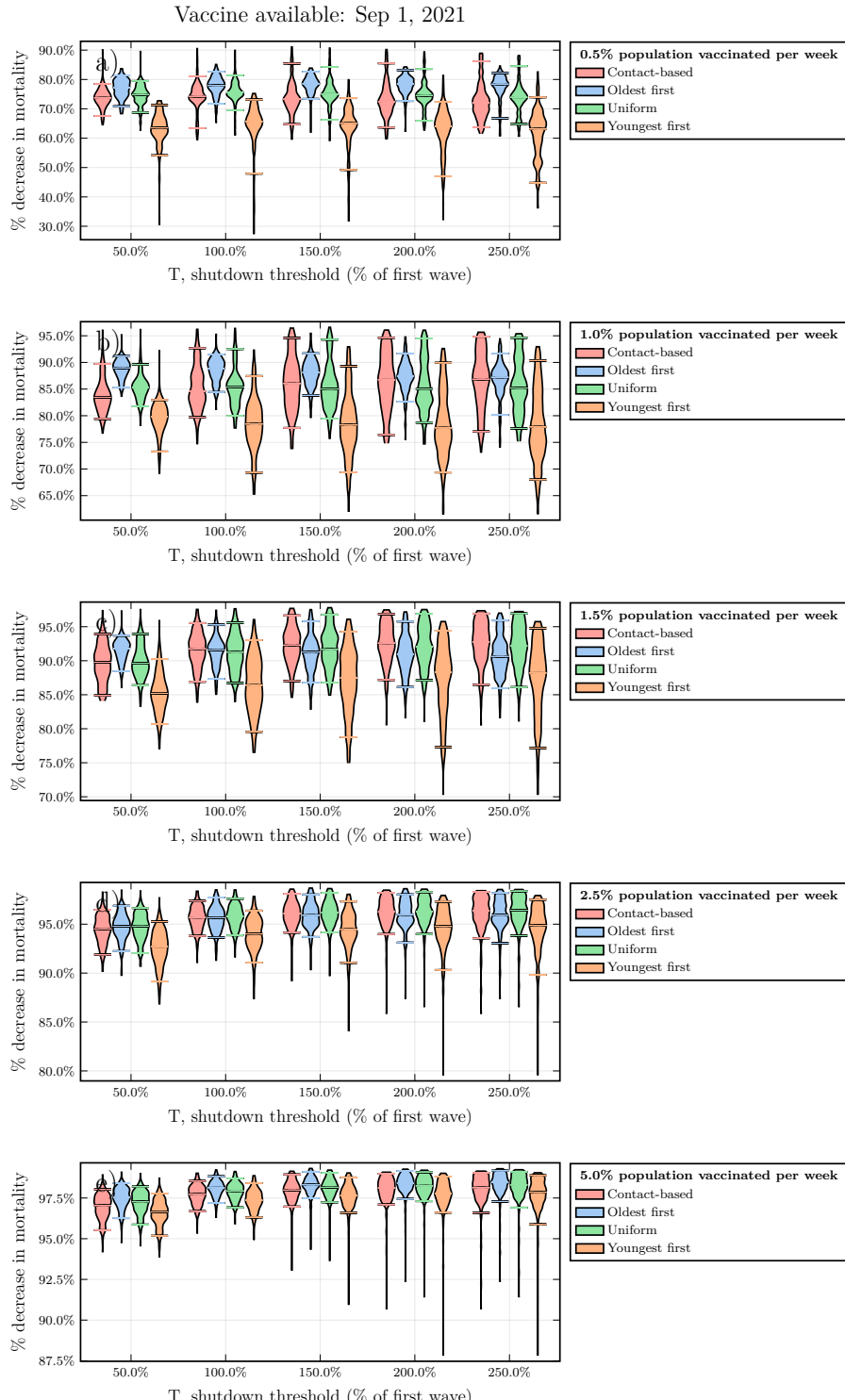


Figure 11: Mortality reductions under various values of T and ψ_0 , late vaccine availability. Violin plots of the percent reduction in mortality under the four vaccine strategies, relative to no vaccination, as a function of the vaccination rate ψ_0 , for September 2021 availability. Horizontal lines represent median values of posterior model projections. Other parameter values in Table S1. Percentage reductions are relative to no vaccination. Projected number of deaths in the absence of vaccination were 25478.8 (CI:

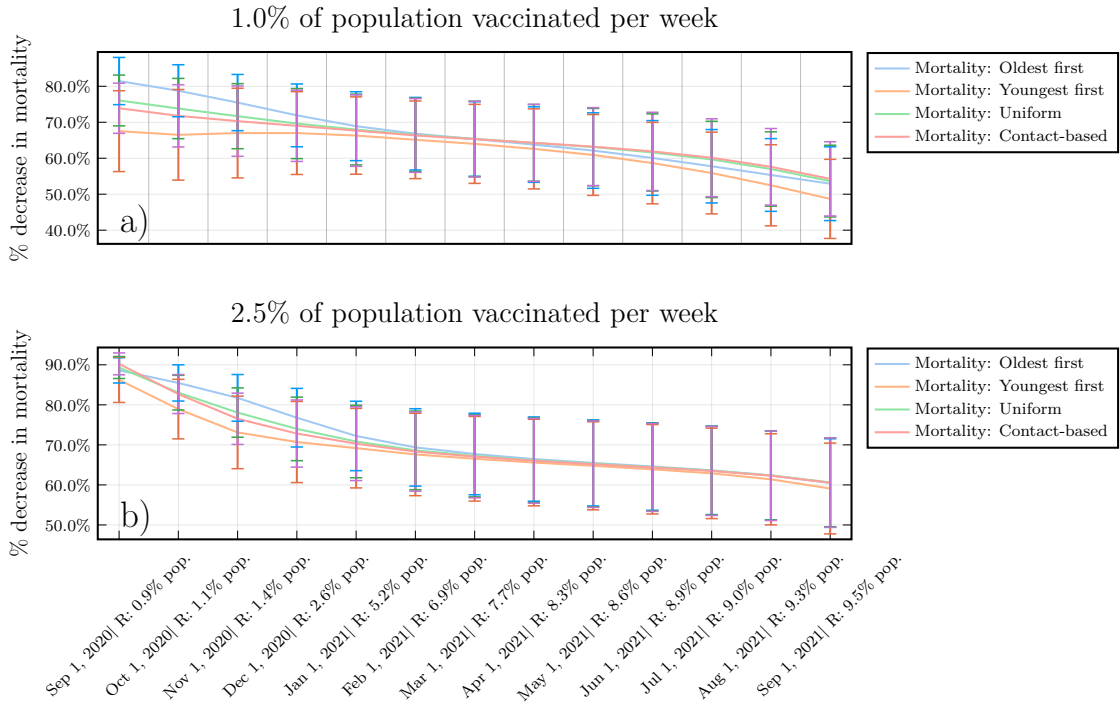


Figure 12: A higher level of natural immunity increases the relative advantage of transmission-interrupting strategies. Median and standard deviation of the percent reduction in mortality under the four vaccine strategies, relative to no vaccination, as a function of the vaccination start date and percent recovered at that time, for (a) $\phi_0 = 1.0\%$ vaccinated per week and (b) $\phi_0 = 2.5\%$ vaccinated per week. Shutdown threshold $T = 200\%$, and other parameter values in Appendix, Table S1.

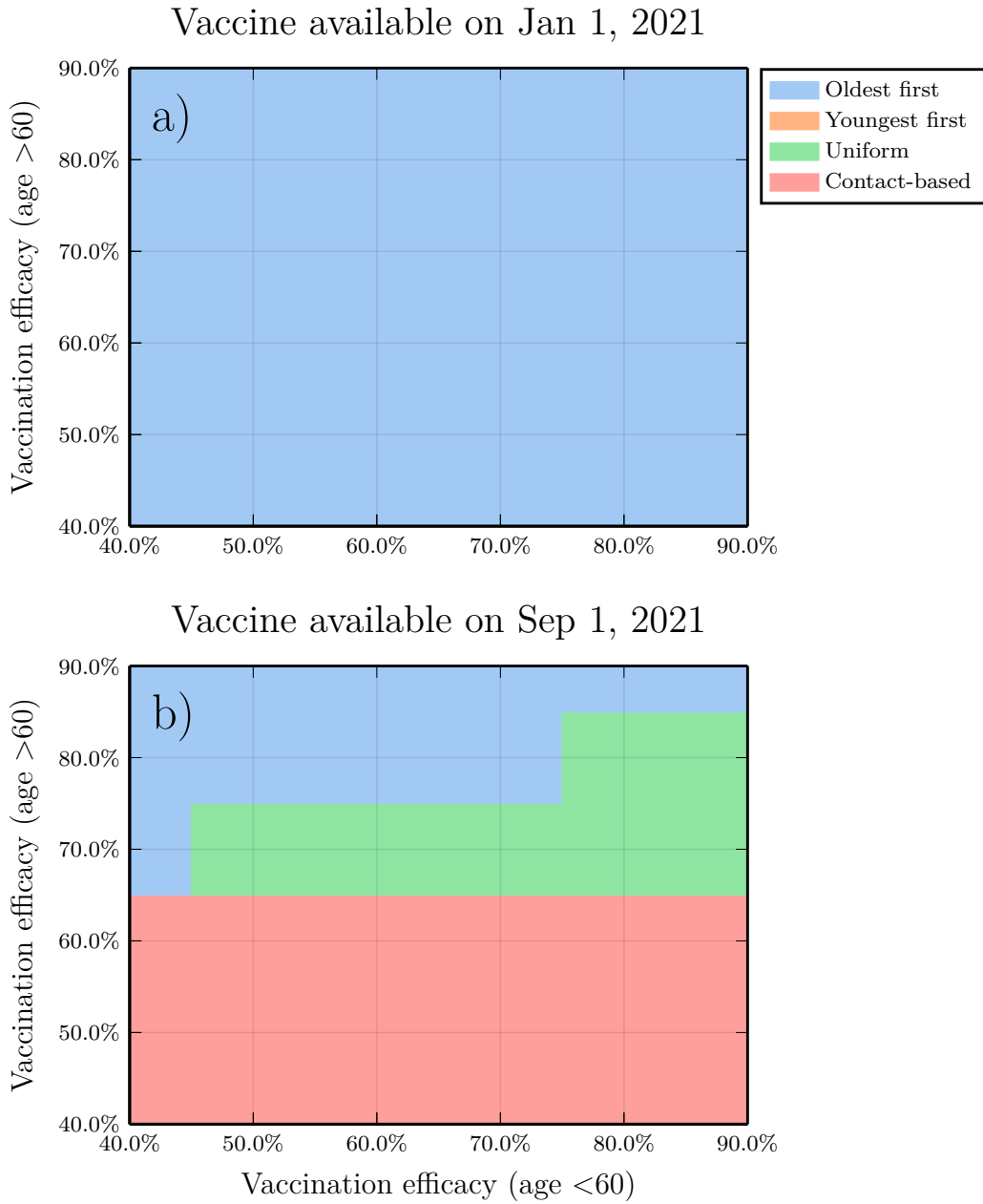


Figure 13: **Sensitivity analysis exploring a range of vaccine efficacy values, for vaccination rate $\phi_0 = 2.5\%$ per week.** Subpanels are parameter planes for January and September availability showing the vaccination strategy that reduces COVID-19 mortality the most as a function of vaccine efficacy in 60+ year-olds versus vaccine efficacy in other age groups. Other parameter values as in Table S1.

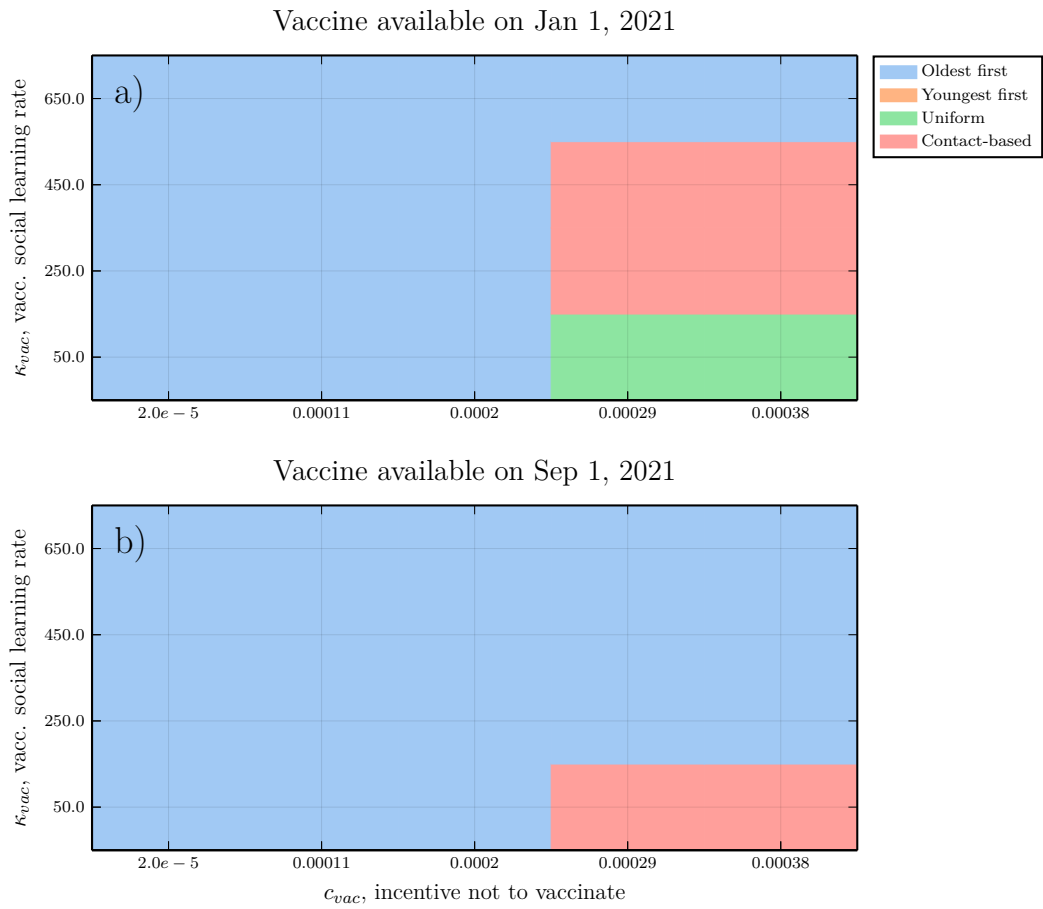


Figure 14: Sensitivity analysis exploring impact of vaccinating behaviour dynamics. $\phi_0 = 2.5\%$ per week, $T = 200\%$. Subpanels are parameter planes for January and September availability showing the vaccination strategy that reduces COVID-19 mortality the most as a function of vaccine social learning rate κ_{vac} and vaccine cost parameter c_{vac} . Other parameter values as in Table S1.

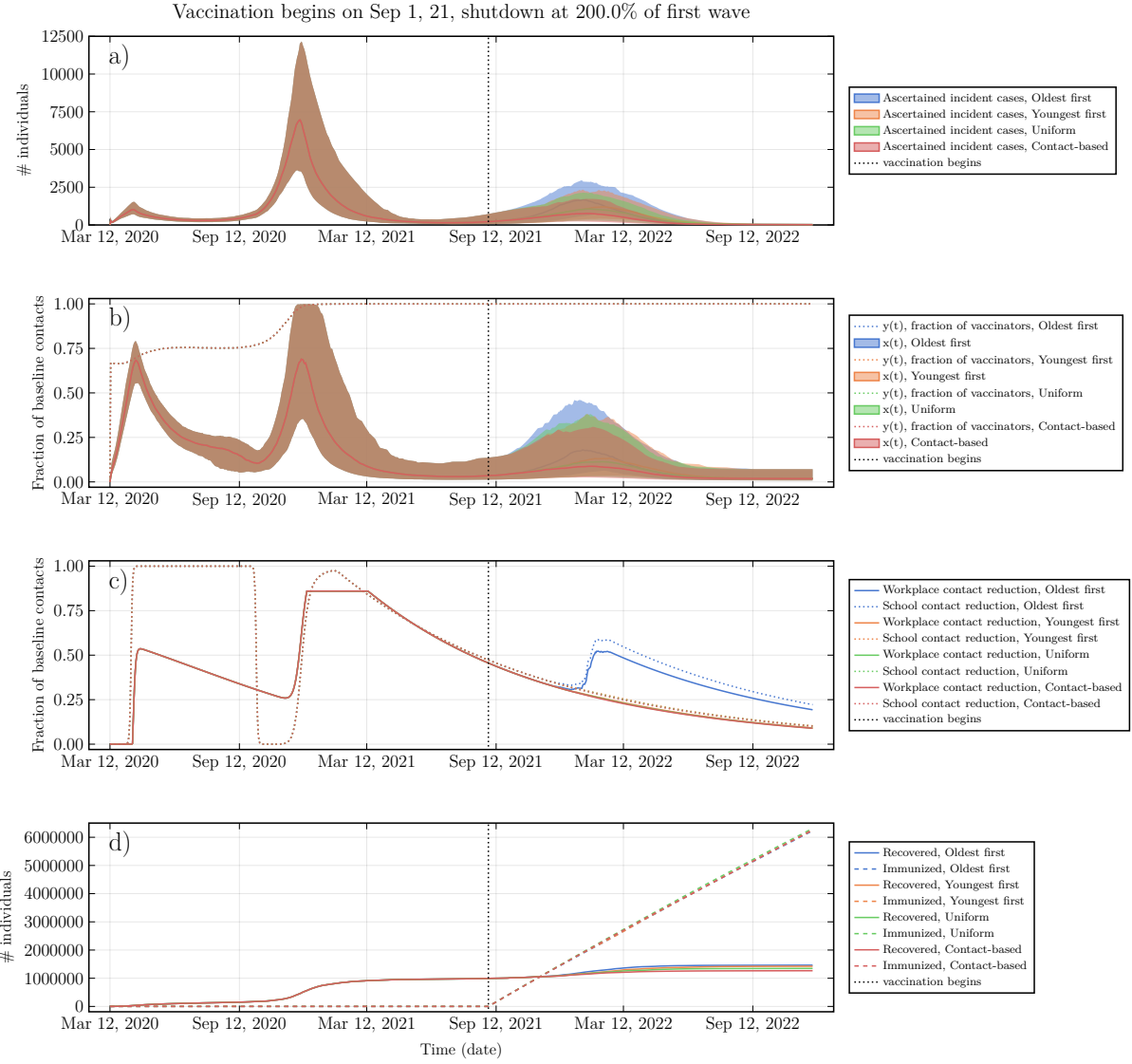


Figure 15: **Epidemic dynamics and social dynamics for both NPI adherence and vaccinating behaviour, when vaccine cost is small, $c_{vac} = 1.1 \times 10^{-4}$.** (a) Ascertained incident COVID-19 cases, (b) proportion x of the population practicing NPIs, (c) Intensity of school and workplace closure, (d) percentage of population with natural or vaccine-derived immunity versus time. $T = 200\%$, $\psi_0 = 1.0\%$ per week (maximum rate in absence of vaccine refusal), vaccine available in September 2021, $\kappa_{vac} = 50/\text{day}$. Other parameters are in Table 2.1.

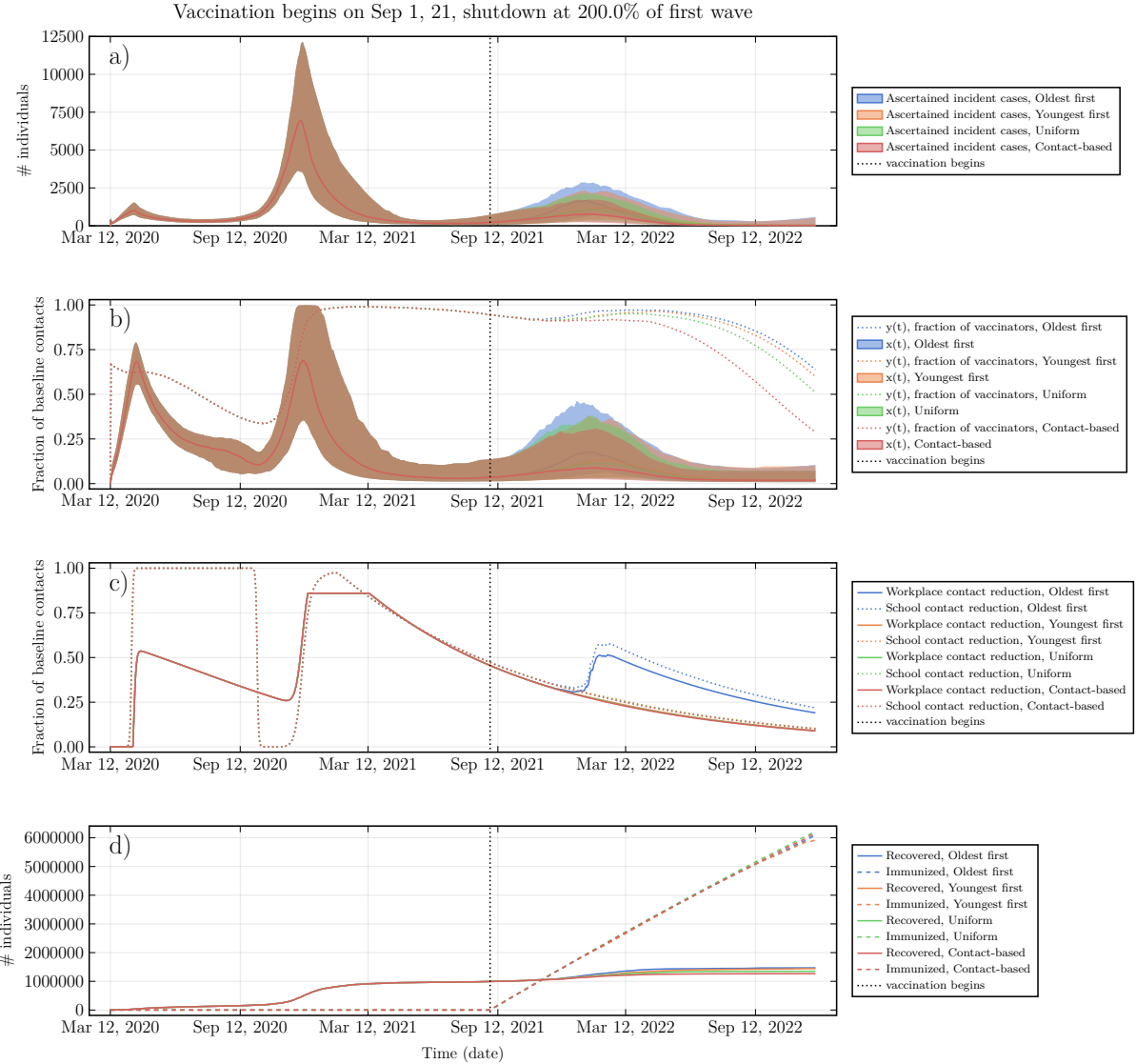


Figure 16: Epidemic dynamics and social dynamics for both NPI adherence and vaccinating behaviour, when vaccine cost is moderate, $c_{vac} = 2.9 \times 10^{-4}$. (a) Ascertained incident COVID-19 cases, (b) proportion x of the population practicing NPIs, (c) Intensity of school and workplace closure, (d) percentage of population with natural or vaccine-derived immunity versus time. $T = 200\%$, $\psi_0 = 1.0\%$ per week (maximum rate in absence of vaccine refusal), vaccine available in September 2021, $\kappa_{vac} = 50/\text{day}$. Other parameters are in Table 2.1.

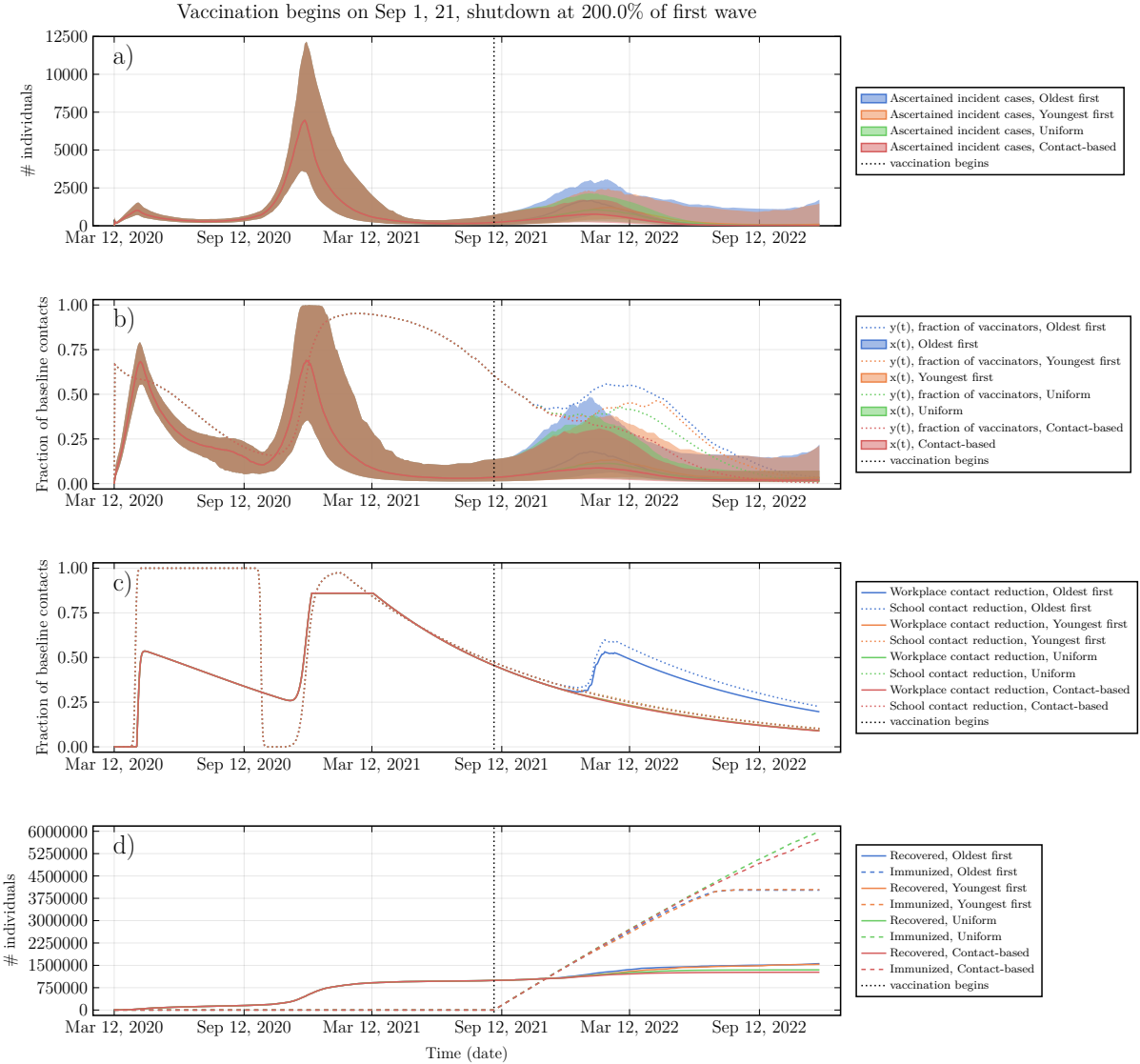


Figure 17: **Epidemic dynamics and social dynamics for both NPI adherence and vaccinating behaviour, when vaccine cost is high, $c_{vac} = 3.8 \times 10^{-4}$.** (a) Ascertained incident COVID-19 cases, (b) proportion x of the population practicing NPIs, (c) Intensity of school and workplace closure, (d) percentage of population with natural or vaccine-derived immunity versus time. $T = 200\%$, $\psi_0 = 1.0\%$ per week (maximum rate in absence of vaccine refusal), vaccine available in September 2021, $\kappa_{vac} = 50/\text{day}$. Other parameters are in Table 2.1.

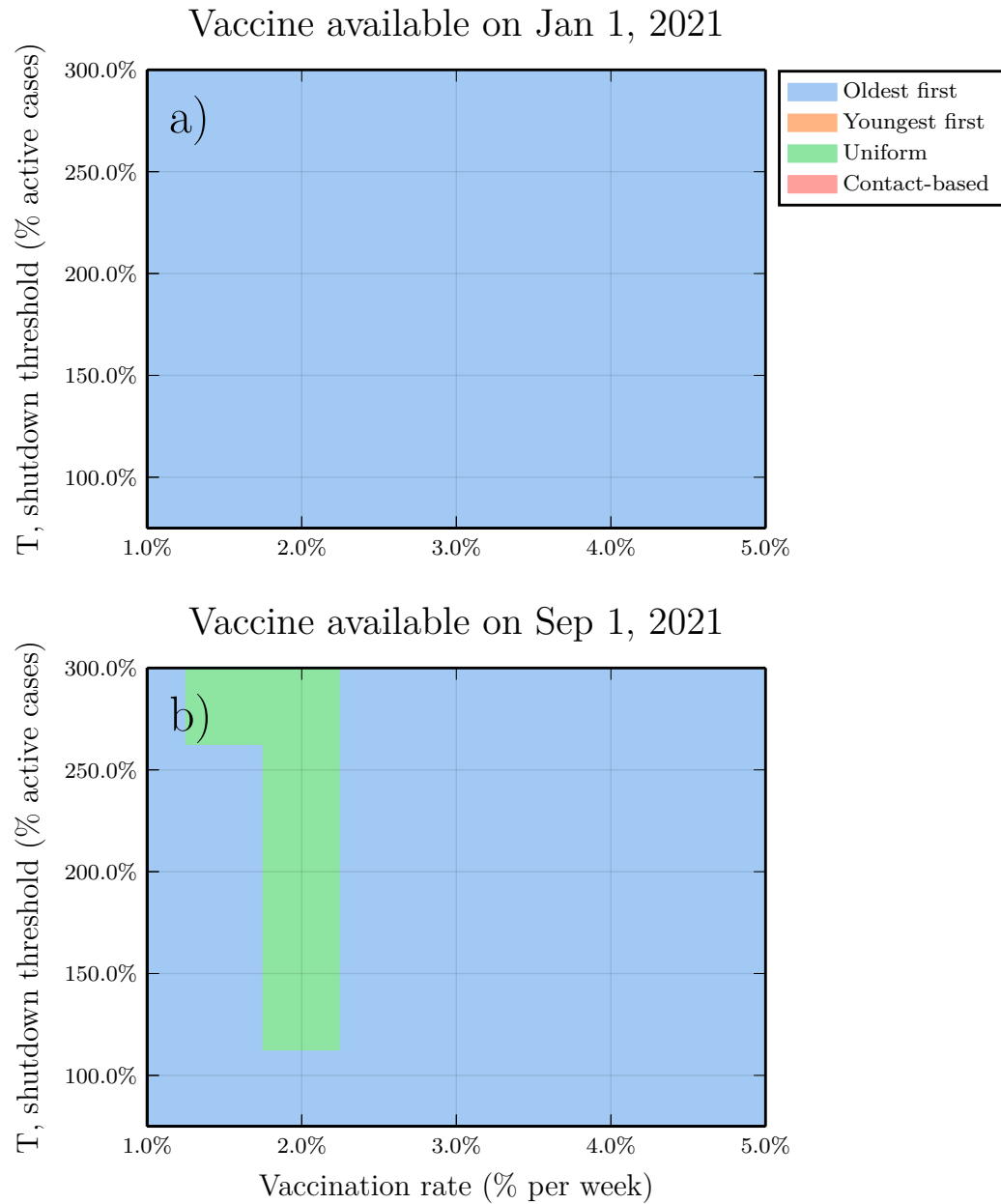


Figure 18: **Sensitivity analysis for the scenario where $R_0 = 2.5$ for December 2020 onward.** Subpanels are (left) parameter planes for January and September availability showing the vaccination strategy that prevents the most COVID-19 deaths as a function of T and ψ_0 , and (right) percentage reductions in mortality. Other parameter values are as in Table S1.

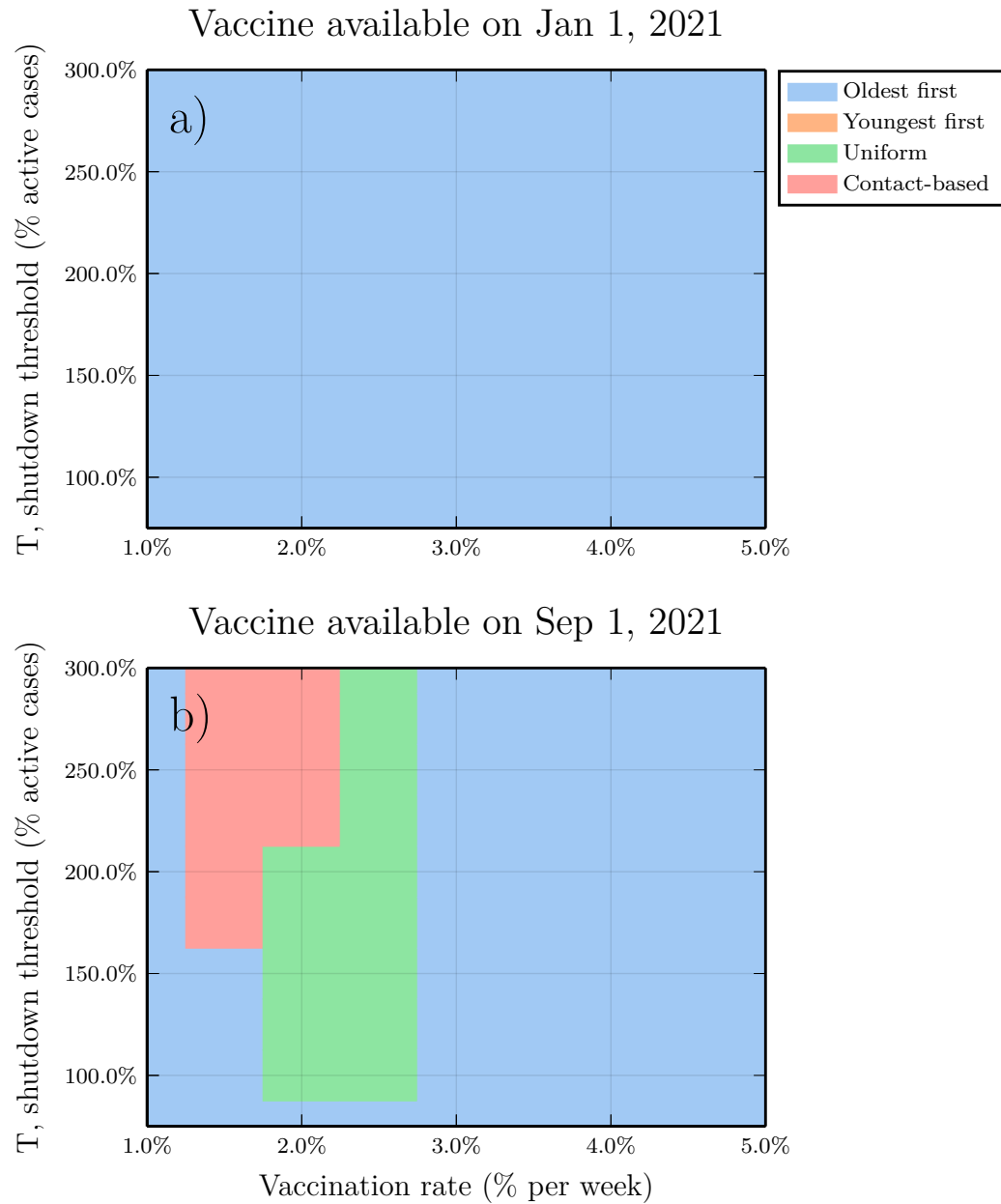


Figure 19: Sensitivity analysis for the scenario of 30% heightened ascertainment across all ages from December 2020 onward. Subpanels are parameter planes for January and September availability showing the vaccination strategy that reduces COVID-19 mortality the most as a function of T and ψ_0 (left) and the corresponding posterior parameter distributions for the refitted parameters (right). Other parameter values as in Table S1.

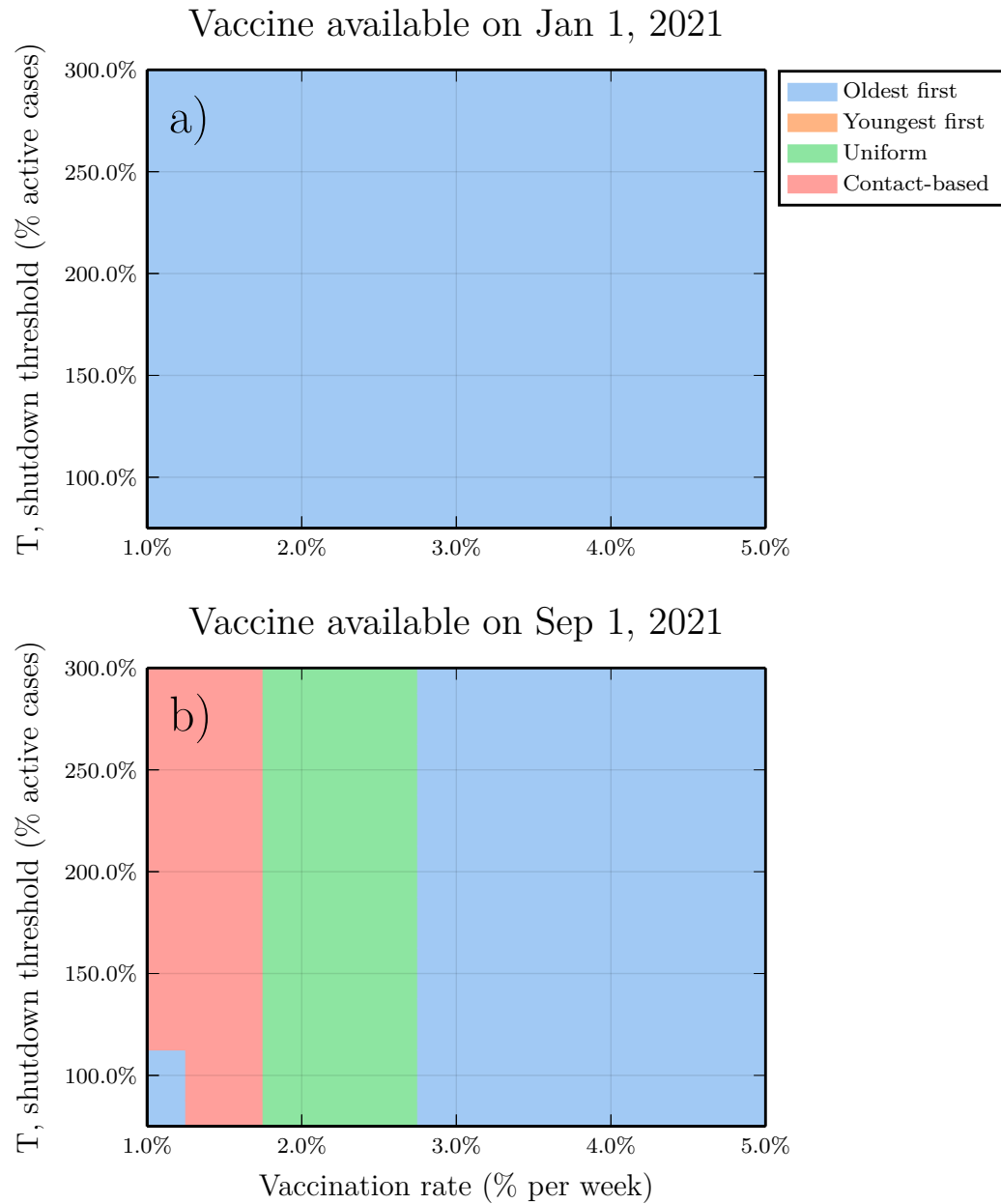


Figure 20: **Sensitivity analysis for the scenario of 30% reduced ascertainment across all ages from December 2020 onward.** Subpanels are parameter planes for January and September availability showing the vaccination strategy that reduces COVID-19 mortality the most as a function of T and ψ_0 (left) and the corresponding posterior parameter distributions for the refitted parameters (right). Other parameter values as in Table S1.

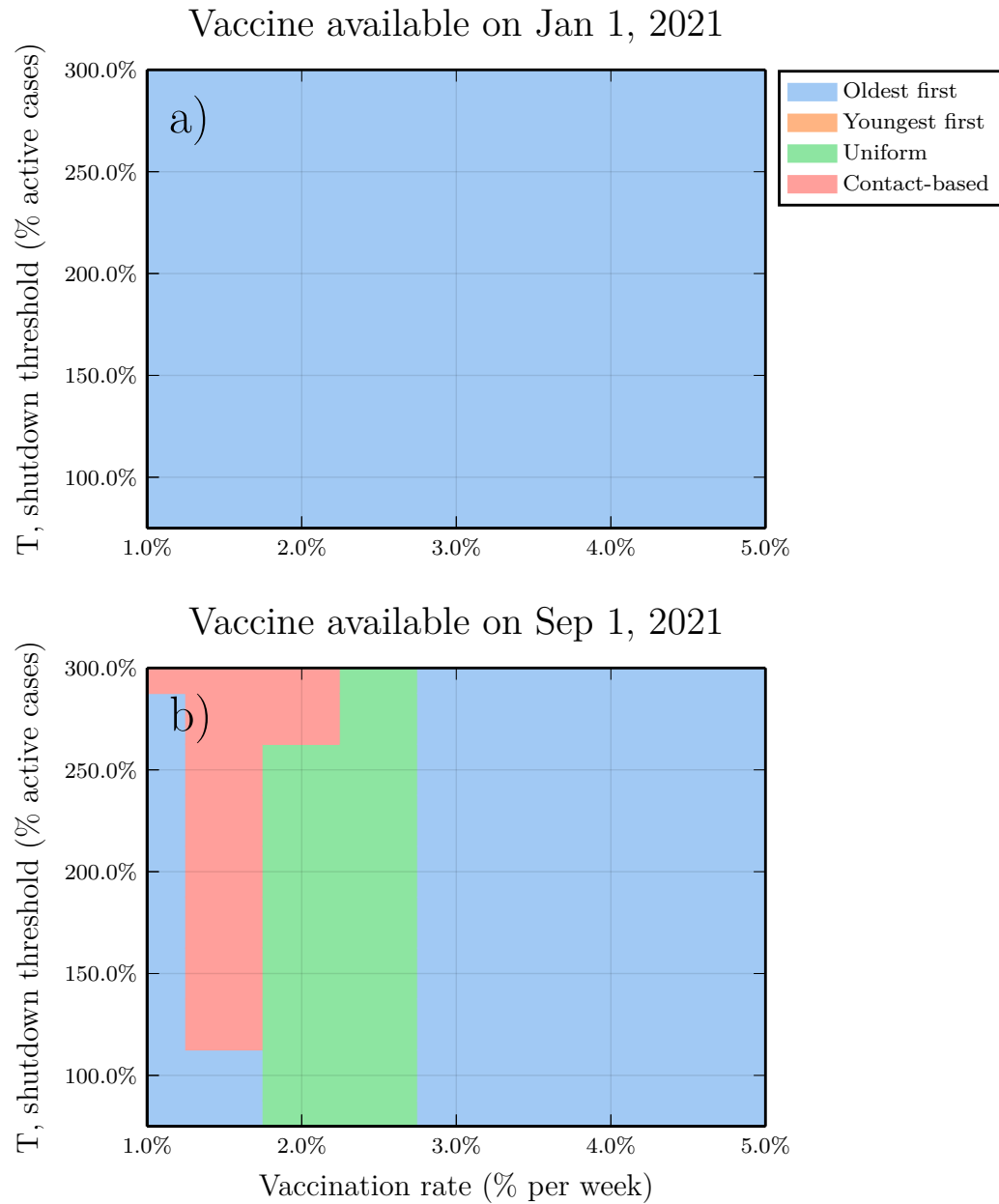


Figure 21: Sensitivity analysis for the scenario of four times the baseline social learning rate from December 2020 onward. Subpanels are parameter planes for January and September availability showing the vaccination strategy that reduces COVID-19 mortality the most as a function of T and ψ_0 (left) and the corresponding posterior parameter distributions for the refitted parameters (right). Other parameter values as in Table S1.

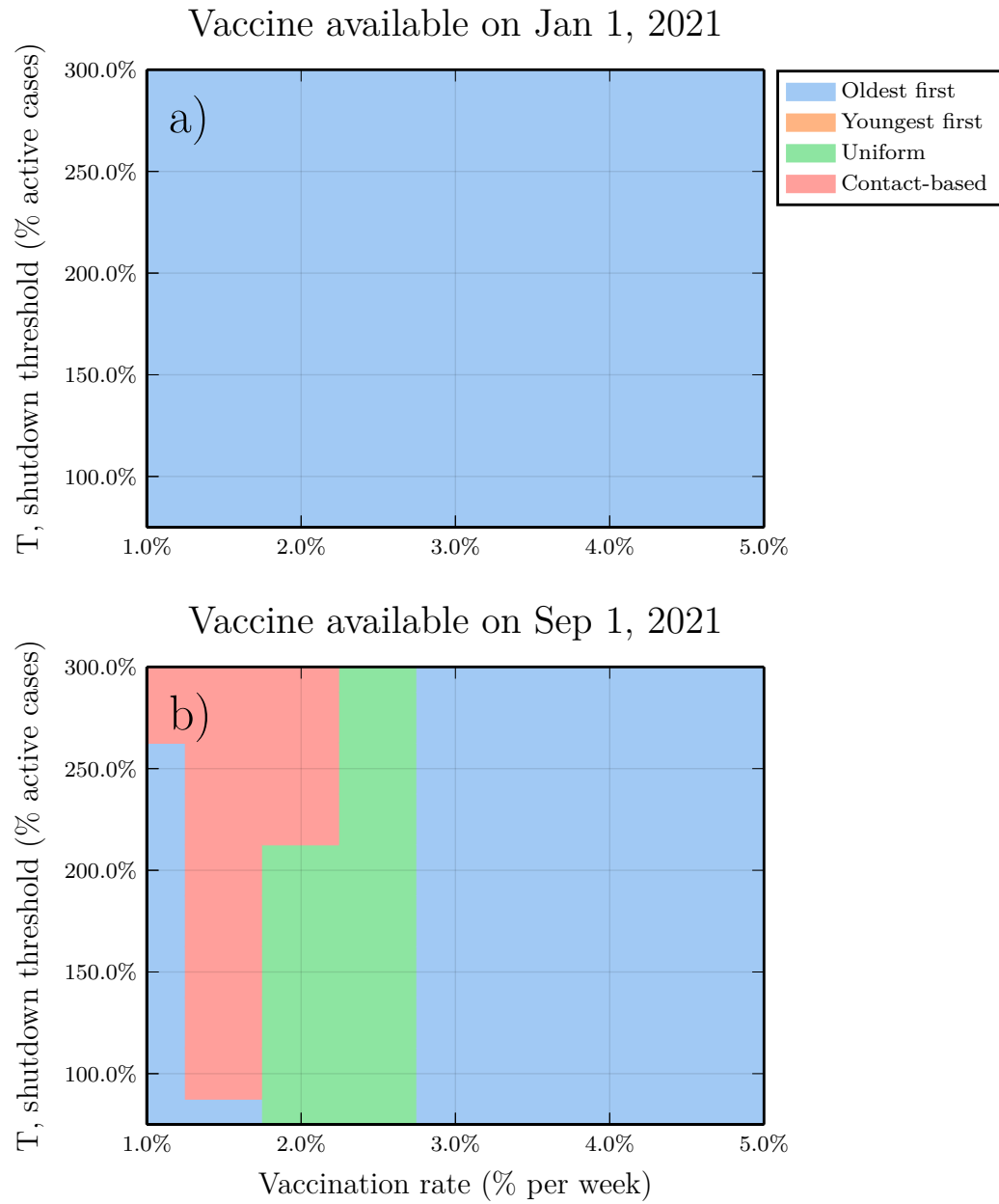
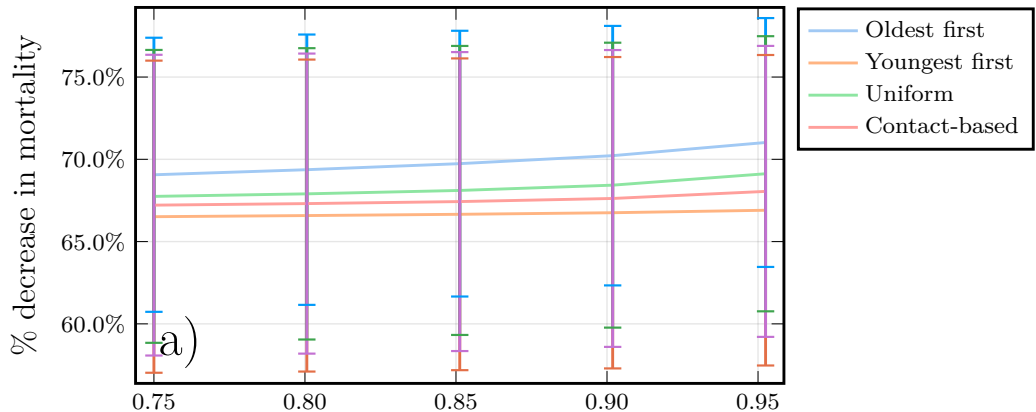


Figure 22: **Sensitivity analysis for the scenario of one-fourth the baseline social learning rate from December 2020 onward.** Subpanels are parameter planes for January and September availability showing the vaccination strategy that reduces COVID-19 mortality the most as a function of T and ψ_0 . Other parameter values as in Table S1.

Vaccine available: Jan 1, 2021



Vaccine available: Sep 1, 2021

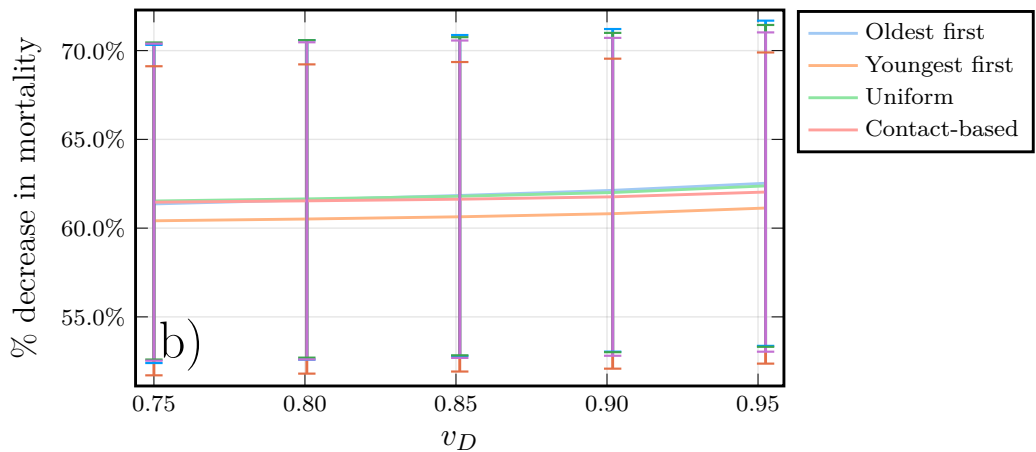


Figure 23: **Sensitivity analysis for the scenario where efficacy against disease v^D is not the same as efficacy against transmission v^T .** Subpanels show percentage reduction in mortality for the four strategies versus v^D when $v^T = 0.75$ but v^D ranges from 0.75 to 0.95, for January and September availability. Other parameter values as in Table S1. Note that mortality in this plot is computed from March 15, 2020 to March 14, 2025.

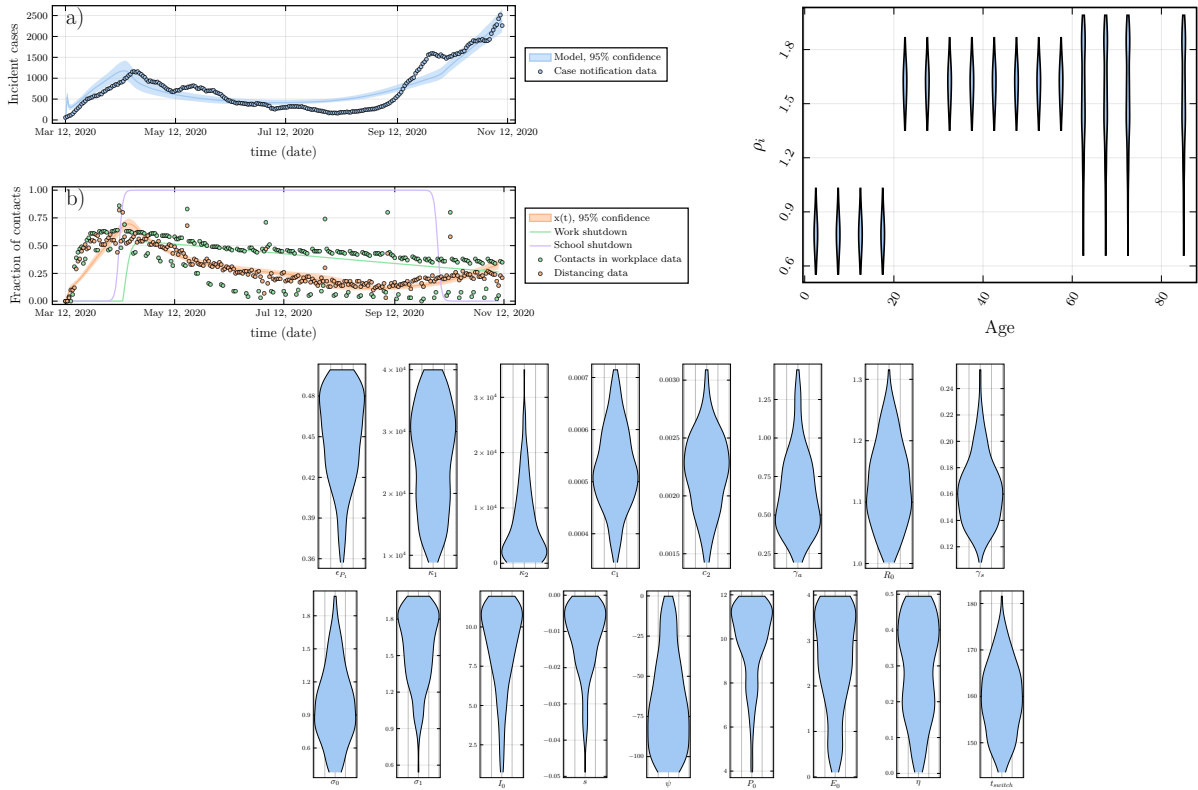


Figure 24: Posterior parameter distributions and model outputs for more stringent particle filtering criteria under Bayesian particle filtering algorithm. Top left panel shows (a) COVID-19 case incidence by date of report in Ontario, 7-day running average (circles) and ascertainment case incidence from best fitting models (lines). (b) Percentage change from baseline in time spent at retail and recreation destinations (orange circles) and at workplaces (green circles) from Google mobility data, and proportion of the population x adhering to NPIs (orange line) and workplace shutdown curve (green line) from fitted model. Top right panel shows posterior parameter distribution for age-specific susceptibility modifier, ρ_i . Bottom panel shows other posterior parameter distributions. Other parameter values as in Appendix, pp. 1-11.

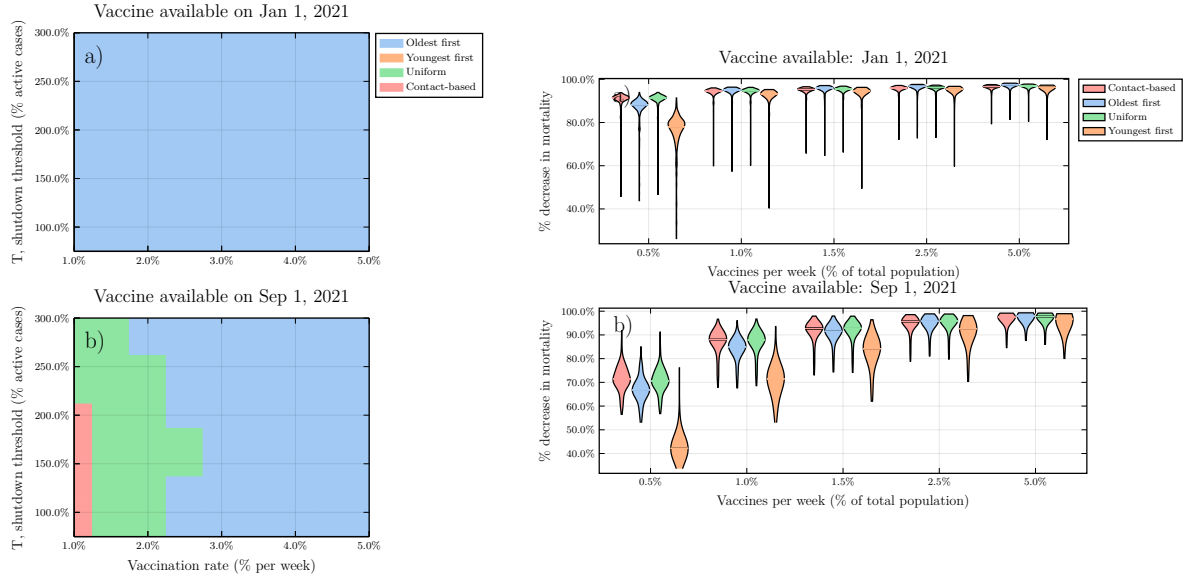


Figure 25: Sensitivity analysis for more stringent particle filtering criteria under Bayesian particle filtering algorithm. Subpanels are parameter planes for January and September availability showing the vaccination strategy that reduces COVID-19 mortality the most as a function of T and ψ_0 (left) and violin plots showing percentage reduction in mortality (right). Horizontal lines represent median values of posterior model projections. Shutdown threshold $T=200\%$ and other parameter values in Appendix, pp. 1-11. Percentage reductions are relative to no vaccination. Projected number of deaths in the absence of vaccination was 72,000 (95% credible interval: 40,000 to 122,000) from January 1, 2021 to March 14, 2025 for (a) and 60,000 (95% credible interval: 31,000 to 108,000) from September 1, 2021 to March 14, 2025 for (b). Ontario Population size: 14.6 million.

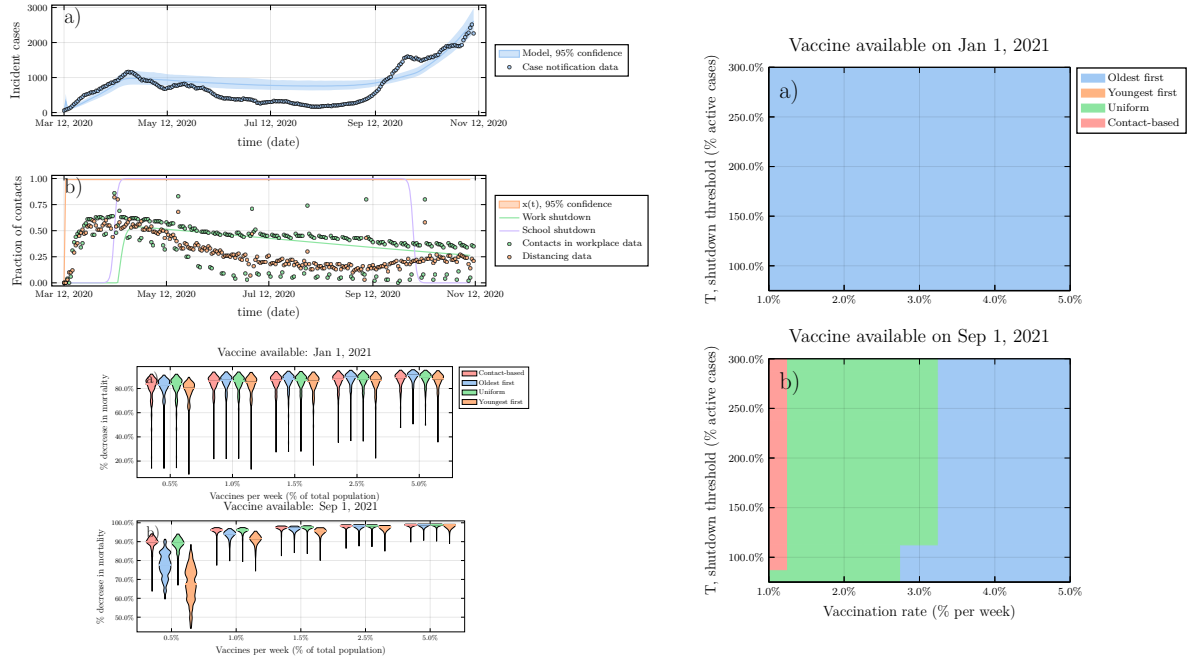


Figure 26: Model fit to data and baseline projections of mortality reductions under the four vaccine strategies, when behaviour is held constant over time.

Top left: a) COVID-19 case incidence by date of report in Ontario, 7-day running average (circles) and ascertained case incidence from best fitting models (lines). (b) Percentage change from baseline in time spent at retail and recreation destinations (orange circles) and at workplaces (green circles) from Google mobility data, and proportion of the population x adhering to NPIs (orange line) and workplace shutdown curve (green line) from fitted model. Bottom left: Violin plots of the percent reduction in mortality under the four vaccine strategies, relative to no vaccination, as a function of the vaccination rate 0, for (a) January and (b) September 2021 availability. Horizontal lines represent median values of posterior model projections. Shutdown threshold $T=200\%$. Percentage reductions are relative to no vaccination. Projected number of deaths in the absence of vaccination was 72,000 (95% credible interval: 40,000 to 122,000) from January 1, 2021 to March 14, 2025 for (a) and 60,000 (95% credible interval: 31,000 to 108,000) from September 1, 2021 to March 14, 2025 for (b). Ontario Population size: 14.6 million. Right: Each parameter combination on the plane is colour coded according to which of the four strategies prevented the most deaths, on average across all model realizations, for (a) January and (b) September 2021 availability. Other parameter values in Appendix, pp. 1-11.

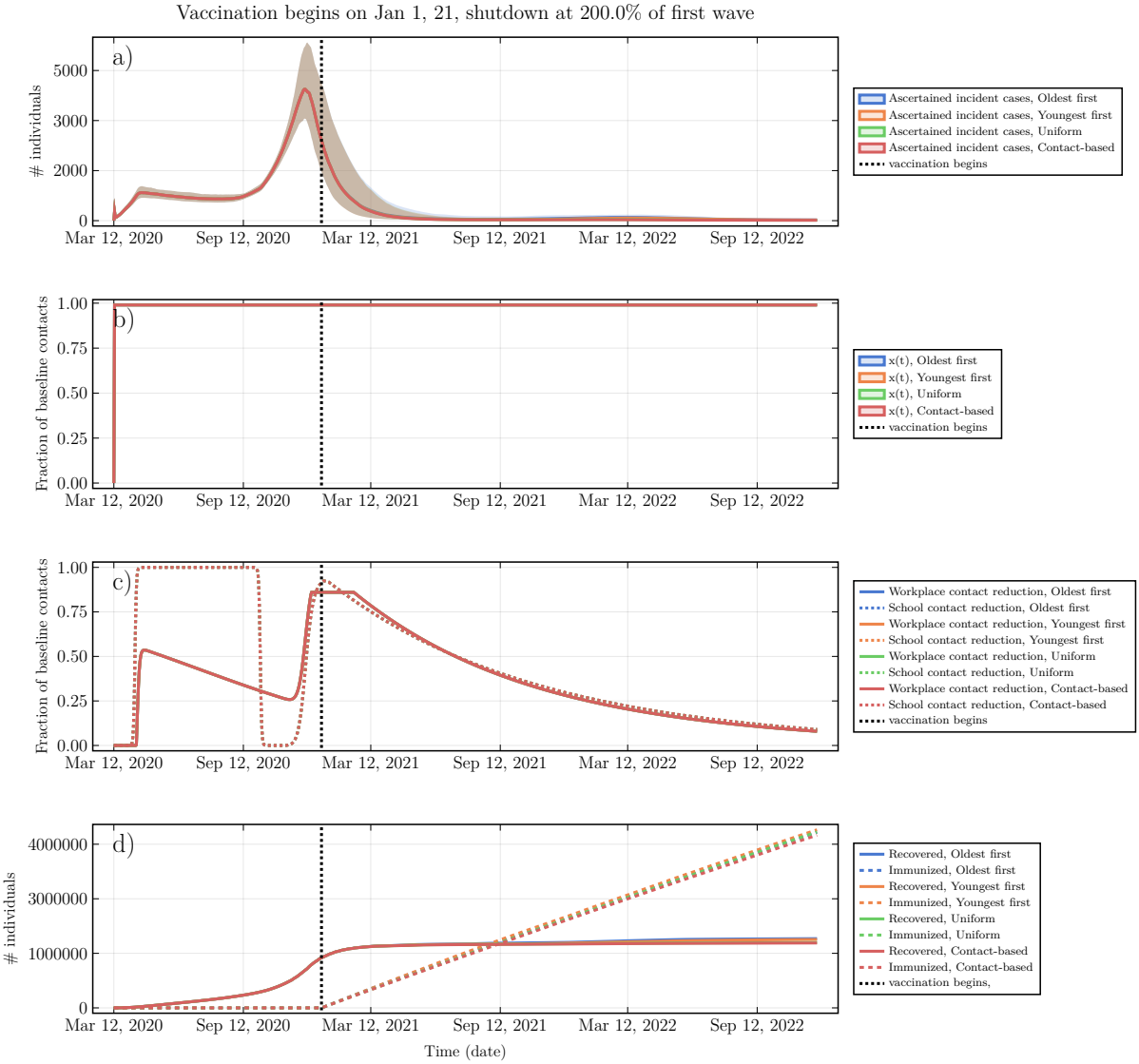


Figure 27: **Epidemic dynamics and social dynamics for both NPI adherence and vaccinating behaviour, when behaviour is held constant over time.** (a) Ascertained incident COVID-19 cases, (b) proportion x of the population practicing NPIs, (c) Intensity of school and workplace closure, (d) percentage of population with natural or vaccine-derived immunity versus time. $T = 200\%$, $\psi_0 = 0.5\%$ per week, vaccine available in January 2021. Other parameters are in Table 2.1.

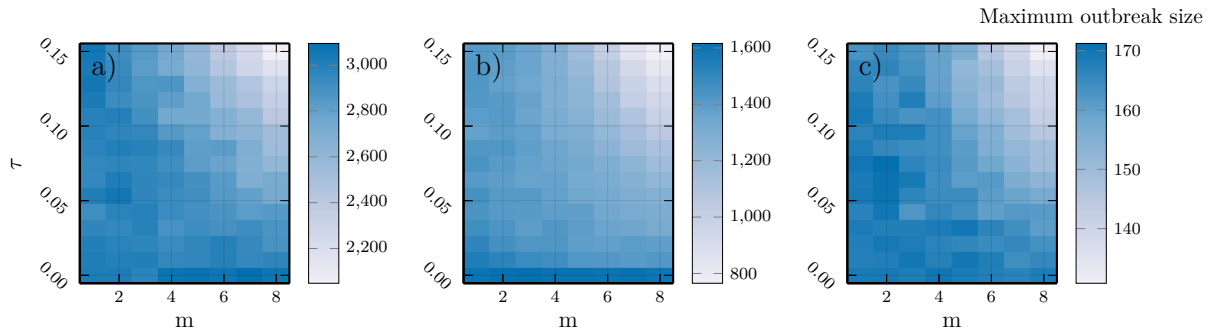


Figure 28: Maximum MPB infestation size within 500 year period, under FTP with respect to τ fraction of m juvenile stands cleared. a) ($\alpha_1 = 0.02, \alpha_2 = 0.0025$), b) ($\alpha_1 = 0.01, \alpha_2 = 0.006$), c) ($\alpha_1 = 0.03, \alpha_2 = 0.0012$.)

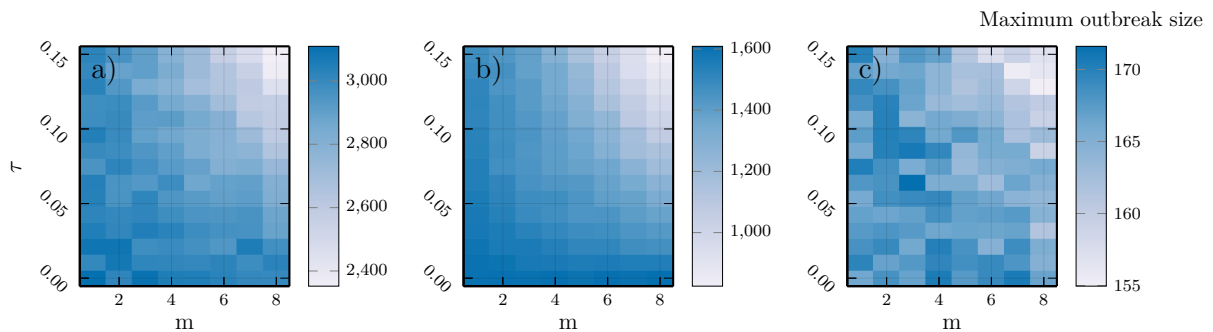


Figure 29: Maximum MPB infestation size within 500 year period, under FTP with respect to τ fraction of m juvenile stands cleared, conducted every *five* years. a) ($\alpha_1 = 0.02, \alpha_2 = 0.0025$), b) ($\alpha_1 = 0.01, \alpha_2 = 0.006$), c) ($\alpha_1 = 0.03, \alpha_2 = 0.0012$.)

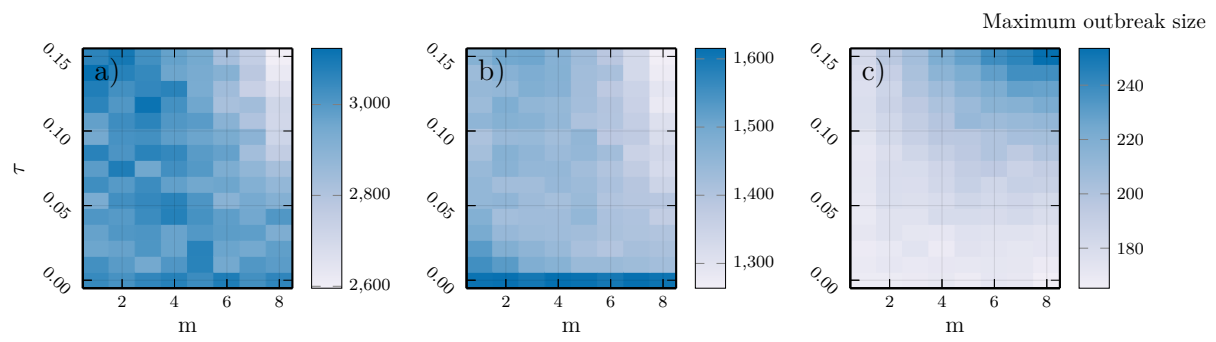


Figure 30: Maximum MPB infestation size within 500 year period, under CBP with respect to τ fraction of m juvenile stands cleared, conducted each year. a) ($\alpha_1 = 0.02$, $\alpha_2 = 0.0025$), b) ($\alpha_1 = 0.01$, $\alpha_2 = 0.006$), c) ($\alpha_1 = 0.03$, $\alpha_2 = 0.0012$.)